Economic significance of platinum group elements and water in asteroids: Insights from chondritic meteorites

by

Cosette Gilmour

A thesis submitted in partial fulfillment of the requirements for the degree of

Master of Science

Department of Earth and Atmospheric Sciences
University of Alberta

Abstract

Asteroids are considered to be rich sources of precious metals, water, and essential volatiles for life. Such a consideration has been derived from the study of meteorites and asteroid reflectance spectra which have both been vital to our understanding of asteroid compositions. The vast amount of valuable resources in asteroids that are in close proximity to Earth (Near-Earth Asteroids; NEAs) has designated such asteroids as prime targets for extra-terrestrial mining. Of the resources that can be extracted from asteroids, the platinum group elements (PGEs) and water are two of the most sought-after materials. The PGEs are highly valuable given their rarity on Earth, while having an available water source in space can help facilitate future space exploration (i.e., rocket fuel, radiation shielding, drinking water, etc.). Before mining of these resources can commence, asteroid miners must develop a detailed understanding of how the different compositions of asteroids can affect the distribution of such resources. Since it is an expensive endeavor to visit asteroids for such an assessment, meteorite studies take precedence in obtaining the necessary information for selecting an asteroid target to mine. The premise of this master's thesis is to provide insight into the PGE and water resources that can be mined from asteroids through the study of chondritic meteorites.

In the first study of this thesis, PGE concentrations have been determined *in situ* in ordinary chondrite metal via laser ablation inductively coupled plasma mass spectrometry (LA-ICP-MS). This is the first study to provide a detailed account of *in situ* PGE concentrations in the metal phases among a suite of ordinary chondrites. *In situ* results reveal that PGE concentrations in ordinary chondrite metal are similar among the different ordinary chondrite groups (H, L, and LL). This discovery is a significant contribution to the asteroid mining industry regarding which ordinary chondrite parent body is most ideal to mine considering that previous

studies have claimed that PGE concentrations vary among the three ordinary chondrite groups. The findings from this PGE study are also pertinent to understanding the formation of metal in ordinary chondrites; the minimal variability of PGEs suggest that metal was formed as nebular condensates. The second part of this thesis addresses the effects aqueous alteration has on the abundance of water in carbonaceous material. For this investigation, the unique Tagish Lake carbonaceous chondrite was selected for analysis given that variable aqueous alteration degrees have been reported for three pristine specimens (TL5b < TL11h < and TL11i; Herd et al., 2011; Blinova et al., 2014). Thermogravimetric analysis (TGA), infrared transmission spectroscopy, and X-ray diffraction (XRD) were used to quantify the extent of aqueous alteration in the Tagish Lake specimens based on how much water they contained and their phyllosilicate/olivine ratio. The findings from this study are congruent with the previously reported alteration sequence (Herd et al., 2011; Blinova et al., 2014), allowing for the addition of two new Tagish Lake specimens (TL4 and TL10a) to be incorporated into the sequence. Reflectance spectra of Tagish Lake were also acquired to re-visit the Tagish Lake parent body connection. This Tagish Lake investigation is relevant to the material processing of asteroid mining given that the TGA method records the temperatures at which minerals break down and release water. Furthermore, investigating the meteorite-parent body connection is pertinent for selecting suitable asteroid targets. The findings of this thesis provide valuable insight into the type of asteroids that are suitable for mining PGEs and water. On this basis, I propose that H chondrite parent bodies are ideal for the extraction of PGEs, while CI and CM carbonaceous chondrite parent bodies are best for water resources.

Preface

This thesis is an original work by Cosette Gilmour.

No part of this thesis has been previously published.

To Mom, Dad, and Sadie

Yard by yard, life is hard.
Inch by inch takes too damn long.

Acknowledgements

I would like to extend my utmost thank you to my supervisor, Chris Herd. I am very fortunate that Chris was open to exploring my interest in asteroid mining and helping me turn it into a thesis. His guidance and patience during this process is greatly appreciated. Thank you for all the wonderful opportunities you have provided me with that have helped me grow as a researcher.

There are very many wonderful people from around the world who I have had the pleasure of getting to know and work with throughout my master's degree. Without these people, this thesis would not have been possible. From the UAlberta Earth and Atmospheric Sciences department I would like to thank: Andy DuFrane (LA-ICP-MS), Guangcheng Chen (solution ICP-MS), Andrew Locock (EPMA and Rietveld refinement), Nathan Gerein (SEM), Diane Caird (XRD), and Martin Von Dollen (sample prep), as well as Benoit Rivard and Robert Creaser for their insight and feedback on my thesis. Thank you also to: Derek MacKenzie (UAlberta Renewable Resources) for granting me use of his TGA instrument and Nduka Ikpo for gathering the TGA measurements; Ed Cloutis, Paul Mann, Matt Cuddy, and Dan Applin (University of Winnipeg Planetary Spectrophotometer Facility) for collecting the Tagish Lake reflectance spectra, providing powdered mineral samples for TGA, and answering my spectroscopy-related questions; Matt Izawa (Okayama University) for answering my Tagish Lake carbonate questions; Conel Alexander (Carnegie Institution of Washington) for providing a sample of Murchison IOM for TGA; Andy Rivkin (Johns Hopkins Applied Physics Lab) for helping me understanding asteroid magnitudes; and Pierre Beck (Institut de Planétologie et d'Astrophysique de Grenoble) for collecting the Tagish Lake transmission spectra. I would like to express gratitude towards the Smithsonian National Museum of Natural History for the loan of Forest Vale, Leedey, Olivenza, and St. Séverin for use in my PGE study.

I would also like to thank my wonderful friends at the U of A who have cheered me on and provided unconditional love and support: Nick Castle, Danielle Simkus, Hector Martinez De La Torre, Ebberly MacLagan, Sasiri Bandara, and Katherine Bramble.

And last, but certainly not least, I would like to thank my parents. They have been my biggest support during this entire process and I am so thankful for their help in making my dreams come true.

This research was supported by: the Natural Sciences and Engineering Research Council (NSERC) Discovery Grant 261740 to C. Herd; the NSERC CGS-M scholarship; the Canadian Space Agency and Western University ASTRO/CPSX Graduate Student Travel Award for travel to University of Winnipeg; the Meteoritical Society Travel Award to attend the 78th Annual Meeting of the Meteoritical Society; and the UAlberta FGSR and GSA travel awards to attend the 2016 Vatican Observatory Summer School.

Table of Contents

List of Tables

List of Figures

Chapter 1. Introduction

Meteorites are fragments of asteroids and other rocky bodies (i.e., moons, terrestrial planets, dwarf planets) that have fallen to the surface of another planetary body. Meteorites hold many clues to understanding the formation of the solar system and the processes that have taken place throughout the solar system's history (e.g., solar nebula condensation, parent body/planetary accretion, secondary alteration processes). The meteorites which fall to Earth allow scientists to study these objects in detail and formulate theories regarding the evolution of the solar system. Meteorites that are collected shortly after an observed fall are referred to as "falls", whereas meteorites that have been collected without context of their fall date are known as "finds". As meteorites are samples of the body from which they came, studying their compositions and textures can help us understand more about their parent bodies. However, the lack of context from where these objects came make it difficult to piece together some parts of the early solar system. Sample return missions (e.g., Apollo 11, Hayabusa 2, OSIRIS-REx) are helpful in providing such context, but these missions are costly and take many years to plan and execute. Reflectance spectroscopic measurements collected from remote sensing of asteroids and in the laboratory for meteorites have aided in elucidating the meteorite-asteroid connection; however, reflectance spectroscopy is not always reliable due to space weathering of asteroids, low albedos, and availability of meteorite samples. Regardless of the lack of context, planetary scientists are still able to gain remarkable insights into the early solar system through the study of meteorites.

In addition to understanding the early solar system, meteorite studies are pertinent to the asteroid mining industry. Studying the composition of meteorites can help asteroid miners understand the types of resources and abundances that can be potentially extracted from their asteroid parent bodies. From petrological studies and spectral measurements (reflectance and transmission) of meteorites, as well as reflectance measurements of asteroids, scientists and asteroid mining companies know that metallic (iron cores) and stony (chondritic) asteroids are rich in precious metals found in low concentrations on Earth, including the platinum group elements (PGEs), whereas carbonaceous (chondritic) asteroids are abundant with water and life sustaining volatiles (Kargel, 1994; Lewis, 1996). Mining asteroids for such resources can provide building materials, life support, and radiation shielding, among many other applications, for future endeavors in space exploration (Kargel, 1994; Ross, 2001; Lewis, 2015).

The improvement of the meteorite-asteroid connection, whether it be through reflectance spectroscopy or sample return missions, is critical for selecting valuable asteroid targets. The implications of asteroid mining are addressed in more detail in Chapter 4.

This introductory chapter provides the necessary background and context of the different meteorites and nomenclature that will be discussed in the following chapters. Meteorites are divided into three major types: stony meteorites, stony-iron meteorites, and iron meteorites. The stony meteorites are further divided into two categories known as chondrites and achondrites. Chondrites are meteorites which contain small, round grains known as chondrules typically made up of olivine and pyroxene; the texture, mineralogy, and geochemistry of these meteorites indicate that they have avoided differentiation (the parent body process in which the body is separated into a metallic core and silicate mantle). The achondrites lack chondrules as they have undergone differentiation, resulting in igneous textures; consequently, metal is mostly absent in achondrites (except for the primitive achondrites) due to fractionation of metal into the core (i.e., iron meteorites). The chondrite meteorites are of particular interest for studying the implications of asteroid mining given that they are the most common meteorite type (83%; Meteoritical Bulletin Database, 2017). This high percentage of chondrite meteorites suggests that the chondrite asteroid parent bodies are abundant in the solar system, which has strong implications when selecting asteroid targets for mining.

The chondrite meteorites are divided into three classes known as ordinary chondrites (OCs), enstatite chondrites (ECs), and carbonaceous chondrites (CCs). These classes are further subdivided into groups and petrologic types (Fig. 1.1), which are discussed in more detail below. The ordinary chondrites are also comprised of two other chondrite groups, R and K (Fig. 1.1), but these two groups are rare and therefore will not be discussed. The chondrite classes have distinct bulk compositions: the abundance of refractory lithophile elements increases in the order EC < OC < CC (Fig. 1.2; Rubin and Wasson, 1995) and the CCs are depleted in volatile lithophile elements relative to OCs and ECs (Fig. 1.2). In terms of siderophile elements, specifically Os to Fe, the CCs have relatively similar abundances, with the exception of the CB and CH groups (Fig. 1.2). There is more variability in siderophile element (Os to Fe) abundances among the OCs and ECs, where the H ordinary chondrites and EH enstatite chondrites have the greatest abundances; all three chondrite classes are depleted in the chalcophile elements (Fig.

1.2). The chondrite classes also have distinct redox states (Fig. 1.3) as well as oxygen isotope values.

The differences in bulk composition, oxygen isotopes, and redox state among the chondrite classes suggest that they formed in different regions in the solar system (e.g., Rubin and Wasson, 1995). It is generally thought that the ECs formed closest to the sun (<1 AU) under the most reducing conditions, the OCs formed at a distance greater than Mars (~2.5 AU), and the CCs formed furthest from the sun (likely beyond the 'snow line' – the distance beyond which water ice is stable) in highly oxidizing conditions (Rubin and Wasson, 1995). The solar system formed from a dense cloud of dust and gas, known as a solar nebula (Boss and Ciesla, 2014), in which the chondrite parent bodies and other planetary bodies formed from the interaction of the dust and gas particles. Condensation of elements occurred in the solar nebula as it cooled (e.g., Larimer and Anders, 1970; Grossman and Larimer, 1974) and the refractory species vaporized closer to the sun (< 1 AU) while the volatile species vaporized further out at greater distances (Boss and Ciesla, 2014). Organic matter and water ice also vaporized at distances greater than the terrestrial planets (Boss and Ciesla, 2014). As the distribution of elemental and molecular constituents varied throughout the solar system, the chondrite classes acquired different abundances of these constituents and developed unique characteristics (i.e., oxygen isotopes, redox states) based on their formation locations as well as post-accretion events (i.e., mixing, alteration, impacts). Given that chondrite meteorites contain metal grains (OC and EC) and hydrous minerals (CC) in variable abundances, the chondrite parent bodies are potentially valuable targets for mining metal and water.

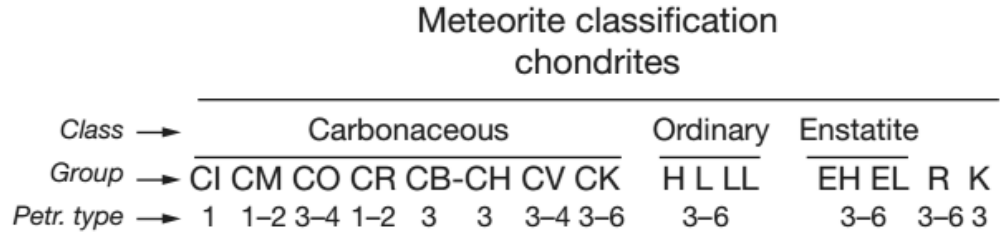

Fig. 1.1. Classification of the chondrite groups divided into class, group, and petrologic (petr.) type. [from Krot et al., 2014]

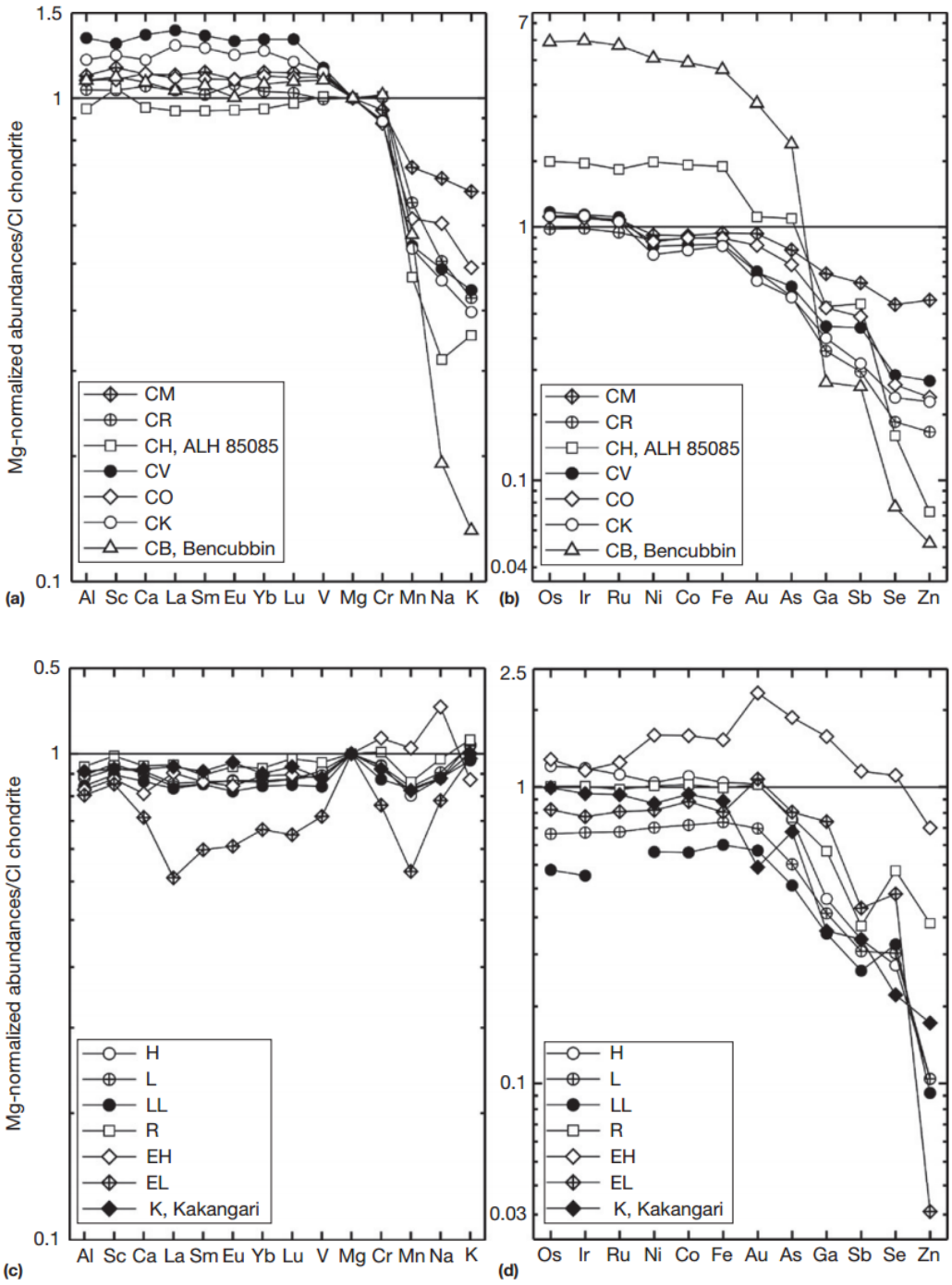

Fig. 1.2. Bulk compositions for the different chondrite groups normalized to Mg and CI chondrites: **(a & c)** lithophile elements **(b & d)** siderophile and chalcophile elements. Volatility of elements increases from left to right. [from Krot et al., 2014]

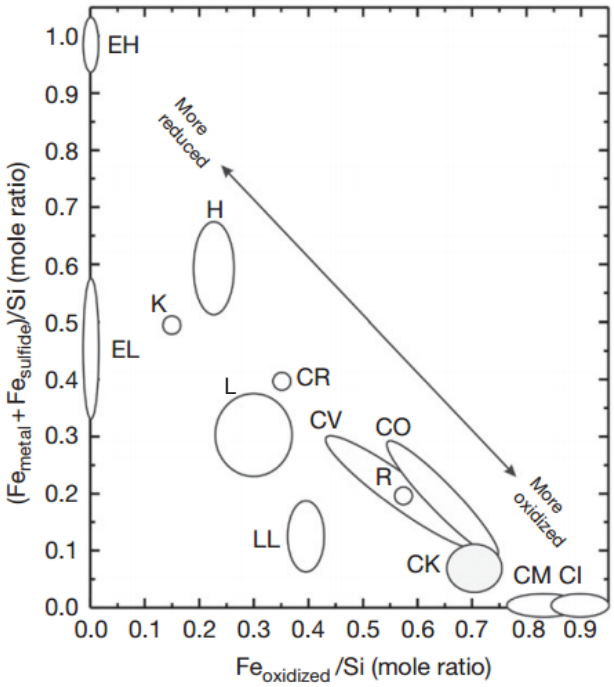

Fig. 1.3. Urey-Craig diagram highlighting the different redox states and iron contents in the chondrite meteorites. Metal and sulphide iron contents are plotted against silicate and oxide iron contents. [from Krot et al., 2014]

1.1 The Chondrites

1.1.1 Ordinary Chondrites

The OCs are the most abundant of the three chondrite classes constituting 90% of the chondrites (Meteoritical Bulletin Database, 2017). The OCs consist of olivine and pyroxene chondrules surrounded by a matrix comprised of silicates (olivine, pyroxene, and plagioclase), FeS (troilite), Fe-Ni metal, and in some cases glass. The OCs are divided into three groups – H, L, and LL (Fig. 1.1) – based on their Fe-Ni metal abundances and total Fe content: H - high metal and high total Fe; L - low metal and low total Fe; LL - low metal relative to total Fe and low total Fe. In terms of modal abundances, the average abundance of metal in the H, L, and LL chondrites is 18.2 wt.%, 8.4 wt.%, and 3.5 wt.%, respectively (Dunn et al., 2010); note that these abundances are for equilibrated OCs (see below for definition). The difference in their metal abundances is controlled by their oxidation states (Fig. 1.4); the H chondrites are the

least oxidized (most reduced) and contain the most metal while the LL chondrites are the most oxidized and have the least metal. The OC groups (and petrologic types) can also be distinguished by their mean olivine (fayalite) and orthopyroxene (ferrosilite) compositions (Fig. 1.4).

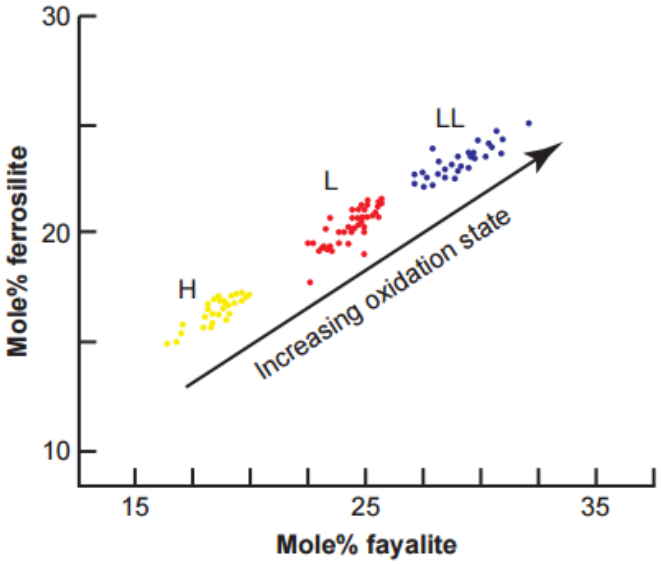

Fig. 1.4. Oxidation states of the ordinary chondrites determined by ferrosilite (orthopyroxene) and fayalite (olivine) compositions. Metal abundances decrease with increasing oxidation state. [from Snelling, 2014]

1.1.2 Enstatite Chondrites

The ECs are the most reduced chondrite class (Fig. 1.3) and are divided into two distinct groups: EH and EL (Fig. 1.1). The E in the group nomenclature stands for "enstatite" and the associated H and L designations of the ECs refer to their total amount of Fe-Ni metal, similar to the OCs. The ECs contain 19-28 wt.% metal (Brearley and Jones, 1998) which is higher than the metal abundances typically found in H ordinary chondrites. This enrichment of metal in ECs is due to the more reducing conditions in which they formed. The ECs get their name from the abundance of the pyroxene Mg-end member (enstatite) present in their composition. This is in large part due to the lack of Fe^{2+} available under the highly reducing conditions when the ECs formed. The ECs also contain unusual sulphides (i.e., Mn, Ca, Cr, Cu, Zn), schreibersite ($FeNi_3P$),

perryite (Ni silicide), graphite, and even carbides; however, olivine is rare (Brearley and Jones, 1998; Krot et al., 2014). Considering that the ECs make up only 1% (Meteoritical Bulletin Database, 2017) of the chondrite meteorites – indicating that their parent bodies are not abundantly available for mining – they were omitted from the research conducted in this thesis.

1.1.3 Carbonaceous Chondrites

The CCs are the most primitive type of meteorites as they contain the oldest objects in the solar system known as Calcium-Aluminum-rich Inclusions (CAIs). The CAIs have a diverse mineralogy, consisting mostly of Ca and Al-rich oxides and silicates, along with refractory mineral phases (i.e., hibonite, spinel, perovskite, anorthite) and in some cases olivine (forsterite) (Brearley and Jones, 1998). The CCs represent ~4% of the chondrites (Meteoritical Bulletin Database, 2017) and are divided into 8 groups (Fig. 1.1): CB, CH, CR, CO, CV, CK, CM, and CI (listed in order of increasing oxidation degree; Krot et al., 2014). The C associated with these designations stands for “carbonaceous” while the second letter represents the name of a type specimen for that group (e.g., Ivuna for CI chondrites). The CH chondrites are the exception to this designation, where the H denotes the high metal content of this group. Iron-nickel metal is not a characteristic constituent of CCs, as it is with the OCs and ECs, but metal does exist in the less oxidized CB, CH, CR, CO, and CV groups (Brearley and Jones, 1998; Krot et al., 2014). In some cases, a CC will not fall into the chemical characteristics of a specific group, and therefore is classified as “ungrouped”. The famous Tagish Lake meteorite is an ungrouped CC.

Despite being depleted in volatile lithophile elements (Fig. 1.2), the CCs are rich in volatiles compared to OCs and ECs due to the presence of organic matter and water in their compositions. The CCs can contain up to 20 wt.% water (Mason, 1963), which is a consequence of aqueous alteration (see below) producing hydrous minerals (i.e., phyllosilicates such as saponite and serpentine). These secondary phyllosilicates are characteristic minerals of CCs. The mineralogy of CCs also includes carbonates (i.e., calcite and dolomite), sulphides (i.e., troilite, pentlandite, pyrrhotite), oxides (notably magnetite), olivine, and pyroxene (Brearley and Jones, 1998).

1.2 Alteration Mechanisms

1.2.1 Parent Body Processes

The petrologic type associated with the chondrite classifications (Fig. 1.1) is designated based on the type and extent of alteration to which the chondrite has been subjected. Chondrites can be altered either by aqueous alteration or secondary metamorphic heating which are thought to both occur on the chondrite parent body (McSween et al., 1988; Zolensky and McSween, 1988). The petrologic types are denoted by the numbers 1 through 6, and criteria for classifying the chondrite petrologic type have been compiled by Van Schmus and Wood (1967), and later modified by Sears and Dodd (1988) and Brearley and Jones (1998) (Fig. 1.5).

Chondrites classified as petrologic type 3 are referred to as unequilibrated chondrites as they have retained their original composition and textures obtained during accretion; they have not been subject to major secondary alteration. Subtle progressive metamorphism can occur among the type 3 chondrites, in which the petrologic type 3 is further subdivided into 3.0 to 3.9 to signify the extent of metamorphism (Brearley and Jones, 1998). The subtle metamorphism that weakly alters the type 3 parent body occurs between 400°C and 600°C (Dodd, 1981; McSween, 1999). Petrologic type 3 specimens occur in all the chondrite groups, except for the CI, CM, and CR chondrites (Fig. 1.1).

Chondrites that have been subject to higher degrees of metamorphism are referred to as equilibrated chondrites and are classified by the petrologic types 4 to 6; these petrologic types represent different degrees of secondary metamorphic heating. The temperature conditions which these different degrees of metamorphism occur are 600 – 700°C (type 4), 700°C – 750°C (type 5), and 750°C – 950°C (type 6) (Dodd, 1981; McSween, 1999). Equilibrated petrologic types 4 to 6 are most commonly associated with the OCs and ECs, however, a few CCs can also undergo metamorphic equilibration (Fig. 1.1; type 4 only: CO and CV; type 4-6: CK). As the degree of metamorphism increases in the equilibrated chondrites, primary compositions and textures are erased; olivine and pyroxene compositions become more homogeneous, the matrix coarsens, and chondrules disappear (Fig. 1.5). Plausible heating mechanisms that could generate metamorphism on the chondrite parent body include the

decay of ^{26}Al (Lee et al., 1976; Grimm and McSween, 1993), collisional heating (Rubin, 1995) and magnetic induction caused by magnetic fields and primordial solar winds (Sonett, 1971).

Chondrites which have undergone aqueous alteration are classified as petrologic types 1 or 2. Petrologic type 1 chondrites have been aqueously altered to a greater extent than type 2, evident by the amount of water present (Fig. 1.5). Aqueous alteration is a low temperature process (<125°C; Bunch and Chang, 1980; McSween, 1999; Guo and Eiler, 2007) that is typically associated with the CCs (specifically CI, CM, and CR; Fig. 1.1), and is determined by the abundance of phyllosilicates present. The phyllosilicates present in CCs were formed on the asteroid parent body from the interaction of liquid water with mafic silicates (i.e., olivine and pyroxene). Prior to the formation of the CCs, water existed in the vapour phase between 5 and 30 AU (Boss and Ciesla, 2014). It is believed that this water vapour later re-condensed into water ice (Lunine et al., 1991) and accreted into the CC parent bodies. How water ice became liquid necessary for aqueous alteration is heavily debated, but the mechanisms proposed are similar to the heating mechanisms for the equilibrated chondrites: short-lived radionuclide decay (Zolensky and McSween, 1988; Grimm and McSween, 1993); impacts on the parent body (Lange et al., 1985); and magnetic induction (Sonett, 1971). Despite the similarity in heating mechanisms between metamorphosed and aqueously altered chondrites, the ice present in the parent bodies acts as a thermal buffer causing low-temperature aqueous alteration instead of metamorphism (Grimm and McSween, 1993).

1.2.2 Weathering and Shock

Additional alteration or modification processes that may occur in the chondrite meteorites are terrestrial weathering and shock metamorphism; not all chondrites are affected by these processes. Meteorites that sit exposed on Earth's surface are subject to terrestrial weathering in varying degrees (e.g., Zurfluh et al., 2016) depending on how long the meteorite has sat exposed; terrestrial weathering is most evident in meteorite finds (vs. falls). Terrestrial weathering can form rust on/within the chondrite due to oxidation of metal and sulphides and may even produce new mineral phases (Zurfluh et al., 2016). Shock metamorphism is a type of alteration that results from impacts on the chondrite body. The extent of shock metamorphism

can be classified based on the changes seen in the textures and mineralogy of olivine, orthopyroxene, and plagioclase grains (Fig. 1.6).

Criterion	*Petrologic type*					
	1	*2*	*3*	*4*	*5*	*6*
Homogeneity of olivine and low-Ca pyroxene compositions		>5% mean deviations		<5%	Homogeneous	
Structural state of low-Ca pyroxene		Predominantly monoclinic		>20% monoclinic	<20% monoclinic	Orthorhombic
Feldspar		Minor primary grains only		Secondary, <2 μm grains	Secondary, 2–50 μm grains	Secondary, >50 μm grains
Chondrule glass		Altered, mostly absent[a]	Clear, isotropic, variable abundance		Devitrified, absent	
Maximum Ni in metal		<20 wt%; taenite minor or absent	>20 wt% kamacite and taenite in exsolution relationship			
Mean Ni in sulfides		>0.5 wt%	<0.5 wt%	<0.5 wt%	<0.5 wt%	<0.5 wt%
Matrix	All fine-grained, opaque	Mostly fine, opaque	Clastic, minor opaque	Transparent, recrystallized coarsening from 4 to 6		
Chondrule–matrix integration	No chondrules	Chondrules very sharply defined		Chondrules well defined	Chondrules readily delineated	Chondrules poorly defined
Carbon (wt%)	3–5	0.8–2.6	<1.5	<1.5	<1.5	<1.5
Water (wt%)	18–22	2–16	0.3–3			<1.5

Fig. 1.5. A summary of the criteria used for classifying the petrologic type of chondrites. [from Krot et al., 2014]

Shock stage	*Description*	*Effect resulting from equilibration peak shock pressure*			*Shock pressure (GPa)*[a]
		Olivine	Plagioclase	Orthopyroxene	
S1	Unshocked		*Sharp optical extinction*, irregular fractures		<4–5
S2	Very weakly shocked	*Undulatory extinction*, irregular fractures	*Undulatory extinction*, irregular fractures	*Undulatory extinction*, irregular and some planar fractures	5–10
S3	Weakly shocked	*Planar fractures*, undulatory extinction, irregular fractures	Undulatory extinction	*Clinoenstatite lamellae on (100)*, undulatory extinction, planar and irregular fractures	15–20
S4	Moderately shocked	*Weak mosaicism*, planar fractures	Undulatory extinction, partially isotropic, planar deformation features		30–35
S5	Strongly shocked	*Strong mosaicism*, planar fractures, planar deformation fractures	*Maskelynite*		45–55
S6	Very strongly shocked	*Solid-state recrystallization* and staining, ringwoodite, melting	Shock melted (normal glass)	*Majorite, melting*	75–90
	Shock melted	Whole-rock melting (impact-melt rocks and melt breccias)			

Fig. 1.6. A summary of the criteria used for determining the shock stage of chondrites. [from Krot et al., 2014]

In this thesis, I assess the economic potential of asteroids by studying PGE and water contents in chondrite meteorites as asteroid analogues. The OCs contain Fe-Ni metal suitable for PGE extraction, while CCs contain the most water compared to other meteorites. PGE concentrations in the Fe-Ni metal phases of OCs were analyzed *in situ* using laser ablation inductively coupled plasma mass spectrometry (LA-ICP-MS) (Chapter 2). Water abundances were determined among different specimens of the unique Tagish Lake CC – which are aqueously altered to different degrees (Herd et al., 2011; Blinova et al., 2014) – using thermogravimetric analysis (TGA) and transmission infrared (IR) spectroscopy (Chapter 3). Chapters 2 and 3 are written independent of asteroid mining to address primary research questions such as the origin of metal in OCs and whether TGA and IR spectroscopy are suitable methods for determining the extent of aqueous alteration in Tagish Lake. The implications these two studies have for asteroid mining are summarized in Chapter 4.

Chapter 2. In Situ Analysis of Platinum Group Elements in Equilibrated Ordinary Chondrite Kamacite and Taenite

2.1 Introduction

Platinum group elements (PGEs) are relatively abundant in extraterrestrial Fe-Ni metal due to their highly siderophile nature. The distribution of PGEs in Fe-Ni metal found in various meteorites has offered insight into diverse planetary science investigations, including: constraining early solar system processes with Re-Os isotope systematics (Chen et al., 1998; Humayun and Campbell, 2000; Walker et al., 2002; Horan et al., 2009); planetary accretion and core formation processes (Kelly and Larimer, 1977; Petaev and Jacobsen, 2004; Day et al., 2007; Righter et al., 2008; Brenan and McDonough, 2009; Walker, 2009); identification of impact projectiles (Palme, 1982; Schmidt et al., 1997; Tagle and Berlin, 2008); and origins of ordinary chondrite metal (Grossman and Wasson, 1985; Kong and Ebihara, 1997; Kong et al., 1998; Meftah et al., 2016). Given that PGE concentrations are relatively low on Earth, there is also interest in the economic development of asteroids to mine these elements (e.g., Kargel, 1994; Elvis, 2014).

Due to their undifferentiated nature, ordinary chondrites provide insights into the processes that occurred in the early solar system, such as metal-silicate fractionation and formation of chondritic metal. Ordinary chondrites are distinguished into three chemical groups based on the proportion of metal to silicates and total Fe content: H chondrites (high metal and high total Fe), L chondrites (low metal and low total Fe), and LL chondrites (low metal relative to total Fe and low total Fe). The major metal phases in ordinary chondrites are dominantly comprised of two major Fe-Ni alloys known as kamacite (low Ni metal phase) and taenite (high Ni metal phase). These two Fe-Ni alloys have different crystal structures where kamacite is body-centered cubic and taenite is face-centered cubic (Wood, 1967). In general, kamacite is most abundant in H chondrites and decreases systematically throughout the ordinary chondrites (H > L > LL), whereas taenite abundances follow an opposite trend: H < L < LL (Afiattalab and Wasson, 1980; Smith et al., 1993; Brearley and Jones, 1998).

Several studies of PGE concentrations in ordinary chondrite metal have been completed using bulk metal analyses (Nichiporuk and Brown, 1965; Rambaldi 1976, 1977a, 1977b; Yongheng et al., 1992; Kong et al., 1995a,b; Kong and Ebihara, 1996, 1997; Horan et al., 2009).

The bulk metal studies in which a suite of ordinary chondrites have been analyzed (e.g., Rambaldi 1976, 1977a, 1977b; Kong and Ebihara, 1997) suggest that PGE concentrations in bulk metal vary between the three ordinary chondrite groups in the order H < L < LL. The PGE variations among the ordinary chondrites have been attributed to fractionation processes, primary formation conditions, and/or secondary metamorphic processes (Rambaldi, 1977b; Rambaldi et al., 1978; Kong and Ebihara, 1997). However, insights from bulk metal analysis is limited as this method is not able to determine PGE and other trace element concentrations in individual metal grains. Therefore, the previous ordinary chondrite bulk metal studies are not able to address whether fractionation occurs between kamacite and taenite, the extent to which the metal phases equilibrate during metamorphism, or if individual kamacite and taenite PGE concentrations are characteristic of each ordinary chondrite group as seen with olivine (fayalite) and low-Ca pyroxene (ferrosilite) compositions. The Rambaldi (1976, 1977a, 1977b) studies, however, hold merit above traditional bulk metal studies as they involved the analysis of separated metallic fractions, which revealed that PGE concentrations do vary among the different metallic fractions within individual ordinary chondrites. Rambaldi attributed these variations to preferential concentration of kamacite in the coarse metallic fraction and taenite in fine and intermediate metallic fractions. However, the extent to which kamacite and taenite are concentrated in these metallic fractions is not clear.

The understanding of metal in ordinary chondrites can be improved on by investigating the behavior and distribution of PGEs among individual metal grains. Analysis of individual metal grains has been made possible through the utilization of *in situ* methods which provide more accurate and precise measurements than bulk metal analysis. *In situ* analysis of PGE concentrations in ordinary chondrite metal has been completed by handful of workers prior to this study (Hsu et al., 1998; Campbell and Humayun, 1999a; Humayun and Campbell, 2000, 2002; Campbell and Humayun, 2003; Meftah et al., 2016). These studies have provided insight into a range of investigations such as trace element analyses, metal origins, and fractionation of PGEs. However, the findings of these studies are limited as most do not report the results for all six PGEs, and only a select few ordinary chondrites have been studied in these investigations. Here I report on the application of laser ablation inductively coupled plasma mass spectrometry (LA-ICP-MS) to determine all PGE concentrations in kamacite and taenite grains in a suite of equilibrated ordinary chondrites (EOCs) of varying group and petrologic type. While these *in situ* results are comparable to those from previous bulk metal analyses,

notable differences are observed. The *in situ* results also reveal significant inter- and intra-grain variability, providing insights into nebular and parent body processes.

2.2 Samples and Methodology

2.2.1 Samples

A representative suite of 14 EOCs were chosen, covering the range of ordinary chondrite groups and petrologic types (Table 2.1). Of these 14 meteorite samples, 10 were obtained from the University of Alberta Meteorite Collection and the remaining four were received on loan from the Meteorite Collection of the Smithsonian National Museum of Natural History. All samples used for analysis were epoxy-mounted specimens, except Buzzard Coulee, Dalgety Downs, and NWA 6204 which were polished thin sections. NWA 6204 (L4-6) is a polymict breccia; however, only metal in the L4 matrix was targeted for analysis. For this reason results from NWA 6204 will be considered representative of an L4. The relatively small number of LL specimens is due to the overall lower abundance of metal in LL chondrites, limiting the number of suitable metal grains for *in situ* analysis. Bjurböle and Knyahinya were originally selected to be representative of the L chondrites; however, these meteorites have geochemical properties that are intermediate between L and LL chondrites (Tandon and Wasson, 1968; Chou and Cohen, 1973; Rambaldi 1976; Rambaldi, 1977a; Kallemeyn et al., 1989). As such, they are representative of the intermediate L/LL chondrite group. PGE concentrations in kamacite were determined in all specimens except for Olivenza; only taenite grains were large enough for analysis in Olivenza. PGE concentrations in taenite were also acquired for Bruderheim, Benares (a), and St. Séverin.

Table 2.1. Equilibrated ordinary chondrite specimens used for PGE trace element analysis.

H Chondrites	Buzzard Coulee **[H4]** (MET11616/1/1/TEP1) Forest Vale **[H4]*** (USNM 2319) Richardton **[H5]** (MET6641) Estacado **[H6]** (MET7113) Kernouve **[H6]** (MET11514/EP)
L Chondrites	Dalgety Downs **[L4]** (MET5257/TEP) NWA 6204 **[L4-6]** (MET11631/1/TEP1) Bruderheim **[L6]** (MET4270/EP-12) Leedey **[L6]*** (USNM 6867)
LL Chondrites	Benares (a) **[LL4]** (MET11540/EP378) Olivenza **[LL5]***(USNM 758) St. Séverin **[LL6]***(USNM 2608)
L/LL Chondrites	Bjurböle **[L/LL4]** (MET10903/EP375) Knyahinya **[L/LL5]** (MET11538/EP371)

* Specimens provided by the Smithsonian National Museum of Natural History. All other specimens are from the University of Alberta Meteorite Collection. Provided with the meteorite name is its classification and specimen number.

2.2.2 Methodology

A New Wave UP213 laser ablation system connected to a Thermo Scientific iCAP Q ICP-MS at the University of Alberta (UAlberta) was used for LA-ICP-MS analysis of kamacite and taenite metal grains. PGE isotopes targeted during analysis were ^{102}Ru, ^{103}Rh, ^{106}Pd, ^{192}Os, ^{193}Ir, and ^{195}Pt; however, results for other trace metal isotopes were also acquired (^{63}Cu, ^{69}Ga, ^{75}As, ^{184}W, ^{187}Re, and ^{197}Au). The isotopes selected for analysis were chosen based on their abundances (i.e., most abundant isotope) and limited interference with other elemental isotopes. All data acquisition and processing was completed using Iolite software. Analytical parameters consisted of a frequency of 5 Hz, a spot size of 40 µm, and a fluence of 10-12 J/cm^2. Utilizing a spot size smaller than 40 µm would have affected the number of counts collected during analysis (i.e., less material being ablated). The internal standard element chosen for

analysis was ^{60}Ni and analysis was completed using He as a gas carrier. The acquisition duration for each spot analysis was a total of 60 seconds: 20 seconds background time followed by a 10 second delay and 30 seconds of analysis. All samples were run using the North Chile (Filomena) iron meteorite as an internal metal standard. North Chile is a hexahedrite iron meteorite; as such, its mineralogy is predominantly kamacite. Details on the establishment of North Chile as an internal standard are provided in Appendix A1.1. A plot of Pd, Os, and Ir in North Chile kamacite obtained during each LA-ICP-MS session in this study is shown in Fig. 2.1, along with accepted values for these elements from Campbell and Humayun (1999b; also obtained by LA-ICP-MS). The North Chile *in situ* concentrations show reproducibility between different analytical sessions and are in good agreement with the accepted values. The overall mean concentrations of all PGE concentrations obtained from North Chile are provided in Table 2.2. The comparability of this study's results with the accepted values demonstrates that North Chile is a good standard and therefore places confidence in the PGE concentrations obtained in this study. The possibility of a nugget effect influencing the LA-ICP-MS results for both North Chile and the ordinary chondrites is obviated by the fact that no unusual peaks were seen in the analytical signals. Furthermore, if a nugget effect did exist, it would likely be small (i.e., sub-micrometer scale) relative to the 40 µm spot size used for LA-ICP-MS analysis.

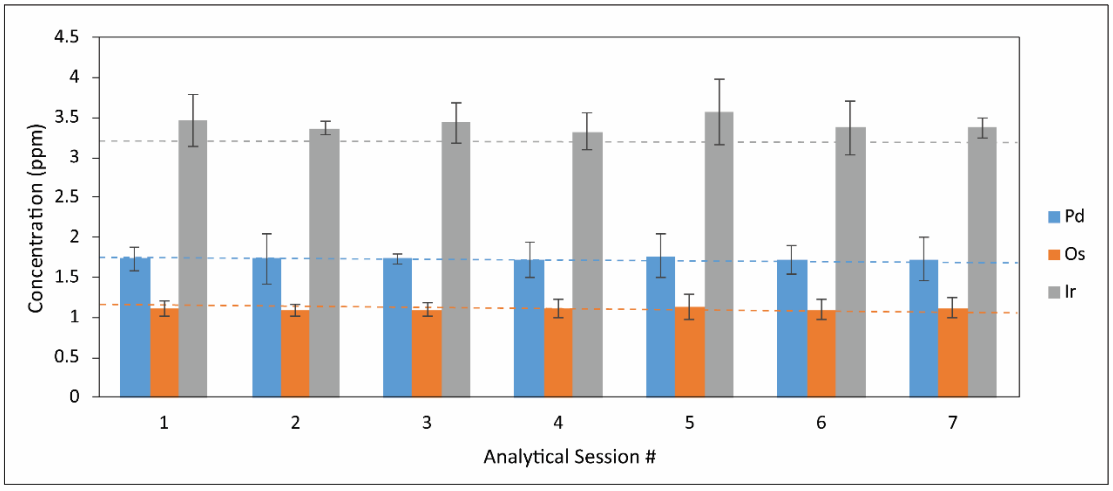

Fig. 2.1. Mean concentrations of Pd, Os, and Ir in North Chile from different LA-ICP-MS analytical sessions conducted during this study. Error bars are one standard deviation from the mean. The horizontal dashed lines of the same corresponding colour are the accepted North Chile values of Pd, Os, and Ir after Campbell and Humayun (1999b).

Table 2.2. Comparison of LA-ICP-MS results of North Chile from this study (n = 77) and Campbell and Humayun (1999b).

PGE	This Study	stdev	Campbell and Humayun (1999b)	error
Ru	15.31	0.97	15.20	0.80
Rh	2.87	0.20	2.86	0.13
Pd	1.72	0.20	1.72	0.15
Os	1.10	0.11	1.09	0.08
Ir	3.39	0.26	3.22	0.21
Pt	20.72	1.72	21.28	1.20

Prior to LA-ICP-MS, backscattered electron (BSE) images were obtained using a Zeiss EVO MA 15 scanning electron microscope (SEM) with a LaB_6 crystal source equipped with a Bruker Silicon Drift Detector for energy dispersive X-ray (EDX) analysis (UAlberta). BSE images were compiled into maps to help identify metal grains in each specimen suitable for analysis based on general metal texture and size, as well as to assist with navigation and locating metal grains during other analyses. Ideal metal grains for LA-ICP-MS analysis were free of inclusions and exsolution, and grains next to troilite were avoided whenever possible. In some cases (e.g., Knyahinya, Olivenza), analysis of exsolved grains was necessary, but care was taken to avoid the exsolution during LA-ICP-MS by ensuring the analytical spot location did not target the exsolved areas. Reflected light microscopy was also used for identifying suitable metal targets for LA-ICP-MS and distinguishing between kamacite and taenite grains. In some cases, it was difficult to differentiate between kamacite and taenite under reflected light, as well as identify the presence of any exsolved grains. To overcome these difficulties, electron probe microanalysis (EPMA) was utilized to gather more detailed images (backscattered electron and secondary electron) and compositional information of the individual metal grain targets.

A JEOL 8900 electron microprobe (UAlberta) under operating conditions of 20 kV acceleration voltage and a 50 nA beam current was used to confirm the identity of the Fe-Ni phase of the selected metal grains and to determine Fe, Ni, and Co concentrations. Pure Fe, Ni, and Co metal standards were used for analysis. The Ni concentrations obtained from EPMA were used to normalize the LA-ICP-MS ^{60}Ni internal standard concentrations. The spots analyzed during EPMA were the same spots targeted for LA-ICP-MS. In some cases, the concentrations of Ni obtained on certain spots by EPMA were averaged for the purpose of normalization of ^{60}Ni due to the relatively larger spot size of the laser. Backscattered and

secondary electron images obtained during EPMA were useful in selecting suitable spot locations for LA-ICP-MS analysis and avoiding grains that were strongly exsolved.

In addition to *in situ* LA-ICP-MS analysis, metal separates of Bruderheim were analyzed by solution ICP-MS analysis to compare *in situ* results with bulk metal results obtained from the same meteorite. Approximately 400 mg of a sample of magnetically-separated Bruderheim (UAlberta Meteorite Collection specimen MET4270/B-74c2/p17) and a 450 mg piece of the North Chile standard were each dissolved in an HF-HCl-HNO_3 solution (refer to Appendix A1.1 for a detailed description of the solution ICP-MS method). Although HF and HNO_3 will dissolve trace silicates, this is not a concern for analysis given that the PGEs are not abundant in silicates (Rambaldi et al., 1978; Horan et al., 2009). North Chile was used as a secondary standard for the Bruderheim analysis. The solutions were analyzed using a PerkinElmer Elan 6000 mass spectrometer (UAlberta) for the same elements analyzed in LA-ICP-MS.

2.3 Results

2.3.1 Kamacite and Taenite LA-ICP-MS

In situ kamacite and taenite results from this study are presented in Tables 2.3 and 2.4, respectively, and the mean results for the three equilibrated petrologic types (4, 5, and 6) are illustrated in Figures 2.2, 2.3, and 2.4. Mean kamacite Ni and Co concentrations are consistent with the reported trends of Ni and Co in ordinary chondrite kamacite (Sears and Axon, 1975; Afiattalab and Wasson, 1980; Rubin 1990): specifically, Ni decreases and Co increases from H to LL chondrites (Table 2.3). The results show an overall agreement in PGE concentrations, within uncertainty, between H and L chondrite kamacite grains (Table 2.3). Average PGE concentrations were not calculated for LL chondrite kamacite in Table 2.3 given the discrepancy in results between Benares(a) and St. Séverin. Benares(a) kamacite PGE results are comparable to the mean kamacite PGE concentrations of the H and L chondrites from this study; however, St. Séverin PGE concentrations (except Pd) are higher relative to all other EOC kamacite results. The kamacite PGE concentrations in the L/LL chondrites are also comparable, within uncertainty, to H and L chondrite PGE concentrations.

Table 2.3. Kamacite metal trace element concentrations (ppm, unless otherwise stated) obtained from LA-ICP-MS analysis.

Meteorite	Type	n	Fe (wt.%)	Ni (wt.%)	Co (wt.%)	Cu	Ga	As	Ru	Rh	Pd	W	Re	Os	Ir	Pt	Au
Buzzard Coulee	H4	18	92.3(0.5)	6.81(0.05)	0.49(0.02)	106(6)	11(1)	30(16)	2.0(0.3)	0.60(0.13)	2.6(0.3)	0.86(0.07)	0.20(0.02)	1.4(0.2)	1.3(0.1)	2.7(0.3)	1.07(0.18)
Forest Vale	H4	18	92.6(0.2)	6.80(0.13)	0.50(0.02)	210(244)	16(1)	13(1)	3.6(0.8)	1.1(0.3)	3.0(0.3)	0.82(0.10)	0.31(0.11)	2.3(0.5)	2.3(0.7)	4.9(1.4)	1.00(0.08)
Richardton	H5	21	93.1(0.7)	6.35(0.59)	0.48(0.01)	115(19)	9(1)	11(2)	2.9(0.7)	0.74(0.16)	2.5(0.5)	0.82(0.11)	0.27(0.07)	2.0(0.7)	1.9(0.6)	3.5(0.8)	1.00(0.17)
Estacado	H6	22	92.9(0.5)	6.32(0.31)	0.50(0.01)	89(10)	11(1)	12(1)	3.8(0.2)	1.1(0.1)	2.8(0.4)	0.96(0.12)	0.37(0.06)	3.1(0.4)	2.6(0.3)	5.0(0.3)	1.06(0.10)
Kernouve	H6	28	92.8(0.4)	6.41(0.22)	0.50(0.01)	92(13)	10(1)	13(1)	4.0(0.5)	1.1(0.1)	2.9(0.4)	0.99(0.10)	0.40(0.05)	2.8(0.3)	2.6(0.3)	5.1(0.5)	1.06(0.14)
Average H	**–**	**–**	**92.8(0.5)**	**6.51(0.38)**	**0.49(0.02)**	**118(108)**	**11(2)**	**15(9)**	**3.3(0.9)**	**0.95(0.26)**	**2.7(0.4)**	**0.90(0.13)**	**0.32(0.10)**	**2.4(0.7)**	**2.2(0.7)**	**4.3(1.2)**	**1.04(0.14)**
Dalgety Downs	L4	15	92.0(0.3)	6.69(0.17)	0.82(0.06)	84(9)	7(9)	10(2)	3.2(1.2)	1.2(0.5)	3.2(0.4)	1.3(0.1)	0.44(0.24)	2.6(1.5)	2.5(1.5)	5.0(2.5)	1.05(0.14)
NWA 6204	L4-6*	8	92.8(0.9)	6.13(1.02)	0.81(0.05)	118(39)	5(2)	11(3)	3.1(2.8)	0.85(0.61)	3.0(0.4)	0.82(0.52)	0.36(0.30)	2.3(2.2)	2.1(2.3)	4.7(3.8)	1.15(0.15)
Leedey	L6	23	92.9(0.4)	6.39(0.22)	0.79(0.07)	77(9)	5.6(0.4)	20(2)	3.3(0.6)	1.0(0.4)	2.9(0.4)	1.3(0.1)	0.38(0.13)	2.7(1.0)	2.5(0.9)	4.4(1.3)	1.22(0.31)
Bruderheim	L6	19	92.3(0.8)	5.94(0.77)	0.87(0.05)	75(11)	4.9(0.7)	18(3)	1.8(0.8)	0.63(0.24)	2.4(0.7)	1.3(0.3)	0.16(0.07)	0.94(0.35)	0.84(0.39)	2.0(1.3)	1.13(0.60)
Average L	**–**	**–**	**92.5(0.7)**	**6.31(0.61)**	**0.82(0.07)**	**83(21)**	**6(5)**	**16(5)**	**2.9(1.4)**	**0.93(0.44)**	**2.8(0.6)**	**1.2(0.3)**	**0.33(0.21)**	**2.2(1.4)**	**2.0(1.4)**	**4.0(2.3)**	**1.15(0.36)**
Benares(a)	LL4	22	92.9(0.4)	6.26(0.32)	0.92(0.11)	81(9)	6(1)	24(2)	3.4(0.8)	1.1(0.2)	3.3(0.5)	1.4(0.2)	0.38(0.12)	2.6(0.9)	2.3(0.9)	4.7(1.5)	1.13(0.10)
St. Séverin	LL6	7	91.7(0.2)	5.27(0.10)	3.03(0.15)	66(35)	0.37(0.51)	55(9)	10.8(1.8)	3.9(0.7)	1.4(0.2)	0.04(0.04)+	1.6(0.2)	9.2(2.0)	9.4(2.4)	16.3(3.5)	0.53(0.08)
Average LL	**–**	**–**	**92.6(0.6)**	**6.02(0.52)**	**1.43(0.93)**	**–**	**–**	**–**	**–**	**–**	**–**	**–**	**–**	**–**	**–**	**–**	**–**
Bjurböle	L/LL4	17	92.3(0.3)	6.38(0.29)	1.38(0.06)	77(9)	2.1(0.4)	28(2)	2.8(1.1)	1.1(0.5)	2.5(0.4)	0.66(0.18)	0.49(0.17)	3.0(1.3)	2.7(1.0)	5.2(1.7)	0.90(0.19)
Knyahinya	L/LL5	17	91.9(0.2)	6.65(0.14)	1.19(0.06)	94(8)	3.7(0.4)	26(1)	2.7(1.4)	0.90(0.37)	2.7(0.3)	1.5(0.2)	0.41(0.20)	2.5(2.1)	2.6(2.4)	4.9(3.3)	1.10(0.14)
Average L/LL	**–**	**–**	**92.1(0.3)**	**6.51(0.26)**	**1.29(0.12)**	**85(12)**	**2.9(0.9)**	**27(2)**	**2.8(1.3)**	**1.0(0.42)**	**2.6(0.3)**	**1.1(0.5)**	**0.45(0.19)**	**2.8(1.8)**	**2.7(1.8)**	**5.1(2.6)**	**1.00(0.19)**

Standard deviations (1σ) of the mean are in parentheses. Fe, Ni, and Co wt.% values are averaged EPMA results corresponding to the targeted LA-ICP-MS spots.

n = Number of laser ablation spots targeted for each sample.

*Metal grains targeted in L4 matrix only.

+Two analyses of ^{184}W were below detection limit.

Table 2.4. Taenite metal trace element concentrations (ppm, unless otherwise stated) obtained from LA-ICP-MS analysis.

Meteorite	Type	n	Fe (wt.%)	Ni (wt.%)	Co (wt.%)	Cu	Ga	As	Ru	Rh	Pd	W	Re	Os	Ir	Pt	Au
Bruderheim*	L6	5	79.9(5.0)	19.9(5.1)	0.40(0.07)	860(305)	12(4)	12(3)	5.4(1.8)	1.4(0.4)	9.4(2.3)	1.2(0.3)	0.59(0.14)	4.1(1.3)	3.3(1.0)	6.9(1.6)	2.4(0.9)
BhT-1		1	72.1[0.2]	28.3[0.1]	0.29[0.02]	1370[180]	18[2]	15[2]	8.3[1.7]	2.0[0.4]	13[2]	1.8[0.3]	0.82[0.28]	6.0[0.9]	4.8[0.5]	9.4[1.7]	3.9[0.9]
Benares(a)	LL4	11	69.8(1.2)	29.9(1.4)	0.34(0.06)	1284(112)	20(4)	17(4)	13.2(4.3)	3.8(1.4)	12.9(1.2)	1.3(0.3)	1.1(0.4)	6.2(2.6)	5.6(2.3)	14.5(7.5)	3.1(0.8)
Olivenza	LL5	20	62.7(2.8)	36.2(2.9)	1.47(0.18)	1254(131)	27(5)	50(4)	9.6(2.1)	2.5(0.5)	16.0(1.4)	3.2(0.3)	1.1(0.3)	6.0(2.8)	6.0(2.6)	12.9(4.1)	5.0(0.3)
Saint-Séverin	LL6	8	64.0(4.1)	35.0(4.4)	1.10(0.28)	1301(163)	5(1)	43(2)	16.6(1.4)	4.6(0.4)	15.2(1.6)	1.6(0.9)	1.6(0.2)	10.1(1.3)	9.6(1.5)	21.5(2.0)	5.0(0.8)
Average LL	**–**	**–**	**65.0(4.1)**	**34.2(4.0)**	**1.08(0.52)**	**1272(131)**	**21(9)**	**39(15)**	**12.1(3.9)**	**3.3(1.2)**	**15.0(1.9)**	**2.3(1.0)**	**1.2(0.4)**	**6.9(3.0)**	**6.6(2.7)**	**15.1(5.9)**	**4.5(1.1)**

Standard deviations (1σ) of the mean are in parentheses. Fe, Ni, and Co wt.% values are averaged EPMA results corresponding to the targeted LA-ICP-MS spots.

n = Number of laser ablation spots targeted for each sample.

* Mean results of a single grain in Bruderheim which is likely plessite, not taenite.

BhT-1 is the singular result from the plessite grain targeted in Bruderheim (see text). Square brackets associated with the concentrations for BhT-1 are 2 times the internal standard error.

PGE concentrations in taenite were found to be higher than in kamacite (Table 2.4). This result is consistent with metal studies of both iron meteorites (e.g., Rasmussen et al., 1988; Campbell and Humayun, 1999b; Hsu et al., 2000; Mullane et al., 2004) and ordinary chondrites (Campbell and Humayun, 2003; Meftah et al., 2016) which demonstrate that PGEs preferentially partition into taenite. This preferential partitioning is controlled by the size and electron configuration of the PGEs as well as the crystal structures of kamacite and taenite (body-centered cubic vs. face-centered cubic) (Hsu et al., 2000); the size and electron configuration favor the taenite face-centered cubic structure. The ionic radius of the PGE main oxidation state has also been related to partitioning between kamacite and taenite (Meftah et al., 2016). This study shows consistently higher taenite PGE concentrations, but also significant variability (Table 2.4; Figs. 2.4, 2.5). Taenite in Bruderheim (Table 2.4) has lower PGE concentrations compared to the LL chondrites, as well as a lower mean Ni concentration (19.9 ± 5.1 wt.%). As taenite Ni concentrations are expected to be >25 wt.%, the most likely explanation is that plessite, a fine-grained mixture of kamacite and taenite reported to have Ni concentrations between ~10 wt.% and ~28 wt.% (Goldstein and Michael, 2006), was inadvertently analyzed instead of taenite in this case; previous studies have identified plessite as one of the metal phases present in Bruderheim (Wood, 1967; Smith and Launspach, 1991). The Bruderheim results listed in Table 2.4 were collected from a single metal grain targeted in five different locations; however, only one of these locations analyzed has a corresponding Ni concentration characteristic of taenite (28.3 wt.%). For the purposes of this study, the results associated with this single location (now referred to as BhT-1) are considered representative of L chondrite taenite, and are included in Table 2.4.

Mean *in situ* kamacite results for the equilibrated H and L petrologic types show that Rh and Pd are the least variable PGEs, while Pt appears to have the greatest variability (Figs. 2.2A, 2.3A, 2.5). PGE concentrations among H4 and H5 chondrites are similar; however, PGEs in the H6 chondrites appear to be enriched (Fig. 2.2A). L chondrites show an opposite trend to the H chondrites: L4 chondrite kamacite is more enriched in PGEs than L6 (Fig. 2.3A). Regardless, the results for all three petrologic types of H and L chondrites are within uncertainty of each other. L chondrites show a larger variability in PGE concentrations than H chondrites among their petrologic types, but the variability in both the H and L chondrites decreases with increasing petrologic type (Fig. 2.5). The depletion of PGEs (notably Os, Ir, and Pt) in the L6 chondrite results is attributable to the lower PGE concentrations in Bruderheim

(Table 2.3); if Bruderheim results are omitted, L6 concentrations (Leedey in this case) match better with the type 4 results (Fig. 2.3A).

As there is only one LL chondrite per petrologic type, each is considered representative of its type for the purposes of this study (Fig. 2.4A), although St. Séverin may not be the most suitable LL6 for this case (see section 2.3.4). The mean taenite PGE concentrations of the three LL chondrites are within uncertainty of each other; however, St. Séverin is enriched in PGEs, except for Pd, relative to the other two LL chondrites (Fig. 2.4A). *In situ* taenite PGE concentrations in LL chondrites behave similarly to the PGE trends seen in H chondrite kamacite (Fig. 2.2A): the LL4 and LL5 chondrites have similar PGE concentrations while there is an enrichment of PGEs in LL6. Despite the greater variability of PGE concentrations in taenite, the observed variability in the LL chondrites decreases with increasing petrologic type (Figs. 2.4A, 2.5), similar to what is observed in H and L chondrite kamacite.

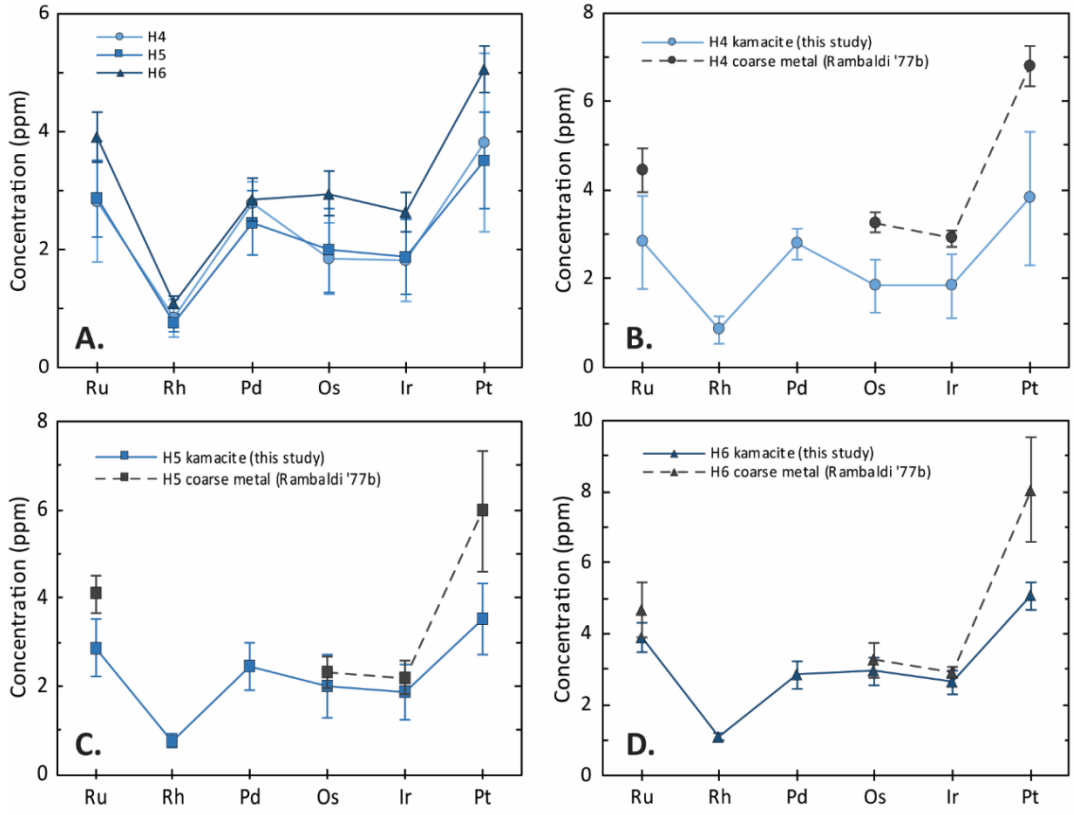

Fig. 2.2. Mean PGE concentrations in H chondrite kamacite metal. Error bars represent one standard deviation from the mean. **(A)** Average *in situ* concentrations of the three H chondrite types. **(B, C & D)** Each H chondrite petrologic type (this study) compared to the results of the H chondrite coarse grained metallic fraction (>100 mesh) from Rambaldi (1977b). Results from Rambaldi are averaged for comparison. In the case of the H5 chondrites (C), Richardton is the only available sample from this study to compare to the H5 Rambaldi results.

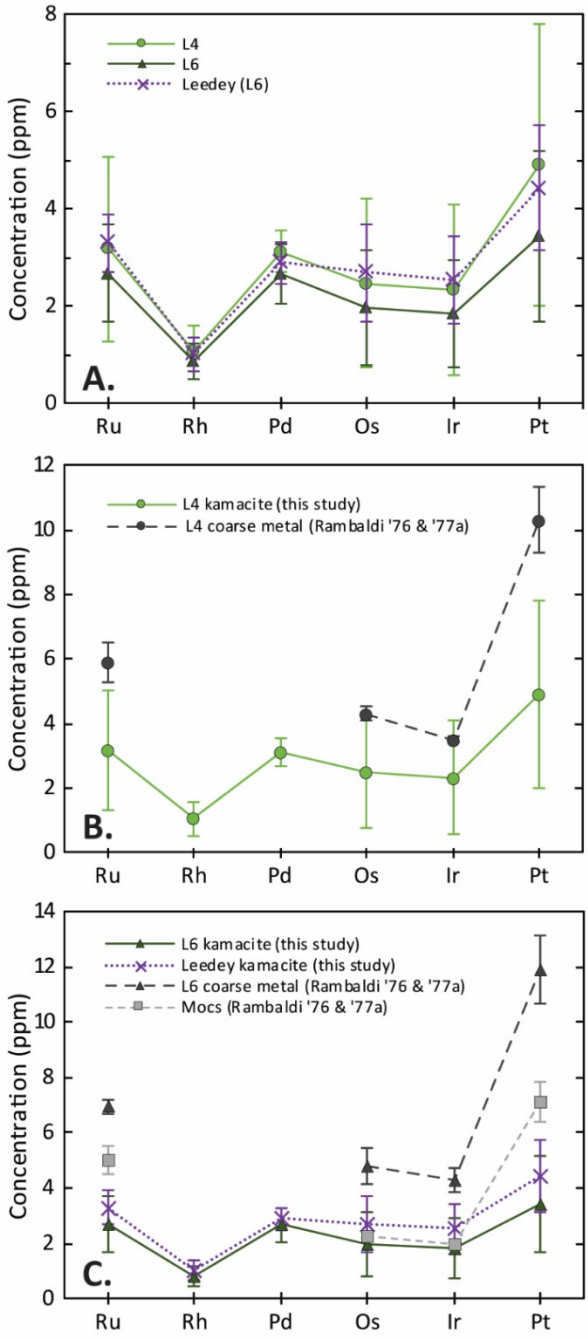

Fig. 2.3. Mean PGE concentrations in L chondrite kamacite metal. **(A)** Average *in situ* kamacite concentrations of L4 and L6 chondrites. Error bars represent one standard deviation from the mean. **(B)** L4 chondrite results (this study) compared to results of the L4 coarse metallic fraction (>100 mesh) from Rambaldi (1976, 1977a). Rambaldi results represent one L4 chondrite (Tennasilm) and the associated error bars are calculated from the precision of the instrumental neutron activation analysis (INAA) method for each element as specified in Rambaldi (1976, 1977a). **(C)** L6 chondrite results compared to Rambaldi (1976, 1977a; excluding Shaw) L6 coarse metallic fraction (>100 mesh). *In situ* results for Leedey (this study) and Rambaldi (1976, 1977a) results for the >>100 mesh metallic fraction of Mocs are also included for comparison (see text). All error bars are one standard deviation from the mean, except for Mocs which is calculated from the precision of INAA for each element.

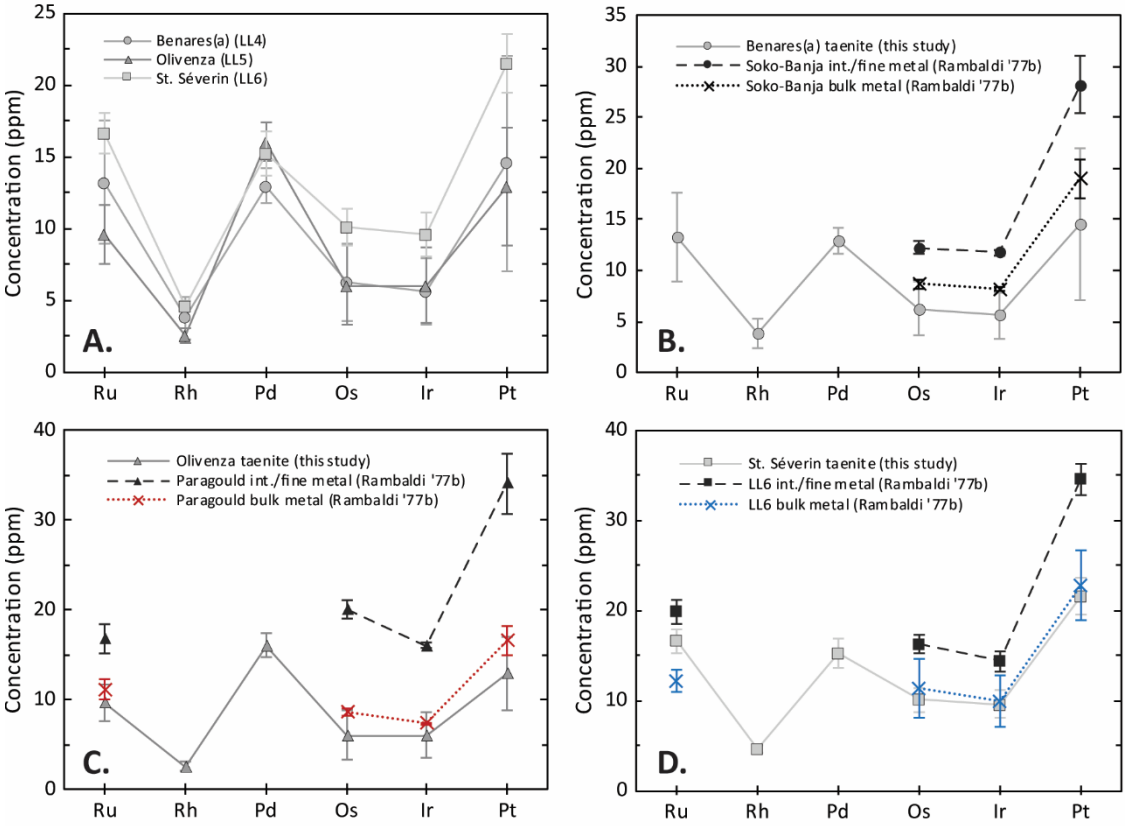

Fig. 2.4. Mean PGE concentrations in LL chondrite taenite metal. **(A)** Average *in situ* taenite concentrations of the three LL chondrites in this study: Benares(a), Olivenza, and St. Séverin. Error bars represent one standard deviation from the mean. **(B)** Benares(a) and **(C)** Olivenza compared to the intermediate and fine metallic fractions of LL chondrites from Rambaldi (1977b) of the same petrologic type (Soko-Banja LL4; Paragould LL5). The intermediate and fine metallic fractions have been added together in appropriate proportions to represent PGE concentrations associated with taenite (int./fine metal). Rambaldi (1977b) bulk metal concentrations are calculated from all three metallic fractions (coarse, intermediate, and fine). Error bars for Rambaldi int./fine. metal and bulk metal are calculated from the precision of the instrumental neutron activation analysis (INAA) method for each element. **(D)** St. Séverin compared to Rambaldi (1977b) LL6 chondrite (St. Séverin and Dhurmsala) intermediate/fine (int./fine) metallic fraction. LL6 bulk metal values are calculated (Rambaldi, 1977b). Error bars are one standard deviation from the mean.

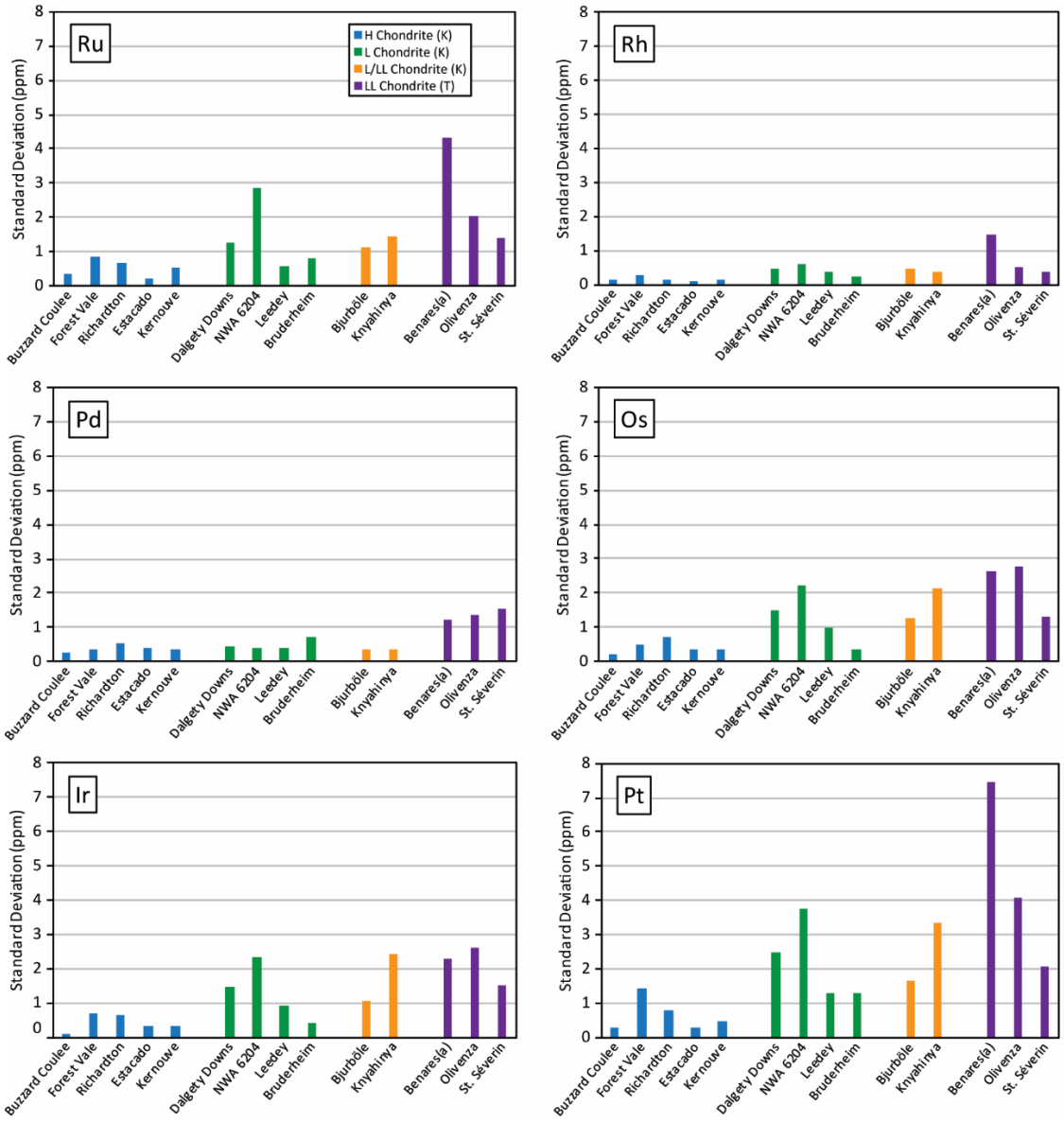

Fig. 2.5. Standard deviations of the mean PGE concentrations for ordinary chondrite kamacite (K) and taenite (T). The ordinary chondrites are ordered from left to right as least equilibrated (type 4) to most equilibrated (type 6) in each group. The standard deviations generally decrease with an increase in petrologic type as a result of less variability.

2.3.2 Bruderheim Bulk Metal ICP-MS

Bulk metal separates from Bruderheim were readily available in the UAlberta Meteorite Collection (MET4270/B-74c2/p17) from early studies of this meteorite (June 1961); therefore, metal separates from this sample were analyzed in addition to *in situ* metal grains. The metal separates are a magnetic fraction that were obtained using a +140 US sieve mesh. According to the UAlberta Meteorite Collection documentation, non-metallic minerals have been found to be embedded on some of the metal particles. Results of the bulk analysis via solution ICP-MS are provided in Table 2.5 and Fig. 2.6, along with *in situ* kamacite and taenite (BhT-1) results and L6 chondrite bulk metal literature values for comparison. These data are used to investigate how the PGEs are distributed in bulk metal concentrations by comparison to *in situ* results. Knowing that PGEs preferentially partition into taenite (e.g., Campbell and Humayun, 1999b; Campbell and Humayun, 2003), it is inferred that the PGE concentrations of the bulk metal will reflect the amount of taenite present. It is expected that Bruderheim's bulk metal composition would fall between the *in situ* kamacite and taenite compositions given that kamacite is the more abundant metal phase in L chondrites (Afiattalab and Wasson, 1980; Kong and Ebihara, 1996; Smith et al., 1993). To test this, bulk metal concentrations for Bruderheim were calculated from the *in situ* kamacite and taenite compositions (Table 2.5; Fig. 2.6) based on the average of known fractions of kamacite and taenite in L6 chondrites (Kong and Ebihara, 1996; Smith et al., 1993). As expected, calculated bulk metal concentrations fall between the *in situ* kamacite and taenite concentrations, closest to the concentrations from kamacite, the more abundant metal phase (Fig. 2.6).

Accordingly, solution ICP-MS Fe, Ni, and Co concentrations are intermediate between the *in situ* kamacite and taenite concentrations (Table 2.5). In terms of PGEs, Fig. 2.6 reveals that solution ICP-MS Pd and Os concentrations also fall between *in situ* kamacite and taenite results, and are comparable to the calculated bulk metal values, within uncertainty. However, the solution ICP-MS Ru, Ir, and Pt concentrations do not behave as expected: Ru is comparable to the *in situ* taenite results, whereas Ir and Pt are more enriched than in *in situ* taenite, although concentrations overlap when uncertainties are considered (Fig. 2.6). All other elements measured by solution ICP-MS have concentrations that fall between the two *in situ* results, except for As and W which are prone to contamination (Fig. 2.6; Table 2.5). The solution ICP-MS results compare quite well with L6 bulk metal concentrations from Rambaldi

Table 2.5. Laser ablation (LA) and solution ICP-MS results for Bruderheim metal.

	LA-ICP-MS		Bulk Metal		L6 Bulk Metal Studies	
	Kamacite	Taenite*	Solution ICP-MS	Calculated	Rambaldi (1976, 1977a)	Kong and Ebihara (1997)
Fe (wt%)	92.3(0.8)	72.1[0.2]	80.0(6.6)	86.4(1.9)	85.4(0.7)	85.1(5.9)
Ni (wt%)	5.94(0.77)	28.3[0.1]	13.7(2.1)	12.4(1.5)	13.8(0.7)	13.5(5.0)
Co (wt%)	0.87(0.05)	0.29[0.02]	0.54(0.10)	0.70(0.08)	0.69(0.05)	0.61(0.11)
Cu	75(11)	1370[180]	799(204)	450(48)	627(140)	1083(646)
Ga	4.9(0.7)	18[2]	15(2)	8.6(2.8)	13(2)	11.6
As	18(3)	15[2]	6.6(0.1)	17(3)	19(2)	16.7(0.1)
Ru	1.8(0.8)	8.3[1.7]	9(2)	3.7(1.3)	7.9(0.2)	5.88
Rh	0.63(0.24)	2.0[0.4]	-	1.0(0.4)	-	1.45(0.03)
Pd	2.4(0.7)	13[2]	7(1)	5.4(1.0)	-	5.69
W	1.3(0.3)	1.8[0.3]	2.5(0.1)	1.4(0.4)	1.3(0.1)	1.09
Re	0.16(0.07)	0.82[0.28]	0.7(0.1)	0.35(0.13)	0.63(0.01)	0.57(0.08)
Os	0.94(0.35)	6.0[0.9]	1.7(0.4)	2.4(1.0)	6.0(0.3)	4.9(0.2)
Ir	0.84(0.39)	4.8[0.5]	6(1)	2.0(0.9)	5.2(0.2)	4.6(0.1)
Pt	2.0(1.3)	9.4[1.7]	13(3)	4.2(2.0)	13.8(0.2)	10(2)
Au	1.13(0.60)	3.9[0.9]	-	1.9(0.7)	1.69(0.05)	1.8(0.3)

*BhT-1

Standard deviations (1σ) of the mean are in parentheses except for the taenite (BhT-1) results which are 2 times the internal standard error represented by square brackets. Considering there was only one taenite result (BhT-1) available for the bulk metal calculations, the error contributed by the taenite phase was assumed to be the same as the relative error for the LL chondrite taenite results (equivalent to the standard deviation of the mean); an exception to this is Fe, Ni, and Co errors which were determined by counting statistics. In some cases, standard deviations were unable to be determined from the literature data given that only one result was reported (e.g., Kong and Ebihara, 1997).

(1976, 1977a) and Kong and Ebihara (1997), with only a few elements (As, W, Os) not in agreement nor within uncertainty (Table 2.5). It is important to note that the use of HCl-HNO_3 in the Bruderheim solution will cause Os to become volatile where it can become lost into the fumehood (R. Creaser, pers. comm.). Compared to the calculated bulk metal concentrations, only a few of the solution ICP-MS results are in agreement within error: Fe, Ni, Co, Pd, and Os. Despite the discrepancies between solution ICP-MS and calculated bulk metal concentrations, there is a reasonable agreement between the calculated bulk metal values and the accepted literature values, except for the notable differences between Os, Ir, and Pt (Table 2.5). This discrepancy in Os, Ir, and Pt concentrations along with the discrepancy between the calculated bulk metal and solution ICP-MS concentrations (e.g., Ru, Ir, Pt) indicates that the calculated bulk metal concentrations for Bruderheim are not accurate. Given the confidence in the *in situ* kamacite results used in the bulk metal calculations (based

on the large number of analyses collected; n = 19), it is therefore possible that the BhT-1 results are not representative of taenite concentrations in Bruderheim. It is predicted that if representative taenite results (i.e., multiple targets) for Bruderheim were to be acquired, they would provide calculated bulk values more comparable to solution ICP-MS results. Alternatively, if Pt and Ir are alloys in the metal, it may be difficult to dissolve these elements in an HCl-HNO3 solution which may have affected the solution results (R. Creaser, pers. comm.).

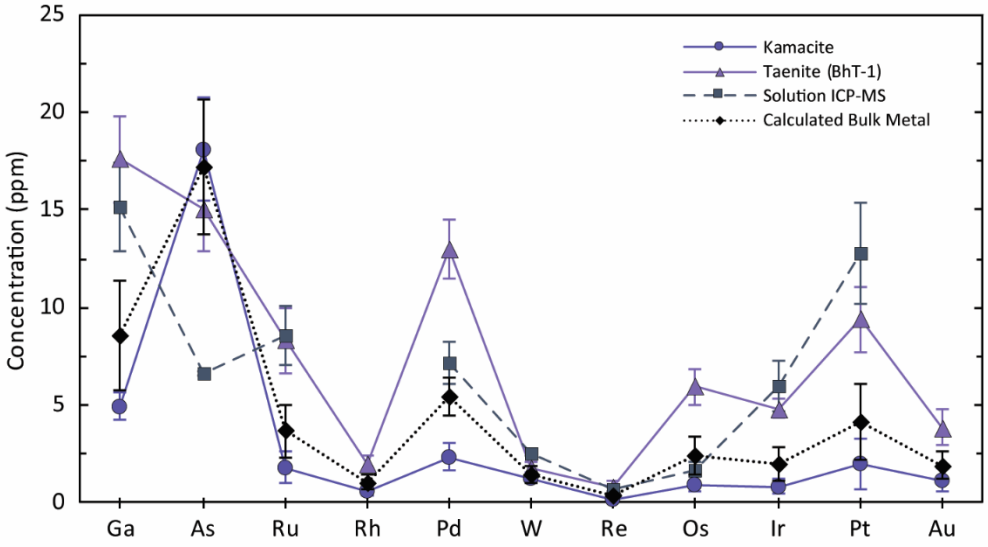

Fig. 2.6. Bruderheim PGE concentrations from *in situ* LA-ICP-MS and bulk metal solution ICP-MS analyses. *In situ* kamacite and taenite (BhT-1) values are both shown. Error bars for *in situ* kamacite and solution results represent one standard deviation from the mean. Error bars for taenite (BhT-1) represent two times the internal standard error. The calculated bulk metal results were achieved by adding together the mean PGE concentrations in kamacite and the BhT-1 PGE concentrations in appropriate proportions; error bars are assumed to be the same as the relative error (standard deviation) for the LL chondrite taenite results.

2.3.3. Comparison to Bulk Metal Studies

In situ results are broadly comparable to results of previous analyses of bulk metal. Mean *in situ* kamacite PGE concentrations for each H and L petrologic type are plotted with corresponding petrologic types from Rambaldi (1976, 1977a, 1977b) (Fig. 2.2B-D; Fig. 2.3B-C). Average Rambaldi PGE concentrations from the coarse metallic fraction (>100 mesh) were used for each petrologic type on the basis that the coarse fraction is where kamacite is preferentially concentrated (Rambaldi, 1976, 1977a, 1977b). Rh and Pd were excluded from the comparisons as these elements were not analyzed in the Rambaldi studies.

In situ H chondrite kamacite results become more comparable to the Rambaldi (1977b) results with increasing petrologic type, with the exception of Pt (Fig. 2.2B-D). This trend is not observed with L chondrites (Fig. 2.3B-C); L6 PGEs are less comparable to results from Rambaldi (1976, 1977a) than L4 chondrites. Despite the large standard deviation of the L4 chondrite *in situ* results (Fig. 2.5), the comparability between the Rambaldi L4 coarse metallic fraction and *in situ* results is minor (Fig. 2.3B); only Os and Ir overlap with the *in situ* error bars. The L6 chondrite *in situ* and coarse metallic fraction values do not overlap with each other at all (Fig. 2.3C). Bruderheim is considered anomalous having significantly lower kamacite PGE (except Pd) and Ni concentrations relative to the other L chondrites (Table 2.3). These lower PGE concentrations in Bruderheim may explain why the mean L6 PGE concentrations do not compare well with the Rambaldi (1976, 1977a) L6 coarse metallic fraction values. However, omitting Bruderheim results (and comparing only Leedey) reveals that there is still a large gap in the comparison (Fig. 2.3C). In an attempt to better match the L6 results with Rambaldi (1976, 1977a), results corresponding to the very coarse (>>100 mesh) metal grains in Mocs from Rambaldi's studies are included in Fig. 2.3C. This metallic fraction of Mocs was specifically chosen for comparison based on having Ni concentrations most like kamacite in the L chondrites. As observed, agreement between the datasets is improved.

Figure 2.4B-D compares PGE concentrations in taenite for each LL chondrite to the intermediate (100-200 mesh) and fine (<200 mesh) metallic fractions of the LL chondrites studied by Rambaldi (1977b). Rambaldi (1976, 1977b) claims taenite is preferentially concentrated in the intermediate and fine metallic fractions, and therefore the results of these two fractions have been added together in appropriate proportions for comparison (hereon referred to as the intermediate/fine fraction). Only one LL4 (Soko-Banja) and one LL5

(Paragould) from Rambaldi (1977b) were available for comparison to Benares(a) and Olivenza, respectively (Fig. 2.4B-C). The Rambaldi LL4 and LL5 chondrite intermediate/fine fraction is enriched in PGEs relative to Benares(a) and Olivenza. Two LL6 analyses from Rambaldi (1977b) (Dhurmsala and St. Séverin) were averaged together for comparison to the St. Séverin results in this study (Fig. 2.4D); the Rambaldi (1977b) LL6 intermediate/fine fraction also reveals an enrichment in PGEs. Furthermore, as the petrologic type increases from 4 to 6, the Rambaldi results remain divergent from the *in situ* results. A possible explanation for the discrepancy is provided below.

As the Rambaldi intermediate/fine fraction for all three LL chondrite petrologic types are not comparable with the *in situ* taenite results, LL chondrite bulk metal results calculated by Rambaldi (1977b) are included in Fig. 2.4B-D for further comparison. It can be assumed that the calculated LL chondrite bulk metal PGE concentrations are representative of true concentrations as earlier work of Rambaldi (1976, 1977a) confirmed such calculations are in general agreement with analyzed bulk metal concentrations. As seen in Fig. 2.4B-D, the LL chondrite bulk metal calculations are in better agreement with the LL chondrite *in situ* taenite results in this study, with the results becoming progressively more similar with increasing petrologic type. It is possible that LL chondrites have more diverse formation histories than H and L chondrites, resulting in a greater range of PGE concentrations in taenite grains. The range in PGE concentrations could be in part due to a large range in Ni concentrations among LL chondrite taenite. Such a range in Ni concentrations has been observed in LL chondrite kamacite relative to H and L chondrites (Rubin, 1990).

Direct comparisons of L/LL chondrite *in situ* kamacite PGE concentrations to the coarse metallic fraction results from Rambaldi (1976, 1977a) for Bjurböle (L/LL4) and Knyahinya (L/LL5) are illustrated in figures 2.7A and 2.7B, respectively. Knyahinya has notably more variable *in situ* kamacite PGE concentrations (Ru, Os, Ir, and Pt) than Bjurböle (Figs. 2.5, 2.7). Compared to the Rambaldi (1976, 1977a) coarse fraction, the *in situ* Ir results for Bjurböle are in good agreement, and the Os results are within uncertainty (Fig. 2.7A). For Knyahinya, only the *in situ* Ir result is comparable to the Rambaldi (1976, 1977a) values (Fig. 2.7B). The discrepancy between these L/LL chondrite datasets is addressed in section 2.4.1.

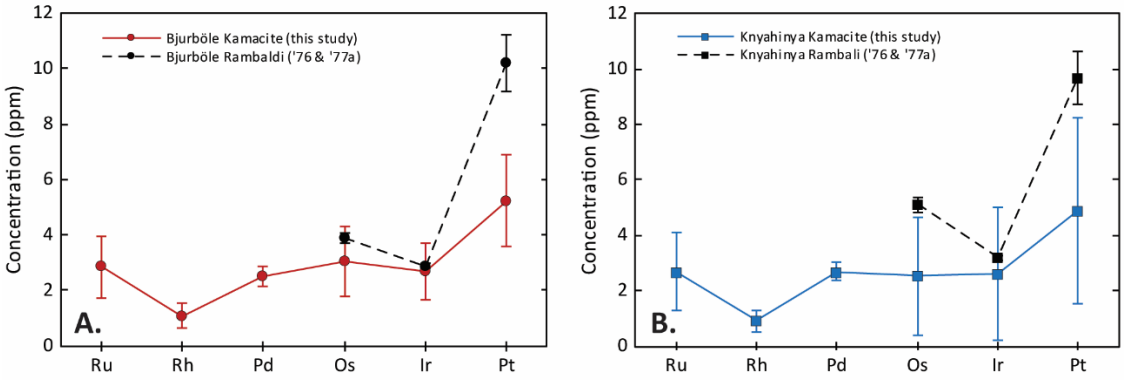

Fig. 2.7. A direct comparison of *in situ* kamacite PGE concentrations (this study) to coarse metallic fraction PGE concentrations from Rambaldi (1976, 1977a) for Bjurböle L/LL4 **(A)** and Knyahinya L/LL5 **(B)**. Ru, Rh, and Pd were not analyzed in the coarse fraction for these meteorites by Rambaldi (1976, 1977a). The error bars on the *in situ* results are one standard deviation from the mean. The error bars for the Rambaldi (1976, 1977a) results are calculated from the precision of the instrument neutron activation method for each element (Os 5%, Ir 3%, Pt 10%).

Further comparison of the mean *in situ* kamacite and taenite results to bulk metal studies is provided in Table 2.6. The *in situ* values are the overall average of PGE concentrations for each EOC group (bolded values in Tables 2.3 and 2.4). Also included in Table 2.6 are averaged LA-ICP-MS results for H and LL chondrites from Campbell and Humayun (2003); the results in this study are in good agreement with theirs. It is apparent that H chondrite *in situ* kamacite results are comparable to the H chondrite bulk metal values, within uncertainty; however, L and LL chondrite bulk metal values are enriched relative to the L and LL *in situ* kamacite results, respectively. *In situ* taenite results are most comparable to the LL chondrite bulk metal values, but are enriched relative to H chondrite bulk metal values. Although the L chondrite *in situ* taenite results (BhT-1) are comparable to the bulk metal studies, the Ni concentrations differ significantly. At this time it is difficult to be confident in this L chondrite comparison based on the result from only one analytical point (BhT-1). Additional analysis of L chondrite taenite is necessary to further investigate the comparability of L chondrite taenite and bulk metal values.

Table 2.6. Mean PGE concentrations in EOC metal.

EOC Groups	Ni (wt.%)	Ru	Rh	Pd	Os	Ir	Pt
H Chondrites							
Kamacite							
This Study	6.51(0.38)	3.3(0.9)	0.95(0.26)	2.7(0.4)	2.4(0.7)	2.2(0.7)	4.3(1.2)
Campbell & Humayun '03	6.47(0.68)	3.4(1.2)	-	2.6(0.3)	2.0(1.4)	1.9(1.4)	6.4(2.0)
Taenite							
Campbell & Humayun '03	27(3)	11(3)	-	15(3)	4.8(2.0)	4.5(1.8)	17(6)
Bulk Metal							
Kong & Ebihara '97	9.1(0.8)	4.4(0.3)	0.90(0.23)	3.9(0.8)	3.1(0.3)	3.1(0.1)	6.9(0.6)
Rambaldi '77b	8.9(0.7)	6.0(0.5)	-	-	4.5(0.5)	4.0(0.4)	10(1)
L Chondrites							
Kamacite							
This Study	6.3(0.6)	2.9(1.4)	0.93(0.44)	2.8(0.6)	2.2(1.4)	2.0(1.4)	4.0(2.3)
Taenite							
This Study*	20(5)	5.4(1.8)	1.4(0.4)	9.4(2.3)	4.1(1.3)	3.3(1.0)	6.9(1.6)
BhT-1	28	8.3[1.7]	2.0[0.4]	13[2]	6.0[0.9]	4.8[0.5]	9.4[1.7]
Bulk Metal							
Kong & Ebihara '97	14(4)	6.5(0.9)	1.6(0.2)	5.8(0.1)	4.7(0.3)	4.5(0.2)	10(1)
Rambaldi '76 &'77a	15(2)	7.8(0.3)	-	-	6.1(0.4)	5.0(0.3)	13.7(0.3)
LL Chondrites							
Kamacite							
This Study⁺	6.3(0.3)	3.4(0.8)	1.1(0.2)	3.3(0.5)	2.6(0.9)	2.3(0.9)	4.7(1.5)
Taenite							
This Study	34(4)	12.1(3.9)	3.3(1.2)	15.0(1.9)	6.9(3.0)	6.6(2.7)	15.1(5.9)
Campbell & Humayun '03	33(5)	12(8)	-	16(3)	5.9(4.2)	5.1(3.5)	14(9)
Bulk Metal							
Kong & Ebihara '97	33(2)	14(3)	3.4(0.3)	17(2)	10(1)	8.8(0.7)	22(2)
Rambaldi '77b	26(4)	12(1)	-	-	10(2)	9(2)	20(4)

Standard deviations (1σ) of the mean are in parentheses except for the BhT-1 results which are 2 times the internal standard error represented by square brackets.
Campbell and Humayun (2003): H chondrite results for kamacite and taenite from Allegan (H5); LL chondrite taenite results from Soko-Banja (LL4).
* Mean results of the single plessite-rich grain in Bruderheim.
⁺ From Benares(a) (LL4) only.

2.3.4. St. Séverin

St. Séverin is unusual given its enrichment of PGEs in kamacite relative to the other EOCs (Table 2.3). Comparison of the PGE concentrations in kamacite and taenite reveals that they are similar, within uncertainty, for all elements except Ru and Pd (Fig. 2.8A). While all PGE plots in this study (Figs. 2.2-2.4, 2.6, 2.7) show a trend of Rh depletion relative to Ru and Pd, the kamacite in St. Séverin does not behave this way; Pd is the most depleted element in St. Séverin kamacite. Also compared in Fig. 2.8A are the results of the coarse and intermediate/fine metallic fractions for St. Séverin obtained by Rambaldi (1977b). Oddly, the coarse fraction compares well with the *in situ* taenite results, while the intermediate/fine fraction shows an enrichment in PGEs overall. BSE images of the metal in St. Séverin reveal that taenite is compositionally heterogeneous on the scale of the analytical spot size (Fig. 2.8B). The unusual metal texture and compositions of St. Séverin metal are likely due to a combination of brecciation, moderate shock (Leroux et al., 1996) and the presence of unequilibrated material (Rambaldi and Cendales, 1977).

Despite discrepancies between *in situ* and bulk metal analyses highlighted in this section and section 2.3.3, there is a broad agreement between the two methods (i.e., H chondrite kamacite and bulk metal; LL chondrite taenite and bulk metal; Table 2.6). However, *in situ* LA-ICP-MS analysis specifically targets individual kamacite and taenite grains, and therefore *in situ* results better reflect the concentrations in kamacite and taenite than results from bulk methods. *In situ* analysis enables the assessment of the distribution of siderophile elements among metal phases, and the characterization of the concentrations in a population of metal grains. On this basis, I now assess the distribution and behavior of PGEs in ordinary chondrite kamacite and taenite as a function of equilibration, and derive implications for accretion and metamorphism of ordinary chondrite parent bodies.

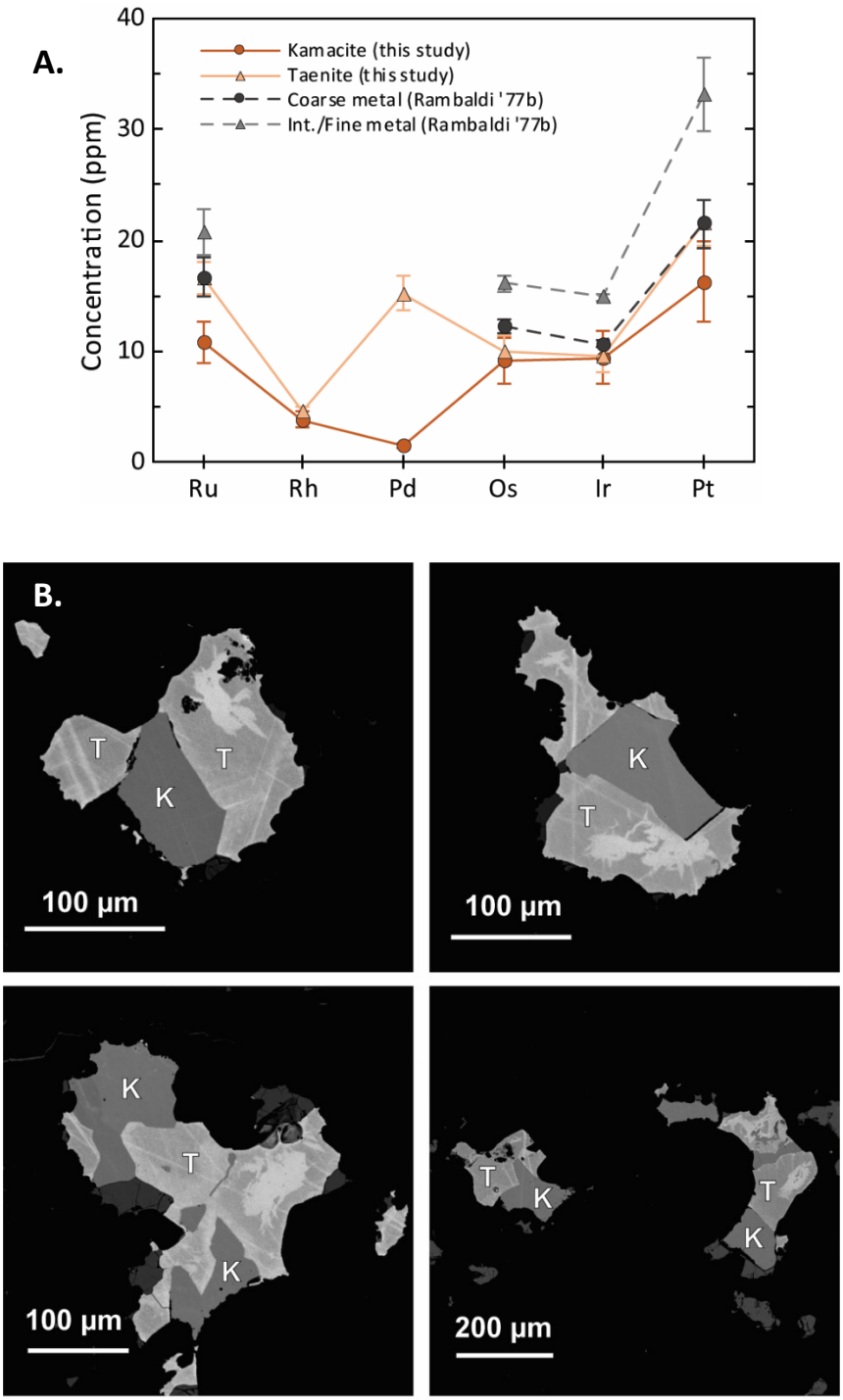

Fig. 2.8. (A) Direct comparison of the mean St. Séverin (LL6) PGE concentrations in kamacite and taenite grains (this study) to the metallic fractions of Rambaldi (1977b). Error bars for the *in situ* data are one standard deviation from the mean, but the error bars for the Rambaldi data are calculated from the precision of INAA for each element. The Rambaldi intermediate and fine fractions have been added together in appropriate proportions (int./fine). **(B)** Backscattered electron images of St. Séverin metal (K = kamacite; T = taenite).

2.3.5 Kamacite and Taenite Inter- and Intra-grain PGE Variability

Significant inter- and intra-grain variability is observed in EOC kamacite and taenite in this study. Figure 2.9 shows the PGE concentrations corresponding to five kamacite grains (see corresponding BSE images) analyzed in Knyahinya (L/LL5). The grains range in size and shape, with taenite exsolution present in some (grains 1, 3, and 5). Rh and Pd have the most consistent concentrations among all five grains, but grains 1 and 3 show higher concentrations of the other PGEs, notably Pt. While it would be easy to argue that the presence of exsolution in grains 1 and 3 is the cause for the increased concentrations, exsolution is also present in grain 5 yet this grain has similar concentrations to grains 2 and 4, which both lack exsolution. The difference in grain size between grains 2 and 4 apparently has no effect on the PGE concentrations.

While Knyahinya is a good example of variability between kamacite grains, Richardton (H5) illustrates variability that can occur both between and within individual grains. The PGE results for Richardton and BSE images of grain targets are shown in Fig. 2.10. Results were collected from five different areas, with some areas having multiple grain targets; results from different grains (labelled A, B, or C) in the same area are separated by gray dashed lines in the PGE plot (Fig. 2.10). The grains in Richardton are irregular in shape and vary in size. Rh is the only element with approximately uniform concentration among all grains targeted in Richardton. All PGE concentrations in Richardton follow a similar pattern specific to each kamacite grain. The grains in areas 1 and 5 show the least variability in PGEs despite a size difference between these grains. Variability that occurs within individual kamacite grains is most prominent in area 2 grain A and area 4 grain A (Fig. 2.10). There is no obvious connection between these two grains that would cause them to have more internal variability than other grains in Richardton.

Intergrain variability is also present in taenite and is shown in Olivenza (LL5) among five taenite grains of different shapes and sizes (Fig. 2.11). PGE concentrations are consistent between grains 1 and 2; however, a notable decrease in Ru, Os, Ir, and Pt concentrations relative to grains 1 and 2 is observed in grain 3. The decrease in these concentrations may be due to the exsolution present in grain 3; however, as seen with Knyahinya (Fig. 2.9), exsolution is not an overall controlling factor for PGE concentrations. Intragrain variation is also present in Olivenza as seen in grains 4 and 5. Despite the intragrain variation in grain 4, most of the Ru,

Rh, Pd, and Pt concentrations in grain 4 are similar to grains 1 and 2, while the Os and Ir concentrations are similar to grain 3. All concentrations except Rh and Pd are enriched in grain 5 relative to the other taenite grains. It is possible that the small size of grain 5 is a factor in the enrichment of these elements, but grain size was proven to not be a factor among the kamacite results for Knayhinya (Fig. 2.9) and Richardton (Fig. 2.10).

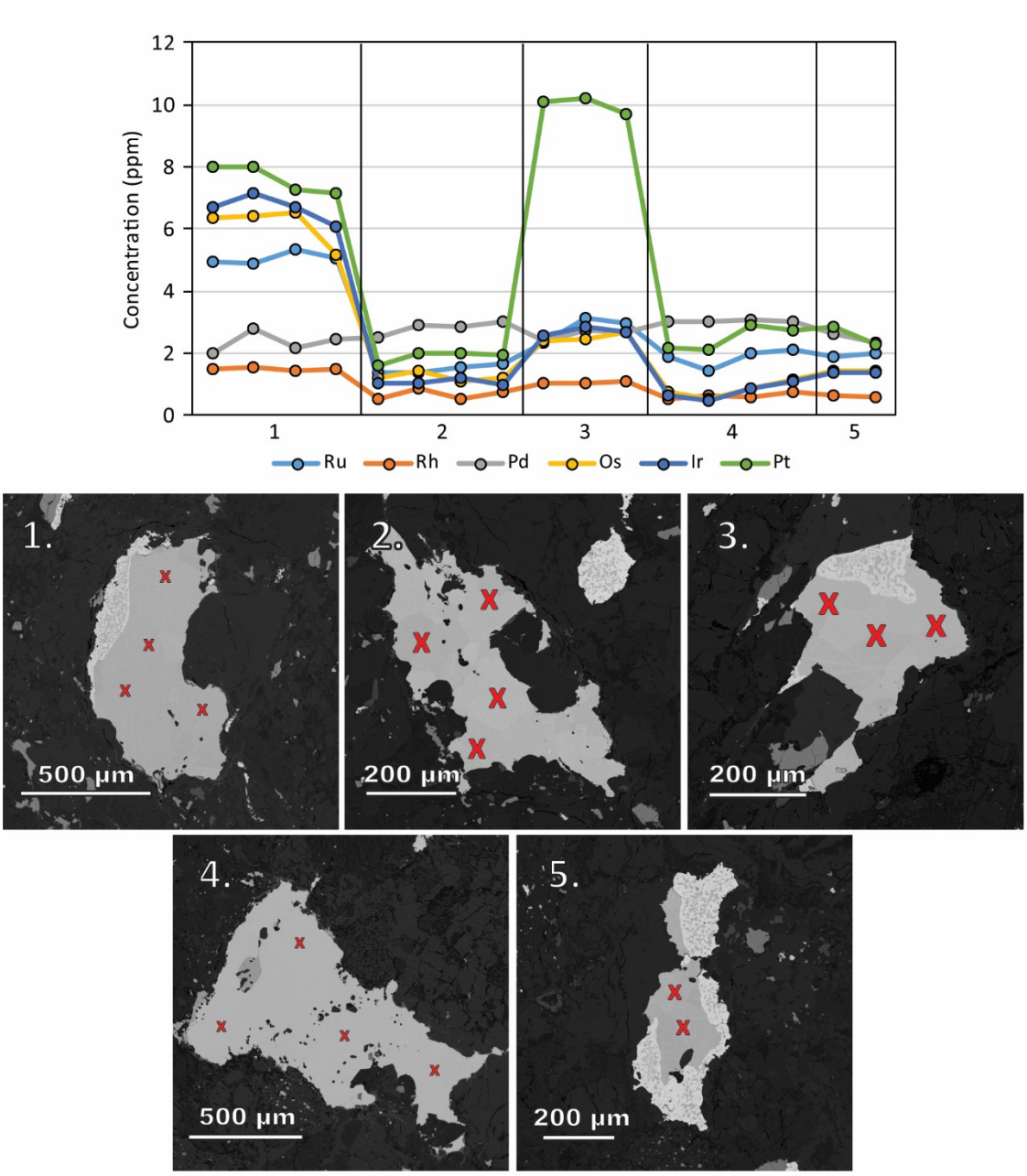

Fig. 2.9. PGE LA-ICP-MS results for five kamacite grains in Knyahinya (L/LL5). The X-axis in the PGE plot specifies the grain analyzed (1-5). BSE images show the grain textures and the red X's indicate the spot size (40 µm) and locations targeted during LA-ICP-MS.

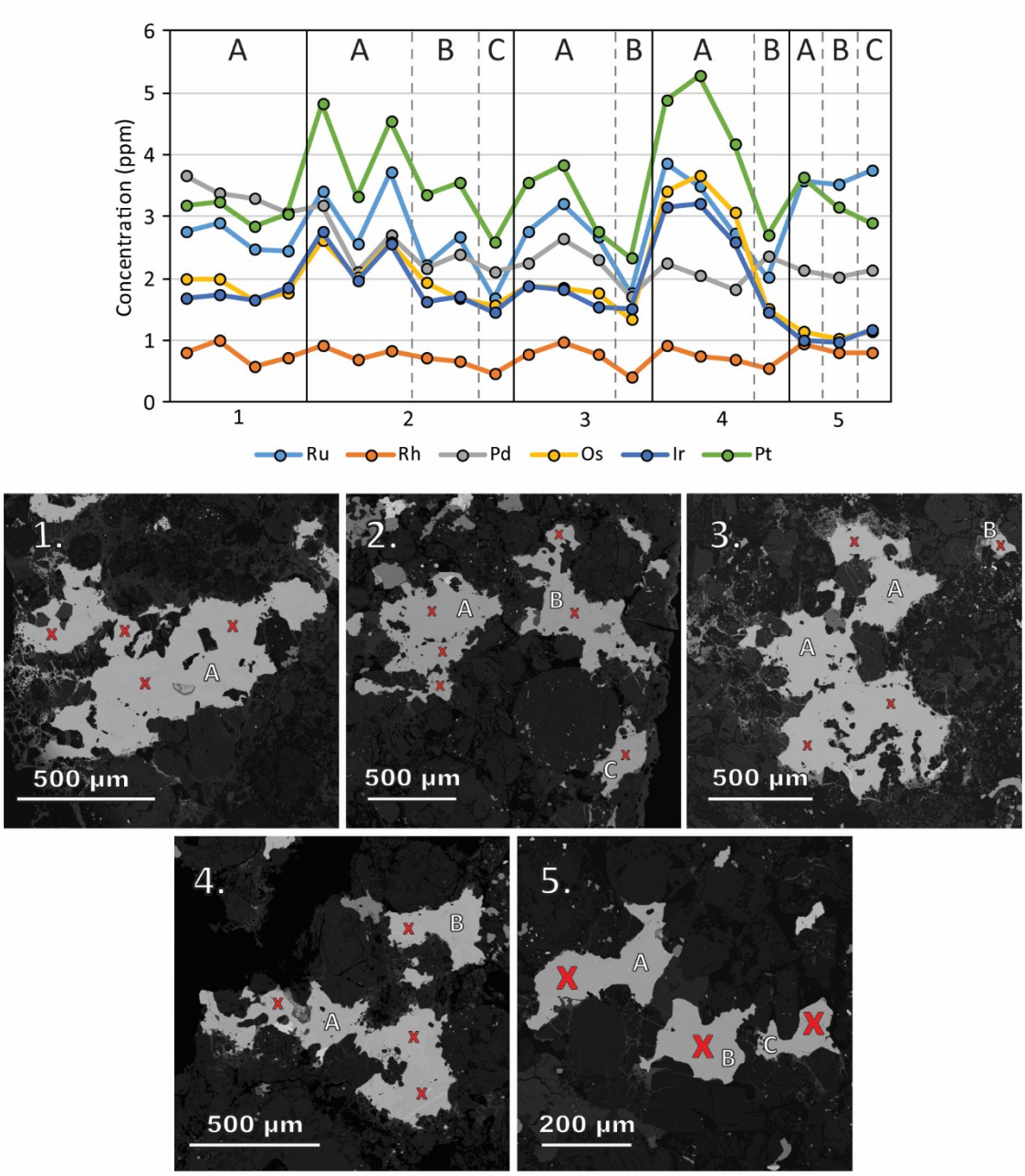

Fig. 2.10. PGE LA-ICP-MS results for kamacite grains in Richardton (H5). The X-axis in the PGE plot specifies the target area (1-5) and the grains within a given area are labelled A, B, or C. BSE images show the grain textures and the red X's indicate the spot size (40 µm) and locations targeted during LA-ICP-MS.

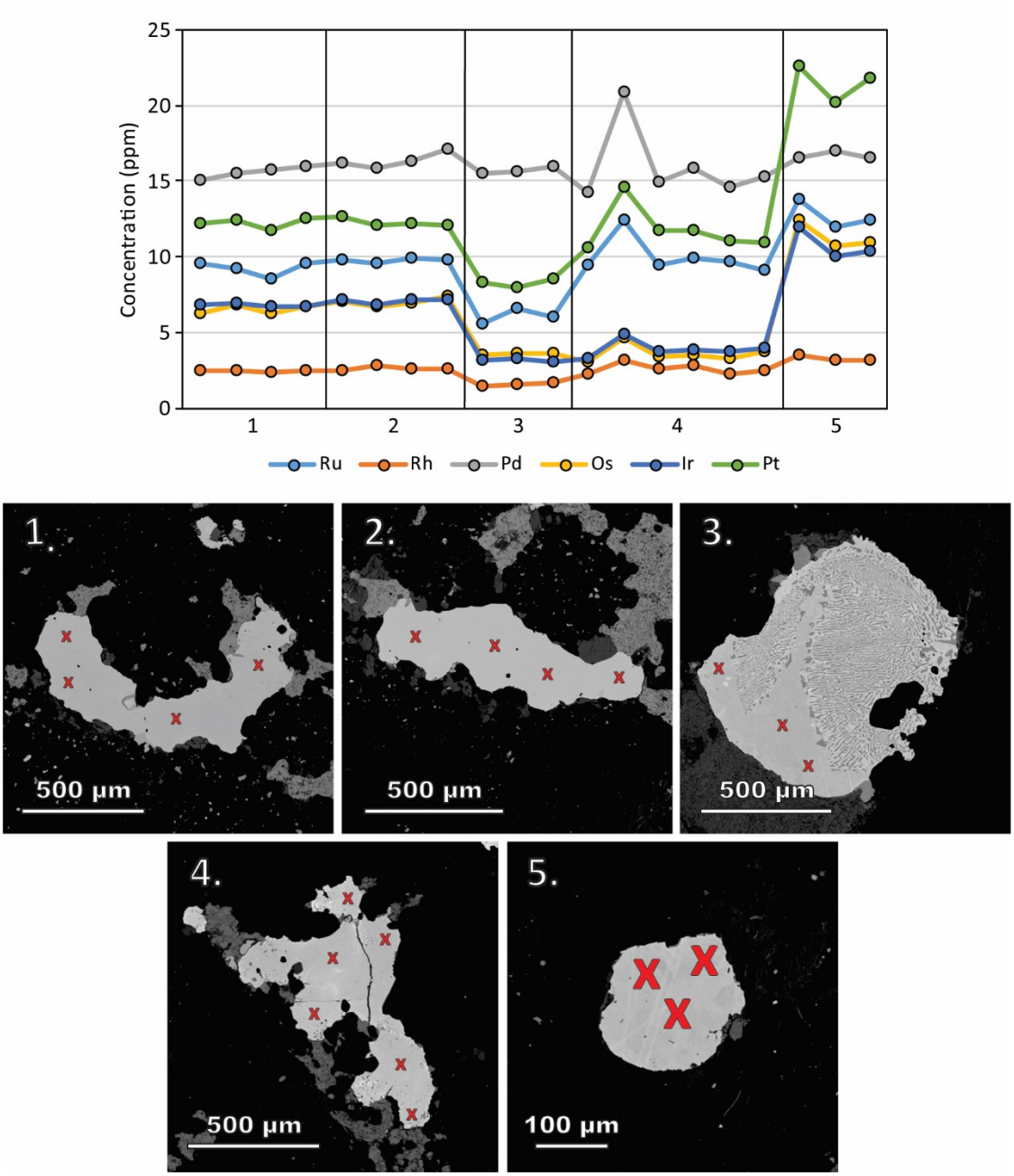

Fig. 2.11. PGE LA-ICP-MS results for five taenite grains in Olivenza (LL5). The X-axis in the PGE plot specifies the grain analyzed (1-5). BSE images show the grain textures and the red X's indicate the spot size (40 µm) and locations targeted during LA-ICP-MS.

PGE inter- and intra-grain variability is present in all kamacite and taenite results obtained in this study, with the exception of Buzzard Coulee (Appendix A1.2). Overall, the variability of PGEs in both kamacite and taenite decreases with increasing EOC petrologic type (Fig. 2.5); however, inter- and intra-grain variability is still evident in type 6 EOC metal (Appendix A1.2). The PGE variability in the metal phases appears to be random: grain size/shape, grain location, and LA-ICP-MS target locations (center vs. rim) seem to have no obvious effect on the variability. The elements Rh and Pd are an exception to this observation given their consistent concentrations regardless of the EOC group or petrologic type (Fig. 2.5; Appendix A1.2). Despite the inter- and intra-grain variability observed in this study, the average PGE concentrations among the ordinary chondrite groups are consistent among the respective kamacite and taenite results (Tables 2.3 and 2.4).

2.4 Discussion

2.4.1. Relationship of PGEs and Ni among the Metal Phases

Comparing *in situ* results to bulk metal studies provides improved insight into the distribution of PGEs in the metal phases among EOCs. It is evident that PGE concentrations are strongly controlled by corresponding Ni concentrations in the metal grains; the greater the Ni, the greater the PGEs. Not only are higher *in situ* PGE concentrations observed in taenite than kamacite, a greater variability associated with these taenite PGE concentrations is also observed. The greater PGE variability in taenite could be a consequence of a larger range of Ni concentrations. For taenite, Ni concentrations range between 25-35 wt.% in the center and 45-55 wt.% at the rims, while kamacite typically has Ni concentrations of 6-7 wt.% in the center and 5-6 wt.% at the rims (Wood, 1967). Therefore, the PGEs in taenite will consequently span a larger range of concentrations, enriched relative to kamacite. The average Ni concentration in kamacite decreases from H to LL chondrites (Table 2.3; Sears and Axon, 1975; Afiattalab and Wasson, 1980; Rubin 1990); however, the kamacite PGEs do not follow this trend as they are similar among the ordinary chondrite groups (Table 2.3). It is likely that the scale of variability between the kamacite Ni contents in the ordinary chondrite groups is too small to have a significant effect on the variability of PGE concentrations. It is apparent that the correlation of

Ni and PGEs is most evident among a larger range of Ni concentrations (i.e., kamacite to taenite Ni concentrations).

Correlation between siderophile elements and Ni in the Allegan (H5) EOC was reported by Campbell and Humayun (2003), who attributed this correlation to kamacite/taenite partitioning. In contrast, a lack of correlation between siderophiles and Ni in the LL4 chondrite Soko-Banja and unequilibrated H chondrite Tieschitz (H3.6) was also reported by Campbell and Humayun (2003), with the exception of Pd and Au. Metal analysis of the Krymka unequilibrated LL chondrite (LL3.2) has also revealed a lack of correlation between Rh, Ir, and Pt and Ni concentrations (Meftah et al., 2016). In order to test whether PGEs correlate with Ni in less-equilibrated chondrite metal, the Benares(a) results from this study are plotted in Fig. 2.12, along with results for Soko-Banja from Campbell and Humayun (2003) and Humayun and Campbell (2002). Based on the Benares(a) results, it is clear that a PGE-Ni correlation does exist for a type 4 chondrite (Fig. 2.12), despite the greater variability of PGE concentrations associated with this petrologic type (Fig. 2.5). The taenite results for Soko-Banja from Campbell and Humayun (2003) are in agreement with the Benares(a) *in situ* taenite results, with the exception of one outlier (Fig. 2.12). The Soko-Banja kamacite results (Os, Ir, and Pt) from Humayun and Campbell (2002) are quite variable, and some results are similar in concentration to those found in taenite (Fig. 2.12). The Ni concentrations for Soko-Banja kamacite are notably low compared to Benares(a) kamacite; however, this is not unusual given that equilibrated LL chondrites are known to have a relatively wide range of mean kamacite Ni concentrations (3.3-7.2 wt.%; Rubin, 1990). Despite being both type 4 LL chondrites, the discrepancy in the variability of the kamacite results between Benares(a) and Soko-Banja suggests that their parent bodies may have undergone differing degrees of secondary heating within the type 4 temperature range, implying that the correlation between PGE and Ni concentrations is an effect of equilibration (see section 2.4.3); that is, the more equilibrated the chondrite, the stronger the PGE-Ni correlation. Therefore, it is understandable that a correlation between PGE and Ni results is not evident for the Tieschitz (Campbell and Humayun, 2003) and Krymka (Meftah et al., 2016) chondrites given the considerable variability of PGEs in the metal grains associated with these unequilibrated meteorites.

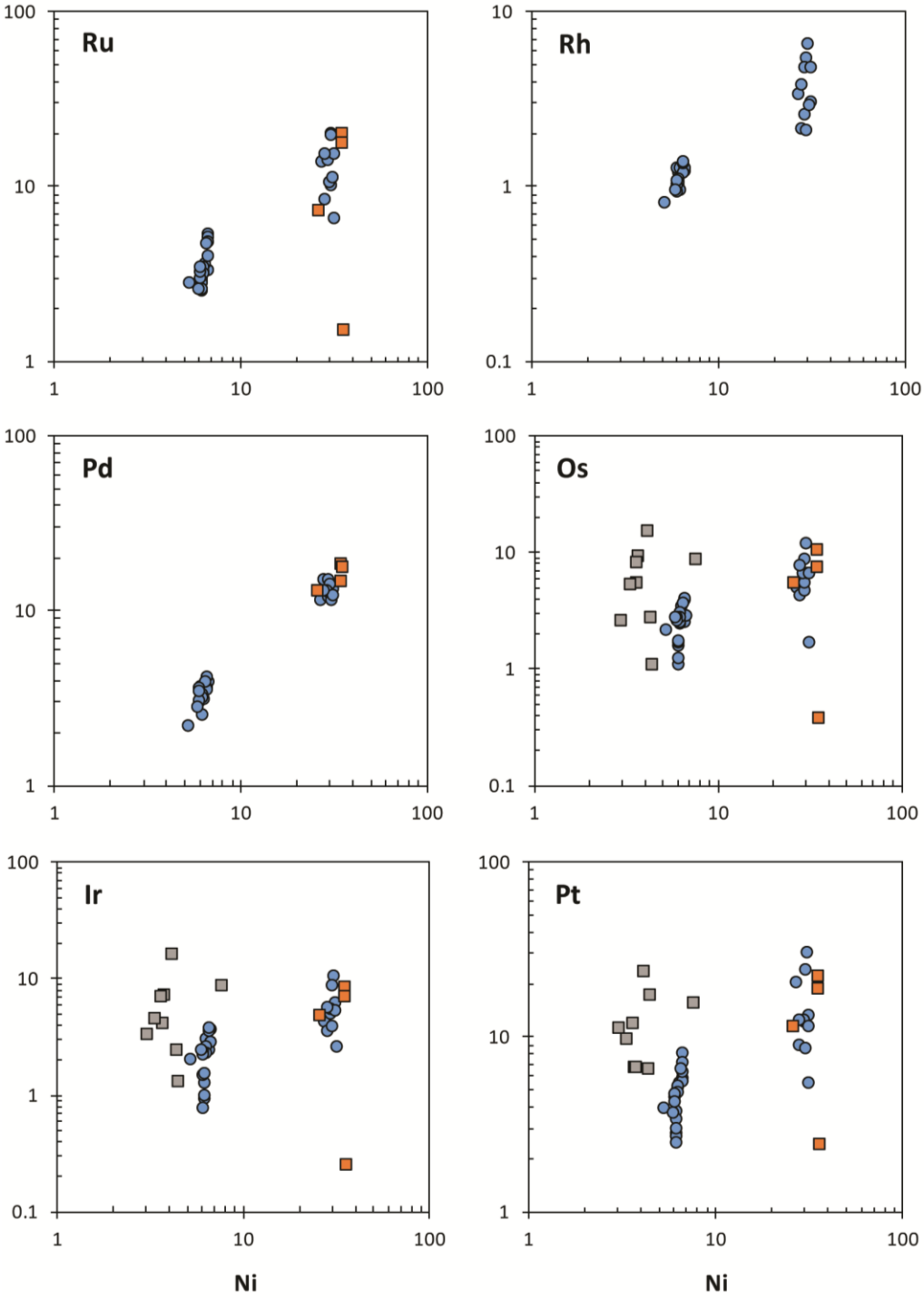

Fig. 2.12. PGEs (ppm) vs. Ni (wt.%) for the LL4 chondrites Benares(a) (blue circles) and Soko-Banja (squares). The two distinct groups of blue circles for Benares(a) correspond to results for kamacite (low Ni) and taenite (high Ni). Taenite results for Soko-Banja from Campbell and Humayun (2003) are represented by orange squares. No Rh results for Soko-Banja were reported by Campbell and Humayun (2003). Kamacite results for Soko-Banja obtained from Humayun and Campbell (2002) for Os, Ir, and Pt are plotted as gray squares. The analyses of Soko-Banja by Humayun and Campbell (2002) and Campbell and Humayun (2003) were completed using the same specimen (Me 319).

PGE concentrations in EOCs are seen to correlate with average Ni concentrations when a mixture of both kamacite and taenite are present (i.e., bulk metal studies). Rambaldi, for example, made a strong effort in his studies (1976, 1977a, 1977b) to separate kamacite and taenite; however, it is clear that a small amount of taenite is present in the coarse metallic fraction of the L and LL chondrites. This is evident from higher Ni concentrations in the coarse metallic fraction which range from 11 wt.% to 12.9 wt.% among equilibrated L chondrites (Rambaldi, 1976; excluding Bjurböle, Knyahinya, and Shaw) and 19.3 wt.% to 29.0 wt.% in equilibrated LL chondrites (Rambaldi, 1977b). The enrichment of Ni in the L chondrite coarse metallic fraction relative to the *in situ* L chondrite kamacite Ni explains the unexpected discrepancy in the L6 chondrite PGE concentrations between Rambaldi and this study (Fig. 2.3C). The mean Ni concentration of the L6 chondrite coarse metallic fraction is 12.3±0.6 wt.%, double the mean Ni concentration of the L6 chondrites in this study (6.2±0.6 wt.%). Consequently, the Rambaldi L6 PGE concentrations are enriched relative to the L6 *in situ* kamacite results. Furthermore, the discrepancies observed in the L/LL chondrite *in situ* and Rambaldi (1976, 1977a) comparisons are also evidently related to the Ni enrichment in the Rambaldi (1976) coarse metallic fractions of Bjurböle and Knyahinya (14.6 wt.% and 16.1 wt.%, respectively) (Fig. 2.7).

The strong correlation between PGEs and Ni also explains why results of the very coarse (>>100 mesh) metallic fraction of Mocs (Rambaldi 1976, 1977a), also illustrated in Fig. 2.3C, better compare with the L6 *in situ* results. The Mocs PGE concentrations are associated with an average Ni concentration of 7.5 wt.%, which is more similar to the average Ni concentrations of the L6 *in situ* kamacite in this study than of the L6 coarse metallic fraction (Rambaldi 1976, 1977a). Furthermore, the Ni-PGE correlation can explain why the H chondrite *in situ* kamacite results better compare with the Rambaldi H chondrite coarse metallic fraction (Fig. 2.2B-D) than the L chondrites between this study and Rambaldi (1976, 1977a). Ni concentrations of the H chondrite coarse metallic fraction range between 5.7 and 7.4 wt.%, which are similar to the H chondrite *in situ* Ni values (Table 2.3); accordingly, there is better agreement in H chondrite PGE concentrations between the two studies.

The results in this study support the use of *in situ* LA-ICP-MS analysis for chondrite metal rather than bulk metal methods to avoid contamination from any taenite present. However, LA-ICP-MS also has limitations when intergrowths are present in the metal. Table 2.4 shows

lower PGE and Ni concentrations in the plessitic grain discovered in Bruderheim relative to the LL chondrite taenite results. As plessite is a fine-grained intergrowth of kamacite and taenite, the spot size of LA-ICP-MS is too large to target the individual phases, therefore resulting in a depletion in Ni, and consequently PGE concentrations, relative to taenite due to the presence of kamacite intergrowths.

2.4.2 PGE Distribution in Bulk Metal

The trend of increasing PGE concentrations in metal from H to LL chondrites reported by previous bulk metal studies is not observed in the *in situ* results (Table 2.6). The relative abundances of kamacite and taenite in each ordinary chondrite group is likely the controlling factor for the increase in bulk metal PGE concentrations from H to LL chondrites. Because PGEs preferentially partition into taenite, the amount of taenite relative to kamacite will govern bulk metal PGE concentrations, as described in section 2.3.2. The similarity of PGE concentrations in H chondrite *in situ* kamacite and bulk metal confirms that kamacite is the more abundant metal phase in H chondrites. As taenite progressively gets more enriched from H to LL chondrites, bulk metal PGE concentrations consequently also become enriched, which explains why LL chondrite bulk metal PGE concentrations are more comparable to the *in situ* taenite values (Table 2.6). *In situ* analysis reveals that PGE concentrations are distributed differently among kamacite and taenite, with PGEs preferentially concentrated in taenite.

2.4.3 Effective Equilibration on PGEs in Kamacite and Taenite

Unequilibrated ordinary chondrite (UOC) metal compositions are found to be more variable than EOCs (Afiattalab and Wasson, 1980; Hsu et al., 1998; Humayun and Campbell, 2002; Campbell and Humayun, 2003; Meftah et al., 2016); however, average PGE concentrations for UOCs and EOCs have been found to be relatively similar. Comparison of unequilibrated and equilibrated H chondrites (Table 2.7) shows similarities in *in situ* PGE concentrations, notably between Os, Ir, and Pt; all PGE values are within uncertainty of each other. Furthermore, bulk metal PGE concentrations for UOCs and EOCs by Kong and Ebihara (1997) reveal some similarities among averaged concentrations. However, the average UOC

and EOC bulk metal concentrations from Kong and Ebihara (1997) are least similar among the LL chondrites. This is believed to be a consequence of greater taenite abundances in LL chondrites (refer to section 2.4.1). Homogenization of taenite grains is controlled by diffusion of Ni (Reisener and Goldstein, 2003), and since Ni diffusion is slower in taenite than kamacite, the result is an M-shape profile of Ni concentrations in taenite (Wood, 1964; Goldstein and Ogilvie, 1965; Wood, 1967; Nagahara, 1979; Hutchison, 2004). Such a pattern could ultimately impact the variability of PGE concentrations in taenite grains, depending on the analytical spot size relative to the grain size.

Table 2.7. Mean i*n situ* kamacite PGE concentrations (ppm) for H chondrites.

PGE	H3	H4-6
Ru	4.1(1.9)	3.3(0.9)
Pd	1.7(1.0)	2.7(0.4)
Os	2.3(2.0)	2.4(0.7)
Ir	2.1(1.7)	2.2(0.7)
Pt	4.9(3.9)	4.3(1.2)

Mean H3 concentrations were obtained from LA-ICP-MS analysis of Tieschitz (H3.6) kamacite grains (Campbell and Humayun, 2003). Mean H4-6 concentrations are from this study (Table 2.3). Standard deviations (1σ) of the mean are in parentheses.

The decrease in PGE variability through ordinary chondrite types 3 to 6 appears to be a result of equilibration. As ordinary chondrites are exposed to increasing temperatures during metamorphism, PGE concentrations become more homogenous throughout metal phases with increasing grade. This same observation has been reported for kamacite Ni and Co concentrations between UOCs and EOCs by Afiattalab and Wasson (1980). Metamorphic temperature ranges from Dodd (1981) and McSween (1999) are as follows: type 3 – 400°C to 600°C; type 4 – 600°C to 700°C; type 5 – 700°C to 750°C; type 6 – 750°C to 950°C. Due to the comparably lower metamorphic temperatures in types 4 and 5, PGE variability is more prominent (and similar) in these types than in the higher metamorphosed type 6 (Fig. 2.5; Appendix A1.2). Importantly, despite the higher metamorphic temperatures associated with

type 6, PGE variability is still evident to some extent in type 6 ordinary chondrite metal. Variable Ir concentrations in type 6 ordinary chondrite metal has been noted by Humayun and Campbell (2002). Overall, the PGE variability seen in EOC kamacite and taenite grains exists both on the inter- and intra-granular scales (Figs. 2.9, 2.10, 2.11; Appendix A1.2).

However, the main question becomes to what extent does the homogenization of PGEs in ordinary chondrite metal occur? Intergrain homogenization has been discussed by Reisener and Goldstein (2003), who compare the homogenization of metal compositions from types 3 to 6 to the redistribution of Fe and Mg between pyroxene and olivine that occurs during metamorphism. While it is agreed that homogenization of PGE concentrations in the metal phases resembles the metamorphic trend of Fe-Mg diffusion, there is no continuous path between the metal grains for diffusion and equilibrium to occur like the silicates. Currently, there is no effective mechanism proposed to explain the diffusion of PGEs throughout metal grains. However, in terms of Fe and Ni, Wood (1967) has advocated that these two elements can easily diffuse through the silicates in order to equilibrate the isolated metal grains. The exact mechanism of Fe and Ni diffusion through the silicates is still debated; however, grain boundary diffusion (Wood, 1967), vapour transport (Wood, 1967; Reisener and Goldstein, 1999), and metal-silicate equilibration (McSween and Labotka, 1993; Reisener et al., 2006) have all been proposed. Regardless, the need for these processes to equilibrate PGE concentrations in metal grains is obviated by the observation that intergrain variability is still present in type 6 metal grains. Furthermore, diffusion of the PGEs between metal grains via the silicates would be a very slow process. Willis and Goldstein (1983) and Reseiner and Goldstein (2003) have eliminated the need for diffusion through intervening silicates on the basis that metal grains are connected 3-dimensionaly. In this case, some diffusion can be facilitated through adjacent metal or troilite grains, or along grain boundaries (Willis and Goldstein, 1983). However, a lack of grain-to-grain conductivity among metal grains in ordinary chondrites (Smith and Launspach, 1991) questions the merit of a 3-dimensional network of metal, especially in terms of equilibration. Also, even with a 3-dimensional network, complete equilibration is not expected between the metal grains given that ordinary chondrites at most contain 20 wt.% metal (equilibrated H chondrites; Dunn et al., 2010) which is randomly distributed throughout the silicates.

As there appears to be no effective process for isolated metal grains to reach equilibrium with each other, homogenization of PGEs in metal must occur at the intragrain scale via self diffusion. Meftah et al. (2016) have also reached a similar conclusion. Given the similarities in average PGE concentrations between UOCs and EOCs discussed above, it needs to be emphasized that primitive concentrations in metal are not necessarily erased during metamorphism, as commonly thought. Instead, it can be assumed that the PGE concentrations are simply redistributed within individual metal grains during metamorphism resulting in more homogenous compositions from types 3 through to 6. During the redistribution, the correlation between PGEs and Ni becomes more apparent in EOCs. The observation that average PGE concentrations in kamacite are consistent among EOCs (Table 2.3) suggests that metal concentrations were established prior to accretion of ordinary chondrites and come from the same population of nebular (or pre-accretionary) metal grains. Once these metal grains were incorporated into ordinary chondrite parent bodies during accretion, subsequent metamorphism homogenized the metal compositions to some degree, although original inter- and intra-grain variability is preserved, even to type 6. It is apparent that the post-accretion history of a given ordinary chondrite can impact the extent of homogenization within metal grains (e.g., Buzzard Coulee, St. Séverin), but overall the metal heterogeneities among the different ordinary chondrite types does not appear to greatly affect average PGE concentrations.

2.4.4 Metal Distribution in Early Solar System

Ordinary chondrite metal analysis completed over many decades has provided a great deal of insight into the metal phases that exist in these meteorites. However, a long-standing debate among researchers has centered on deciphering the origin of chondritic metal. It has been proposed that chondritic metal formed: 1) *in situ* on the parent body through metamorphic and diffusional processes (Wood, 1967; Kong and Ebihara, 1996); 2) during chondrule formation and/or melting events via silicate reduction (Scott and Taylor, 1983; Connolly et al., 1994; Zanda et al., 1994; Lauretta et al., 2001); 3) via devolatilization of FeS due to chondrule melting (Shimaoka and Nakamura, 1989; Hewins et al., 1997; Zanda et al., 1997); 4) during nebular condensation (Grossman and Olsen, 1974; Grossman et al., 1979; Rambaldi et al., 1980; Grossman and Wasson, 1985). The theory that metal formed *in situ* after the

parent bodies accreted is discounted based on the findings that PGE concentrations are similar among their respective metal phases. If metal was an *in situ* product, the metal phases would be expected to contain PGE concentrations characteristic of each ordinary chondrite group and petrologic type, as seen with olivine and pyroxene compositions. The formation of metal from the reduction of silicates can only account for some of the metal in chondrites, such as the grains associated with chondrules (e.g., Scott and Taylor, 1983) and dusty olivine grains (e.g., Leroux et al., 2003). Considering that condensation of the lithophile and siderophile elements and metal-silicate fractionation is believed to have occurred before the formation of chondrules (Larimer and Anders, 1970; Grossman and Larimer, 1974; Hutchison, 2004), the amount of siderophile elements contained in the metal formed by silicate reduction during chondrule formation and melting processes would be low (Horan et al., 2009). Devolatilization of FeS also seems like an unlikely formation mechanism given that FeS formed prior to chondrules at temperatures below which metal-silicate fractionation has occurred (Larimer and Anders, 1970; Hutchison, 2004). In this case, it is assumed that metal compositions would be well established before the formation of FeS. Despite the ordinary chondrite parent bodies having diverse formation histories, silicate compositions, and oxidation states (e.g., Rubin et al, 1988; Kallemeyn et al., 1989; Rubin 1990; Kong and Ebihara, 1997; Hutchison, 2004), the similar metal compositions found in this study strongly suggest that chondritic metal is a product of nebular condensation.

Thermodynamic calculations have revealed that the PGEs, excluding Pd, condense at temperatures greater than those of Fe and Ni (Palme and Wlotzka, 1976; Fegley and Palme, 1985; Sylvester et al., 1990; Campbell et al., 2001). By the time Fe starts to condense, the five refractory PGEs have fully condensed (Campbell et al., 2001) and are believed to have formed their own metallic alloy (Palme and Wlotzka, 1976; Palme, 2008). These refractory metal alloys were later incorporated and preserved in Fe-Ni metal during the condensation of Fe and Ni (Grossman and Wasson, 1985; Horan et al., 2009). Palladium is a non-refractory element which has condensation temperatures similar to Fe and Ni, and therefore Pd condensed with Fe and Ni to become part of the Fe-Ni metal alloys (Fegley and Palme, 1985; Campbell et al., 2001); this ultimately effects the behavior of Pd relative to the other PGEs (Palme, 2008). Notably, Pd is the only PGE to strongly correlate with Ni in ordinary chondrite metal, regardless of the petrologic type (Fig. 2.12; Campbell and Humayun, 2003). Palladium concentrations in kamacite and taenite are also consistent among the different ordinary chondrites (Fig. 2.5;

Appendix A1.2), which is attributable to the similar volatilities of Pd and Fe (Campbell et al., 2001; Palme, 2008). The results in this study show that Rh also has consistent concentrations among the metal phases (Fig. 2.5; Appendix A1.2), which is unusual given that Rh condenses at higher temperatures than Fe (e.g., Campbell et al., 2001). While these results seem to imply that the previously calculated Rh condensations temperatures may be incorrect, and instead Rh condenses at temperatures similar to Fe, making such an assumption is avoided given that the previous studies are congruent in their results (Palme and Wlotzka, 1976; Fegley and Palme, 1985; Sylvester et al., 1990; Campbell et al., 2001). Also, Rh variability has been observed in zoned metal grains of the QUE94411 carbonaceous chondrite (Campbell et al., 2001), further supporting the idea that Rh condenses before Fe. Instead, it is possible that because Rh is the least refractory PGE, it is effectively homogenized in type 4 ordinary chondrites during equilibration. Further metal analysis including UOCs is needed to confirm this.

2.5 Conclusions

In situ analysis of individual kamacite and taenite grains has provided a better understanding of the behavior and distribution of PGEs in EOC metal. This *in situ* study is the first of its kind to provide an extensive report of PGE concentrations in kamacite and taenite among several EOCs of varying group and petrologic type. PGEs are not distributed throughout metal among the ordinary chondrite groups in varying concentrations (i.e., H < L < LL) as indicated in previous bulk metal studies. Instead it is discovered that average PGE concentrations in kamacite are consistent among the different ordinary chondrite groups and petrologic types. Taenite PGE concentrations are enriched relative to kamacite, confirming the preferential partitioning of PGEs into taenite. PGE concentrations in taenite are also more variable than kamacite concentrations, which may be attributable to a larger range of Ni concentrations in taenite than in kamacite. It is apparent that a correlation between PGEs and Ni exists among the EOC metal grains.

Compared to the bulk metal data, the *in situ* results from this study are most similar among the H and LL chondrites. Kamacite PGE concentrations are similar to H chondrite bulk metal values, consistent with kamacite being the primary metal phase and major carrier of

PGEs in these meteorites. Taenite PGE concentrations are similar to bulk metal values for LL chondrites, consistent with taenite being the primary metal phase in LL chondrites. These observations are significant for explaining why bulk metal PGE concentrations differ among the H, L, and LL chondrites. As kamacite and taenite are not allocated equally among the ordinary chondrite groups, the bulk metal results reflect the concentration of the dominant metal phase.

In situ analysis has revealed that PGE concentrations vary between and within the metal grains. This variability decreases with increasing petrologic grade, yet is not completely diminished in the type 6 ordinary chondrites. The geochemical characteristics of PGEs and the absence of a connecting network of metal grains limits the extent to which equilibration can occur between metal grains. Homogenization of PGE concentrations in kamacite and taenite is believed to occur within individual metal grains via self diffusion during metamorphism. Despite the heterogeneities seen between and within different metal grains for a given ordinary chondrite, when averaged these variabilities become negligible. The similarities of the PGE concentrations seen in the kamacite grains of the EOCs suggests that the metal grains formed as nebular condensates, and were partially homogenized after accretion during metamorphism.

Chapter 3. Water Abundance in the Tagish Lake Meteorite from TGA and IR Spectroscopy: Evaluation of Aqueous Alteration

3.1 Introduction

The Tagish Lake meteorite is one of the most well studied carbonaceous chondrites due to its primitive nature and unique chemical and physical properties. Tagish Lake is a dark, organic-rich, ungrouped, type 2 carbonaceous chondrite breccia with similarities to CI and CM chondrites (Brown et al., 2000; Zolensky et al., 2002). The bulk mineralogy of Tagish Lake consists of olivine (forsterite-rich) and pyroxene (enstatite-rich) found as chondrules, aggregates, and isolated grains in the matrix, as well as magnetite, carbonates, sulphides, and abundant phyllosilicates (saponite and serpentine) (Brown et al., 2000; Zolensky et al., 2002; Bland et al., 2004; Izawa et al., 2010; Blinova et al., 2014). Tagish Lake has the lowest density ever recorded for any meteorite (1.6 g/cm^3), and is also quite porous (~40% porosity) and extremely friable (Brown et al., 2002; Zolensky et al., 2002; Bland et al., 2004; Ralchenko et al., 2014).

Tagish Lake specimens are classified as either “pristine” or “degraded” depending on how soon they were collected after the fall on January 18, 2000. Specimens collected after Tagish Lake’s fall and kept in cold conditions are the pristine specimens, whereas those collected after the spring melt are referred to as degraded. Of the pristine samples collected, three specimens (TL5b, TL11h, and TL11i) have been studied in detail (Herd et al., 2011; Alexander et al., 2012; Blinova et al., 2014). Petrological studies of TL5b, TL11h, and TL11i have reported mineralogical variations among these three specimens that are indicative of varying degrees of aqueous alteration in the order TL5b (least altered) < TL11h < TL11i (most altered) (Herd et al., 2011; Blinova et al., 2014). Variations in hydrogen abundances (water and bulk) have also been reported for these three specimens, but interestingly in the opposite order of TL5b > TL11h > TL11i (Alexander et al., 2012).

While petrologic investigations are useful for determining the extent of aqueous alteration a carbonaceous chondrite has undergone, recent aqueous alteration studies have revealed that it is possible to determine relative aqueous alteration degrees from phyllosilicate water abundances as well as from the ratio of phyllosilicates to anhydrous silicates (Beck et al., 2010; Beck et al., 2014; Garenne et al., 2014; Howard et al., 2014; King et al., 2015). As

phyllosilicates are aqueous alteration products of anhydrous materials (i.e., olivine, pyroxene, and chondrule mesostasis; Browning et al., 1996; Hanowski and Brearley, 2001; Rubin et al., 2007), the amount of phyllosilicates/water present should reflect the degree of aqueous alteration in a given sample (e.g., Garenne et al., 2014). This study uses thermogravimetric analysis (TGA) to determine the amount of water in pristine Tagish Lake samples. TGA is a quantitative method where the mass loss of a given substance is measured as a function of temperature while the substance is subject to a controlled temperature. Given that TL5b, TL11h, and TL11i have been exposed to variable degrees of aqueous alteration (Herd et al., 2011; Blinova et al., 2014), it is expected that the TGA results will show a variance in water abundances between the samples correlative with the alteration degrees (e.g., Garenne et al., 2014; King et al., 2015). Infrared (IR) transmission spectroscopy can also be used to quantify the amount of water in addition to determining the relative ratio of phyllosilicates to olivine from the depth of absorption bands (Beck et al., 2010; Beck et al., 2014); the stronger the olivine band, the less altered the sample. TGA and IR spectroscopy are used to help address a significant unknown: whether the total water abundance in Tagish Lake corresponds to the degree of aqueous alteration; secondary to this question is which alteration phases are the reservoirs for water. In addition to the aqueous alteration investigation, reflectance spectroscopy of Tagish Lake was gathered to provide additional information pertaining to connecting the Tagish Lake meteorite to its asteroid parent body.

3.2 Samples

Five pristine Tagish Lake specimens (TL5b, TL11h, TL11i, TL4, and TL10a) were available for study from the University of Alberta Meteorite Collection (Fig. 3.1); these pristine specimens have been kept cold (-28°C) and dry, and have not been warmed to temperatures above 0°C. The pristine nature of these specimens is ideal for an aqueous alteration investigation as the material best represents the actual parent body composition due to the lack of terrestrial weathering or contamination. The petrological study of TL5b, TL11h, and TL11i by Blinova et al. (2014) revealed that the matrix, composed of a fine-grained mixture of saponite and serpentine, varies in abundance between TL5b, TL11h, and TL11i with 20 vol.%, 40 vol.%, and 50 vol.%, respectively, in conjunction with their alteration degrees. TL4 and TL10a have not been studied in petrologic detail prior to this study. Little is known about their

mineralogy and degree of aqueous alteration, although TL10a looks macroscopically similar to TL5b. TL4 has unusual bulk physical properties as it has a much higher grain density and porosity relative to other Tagish Lake specimens (Ralchenko et al., 2014). One of the goals of this study is to introduce TL4 and TL10a into the reported aqueous alteration sequence of TL5b, TL11h, and TL11i (Herd et al., 2011; Blinova et al., 2014); this will be possible if the reported sequence can be replicated with TGA and IR spectroscopy.

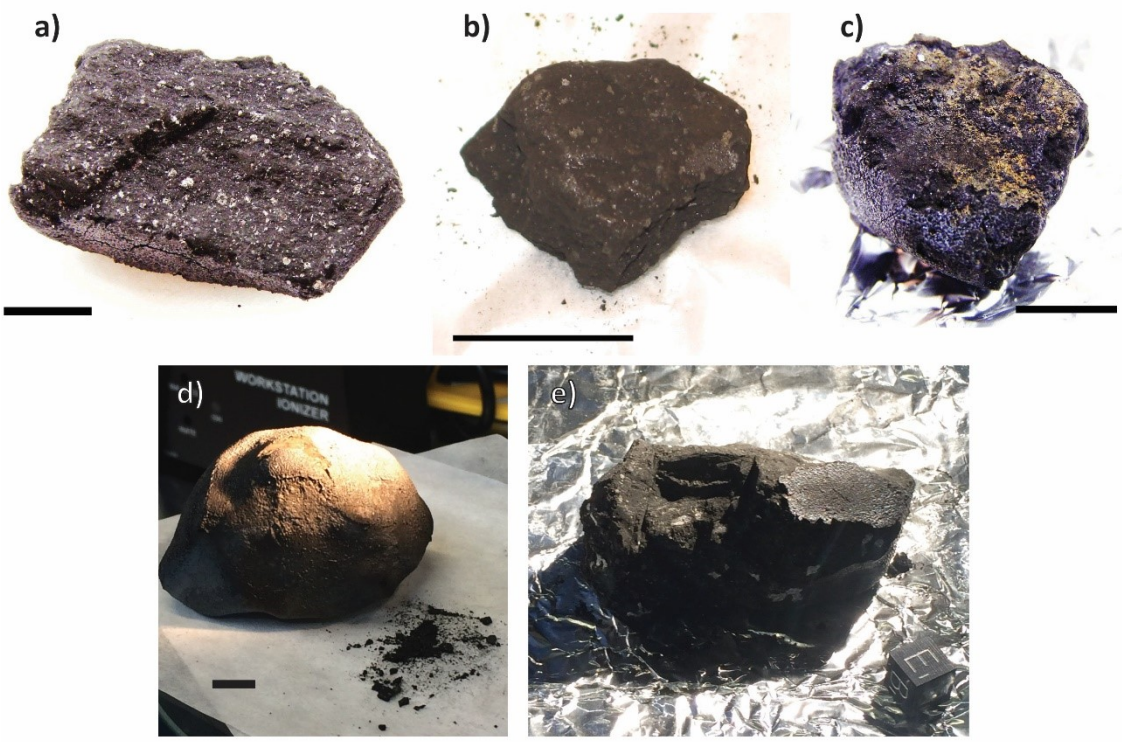

Fig. 3.1. Images of the five Tagish Lake specimens in this study: a) TL5b; b) TL11h; c) TL11i; d) TL4; and e) TL10a. Note the dark colour of the specimens. TL4 shows fusion crust as well as the very fine grained, friable material which is characteristic of Tagish Lake. Scale bars for TL5b, TL11h, TL11i, and TL4 are 1 cm. Included in the TL10a image is a 1 cm cube for scale.

3.3 Methodology

TGA and transmission IR spectroscopy were selected for this aqueous alteration investigation of Tagish Lake based on the study of Garenne et al. (2014) where these methods were used to characterize degrees of aqueous alteration among several different carbonaceous chondrite types. Both methods are individually suited for determining the extent of aqueous alteration; however, these two methods are complimentary and are expected to be congruent with one another (Garenne et al., 2014).

TGA was completed in the Department of Renewable Resources at the University of Alberta; two analytical sessions were completed on separate occasions. Each Tagish Lake sample was a loose, heterogeneous mixture of chondrules and matrix. Approximately 12 to 20 mg were collected for analysis. For the first TGA session, TL5b, TL4, and TL10a were crushed and homogenized by a mortar and pestle. This was done to assess if homogenization has an effect on the TGA results. All remaining analyses were completed with samples as collected (heterogeneous mixtures).

The analytical procedure for TGA was intended to replicate the conditions used by Beck et al. (2013) and Garenne et al. (2014), but due to instrument differences the conditions used in this study vary slightly. Tagish Lake samples were analyzed using a Perkin Elmer STA 6000 instrument under an inert N_2 atmosphere of 20 mL/min. Samples were put into a 30 µL ceramic crucible and heated from 30°C to 900°C at a rate of 10°C/min. Measurements in Garenne et al. (2014) were completed up to 1200°C, however the Perkin Elmer instrument used in this study is only capable of heating to 900°C. This temperature limit is not a concern as the water/OH abundances of interest are associated with saponite and serpentine which release OH at temperatures < 850°C (Mielenz et al., 1953; Nozaki et al., 2006; Földvári, 2011; Lafay et al., 2012; Garenne et al., 2014; King et al., 2015). Mineral references were also analyzed via TGA which include saponite, greenalite, clinochlore, calcite, dolomite, and siderite. A sample of insoluble organic matter of the Murchison (CM) carbonaceous chondrite (courtesy of C. Alexander) was also analyzed with TGA for comparison to Tagish Lake. These reference materials were chosen based on the petrological study of Tagish Lake by Blinova et al. (2014).

Analysis of reference material by TGA has revealed that minerals have characteristic peak temperatures at which they break down and in some cases re-crystallize (e.g., Földvári,

2011). These peak temperatures can be determined by calculating the derivative of the TGA results which produces a derivative thermogravimetric (DTG) curve. The DTG curves represent the rate of weight loss during TGA (i.e., wt.%/°C). Peaks on the DTG curves were used to identify the temperatures where water/OH is released from the hydrous mineral phases in Tagish Lake. The breakdown of other carbonaceous chondrite constituents such as organics, carbonates, (oxy)-hydroxides, and even sulphides can also be recorded by TGA/DTG (e.g., Miyazawa et al., 2000; Földvári, 2011; Garenne et al., 2014). By obtaining TGA/DTG results for mineral references, a general idea of the decomposition temperatures of the different constituents in Tagish Lake, notably the phyllosilicates, can be determined. Compositional variations of a given mineral can shift the position of the DTG peak (Földvári, 2011) making it difficult to identify the specific mineral phases in Tagish Lake from the DTG curves given that the compositions of the reference material are not the same as the minerals in Tagish Lake. Therefore, identification of the hydrous mineral phases via DTG was not attempted in this study.

Transmission IR spectra were measured at the Institut de Planétologie et d'Astrophysique de Grenoble using a Bruker Vertex 70 Fourier transform infrared (FTIR) spectrometer with an 8 mm collimated beam. Prior to analysis, 1.0 mg of homogenized Tagish Lake powder (via mortar and pestle) of each specimen was mixed with 300 mg of ultrapure KBr powder and mechanically ground. The mixture was compressed (400 bars) into a 13 mm diameter pellet for transmission analysis. Spectra were measured over the range of 4000 to 400 cm^{-1} (2.5 to 25 µm) from 64 scans at 8 cm^{-1} spectral resolution.

Reflectance spectra of TL5b, TL11h, TL4, and TL10a were measured at the University of Winnipeg Planetary Spectrophotometer Facility (UWPSF) using an Analytical Spectral Devices (ASD) FieldSpec Pro HR spectrometer with a 5 mm field of view and a spectral resolution between 2 and 7 nm. Samples were homogenized into a fine-grained powder via mortar and pestle prior to analysis. A spectrum for TL11i was not acquired due to limited availability of the sample. The spectra were measured in the visible and near infra-red (0.35 to 2.5 µm) at an incidence (i) angle of 30° and an emergence (e) angle of 0° relative to a Spectralon reflectance standard. The spectra were corrected for minor irregularities in absolute reflectance and detector offsets. A lampblack-coated aluminum mask (5 mm diameter central hole) was placed over the samples and reflectance standard as the amount of sample available

for analysis did not fill the sample cup. The use of a mask is to ensure that aluminum features from the sample cup are not reflected back during analysis.

Bulk mineralogy of specimens TL4 and TL10a was determined by X-ray diffraction (XRD) for comparison to TL5b, TL11h, and TL11i from Blinova et al. (2014). XRD analysis was completed under the same operating conditions as Blinova et al. (2014). TL4 and TL10a were ground in an alumina mortar and pestle prior to analysis. The fine-grained powdered samples were analyzed using a Rigaku Ultima IV Powder Diffractometer equipped with a Co tube and a high-speed Si strip detector. Samples were mounted onto a zero-background plate and spun at a rate of 0.5 Hz. Conditions for analysis included using Co Kα radiation (λ =1.78899 Å) and a step size of 0.02° 2θ with 0.6 second count time per step. Results were acquired over the range of 5-80° 2θ. Rietveld refinement was used to identify the mineral phases in TL4 and TL10a and quantify their relative abundances. Rietveld refinement is a quantitative technique that fits measured diffraction patterns to calculated data using the nonlinear least-squares fit method (Rietveld, 1967; Young et al., 1977). The JADE 9.0 software (Materials Database Inc.) was employed for Rietveld refinement utilizing whole pattern fitting over the range of 15-70° 2θ.

3.4 Results

3.4.1 XRD and Rietveld Refinement

The mineral phases present in Tagish Lake and their modal abundances determined by XRD and Rietveld refinement are provided in Table 3.1. The vol.% of each phase was calculated from the XRD results using the density of each mineral phase. Results show that the Tagish Lake specimens are comprised of forsterite, magnetite, pyrrhotite, enstatite, carbonates, and amorphous material in varying abundances (Table 3.1). Calcite was one of the carbonate phases detected, although the relative abundances are quite low. The errors associated with calcite for TL4 and TL10a are close to the detected values, implying that calcite may or may not have been detected during XRD in the refinement process for these two specimens. The same can also be said about enstatite in TL10a. Aragonite was detected in TL10a and TL4, but not in TL5b, TL11h, and TL11i. The similarity between the abundance and associated error of aragonite in TL4 and TL10a again suggests that aragonite may not actually be present; however, aragonite has been detected via XRD in Tagish Lake by Nakamura et al. (2003). Siderite was

also detected among the specimens; although, Blinova et al. (2014) states that they did not come across any siderite grains in their analysis. However, the presence of siderite has been reported in other Tagish Lake studies (Noguchi et al., 2002; Zolensky et al., 2002).

It is known from previous Tagish Lake studies that the matrix is dominated by a fine-grained mixture of saponite (smectite) and serpentine (e.g., Zolensky et al., 2002; Blinova et al., 2014). However, it is difficult to positively identify this fine-grained material in Tagish Lake using the Rietveld refinement method. The Rietveld method is not suitable for the characterization of clay minerals (i.e., saponite) for a number of reasons, including: (1) particle size is too fine-grained for single-crystal analysis; (2) clays have low symmetry (monoclinic and triclinic) and variable degrees of planar disorder; (3) chemical compositions vary due to cation substitutions; (4) the amount of molecular water in clays can vary; and (5) clays tend to have a preferred orientation (sit flat) rather than random orientation due to their platy characteristic (Brindley, 1980; Środoń et al., 2001; Gualtieri et al., 2008). With these limitations, it is very difficult to find a suitable fit for the diffraction pattern of clays. Blinova et al. (2014) were able to model their saponite-serpentine clay matrix using clinochlore as a best fit. Unfortunately, the clay bands from the XRD scans in this study were not adequate to be fit with a model for Rietveld refinement. In TL4 and TL10a there is an abundance of material that was modeled as "clays + amorphous" (Table 3.1) which is most likely saponite and serpentine. For comparison purposes, the abundance of clinochlore (saponite-serpentine) for TL5b, TL11h, and TL11i from Blinova et al. (2014) was added together with their amorphous abundances and reported as "clays + amorphous" in Table 3.1. TL11h and TL11i have relatively similar abundances of this material (50 wt.%), while TL10a, TL4, and TL5b have significantly less (TL10a > TL4 > TL5b).

Table 3.1. Bulk mineralogy of Tagish Lake from Rietveld refinement (XRD).

Mineral	Density (g/cm^3)[a]	TL4		TL10a		TL5b[b]		TL11h[b]		TL11i[b]	
		wt.%	vol.%	wt.%	vol.%	wt.%	vol.%	wt.%	vol.%	wt.%	vol.%
Forsterite	3.28	37.1(5.5)	40	29.2(2.5)	32	39	44	15	15	19	20
Magnetite	5.18	22.1(2.0)	15	26.2(1.5)	18	30	21	18	12	19	12
Pyrrhotite	4.60	7.6(2.0)	6	7.3(1.0)	6	3	3	n/d	n/d	n/d	n/d
Enstatite	3.20	11.6(4.5)	13	2.3(2.0)	3	8	6	8	6	4	3
Dolomite	2.84	n/d	n/d	n/d	n/d	2	3	n/d	n/d	n/d	n/d
Siderite	3.96	2.2(1.5)	2	11.2(1.5)	10	10	9	10	9	7	6
Calcite	2.71	1.6(1.5)	2	1.4(1)	2	2	2	0	1	1	1
Aragonite	2.95	1.3(1.5)	2	2.6(1.5)	3	n/d	n/d	n/d	n/d	n/d	n/d
Clays + amorphous	2.65	16.4(1.5)	22	19.7(2.5)	27	7.6	10.7	50	65	51	65
Total		100	100	100	100	100	100	100	100	100	100

[a] Density values from www.mindat.org. These densities are the same as those used in Blinova et al. (2014). The density for the clays + amorphous material is equivalent to the density of silica.

[b] XRD results from Blinova et al. (2014).

n/d = not detected

Vol.% values are calculated from wt.% and mineral densities.

3.4.2 TGA of Tagish Lake

The TGA and DTG curves for the Tagish Lake specimens from the two analytical sessions are shown in Figs. 3.2 and 3.3. To address the different DTG peaks, the results have been divided into temperature ranges corresponding to the decomposition of the mineral phases present in Tagish Lake (Table 3.2; Fig. 3.4). Dehydration of the Tagish Lake samples occurs between 30°C and 200°C. All the Tagish Lake samples have a DTG peak that occurs at ~75°C (Figs. 3.2, 3.3) which corresponds to the release of adsorbed H_2O (Yoldi-Martinez et al., 2011; Garenne et al., 2014); this is consistent with the TGA analysis of Tagish Lake by Yoldi-Martinez et al. (2011). The water released in this temperature range is not pertinent to aqueous alteration studies given that most of the water is terrestrial (Garenne et al., 2014). The next temperature range, 200°C to 400°C, is characteristic of the dehydroxylation of (oxy)-hydroxide minerals (Földvári, 2011; Garenne et al., 2014; King et al., 2015). However, for Tagish Lake the DTG peaks that occur between 200°C and 400°C (Figs. 3.2, 3.3) are not characteristic of (oxy)-hydroxides given that such minerals are not present in the pristine samples of Tagish Lake, as indicated by the XRD results in this study and the findings of Blinova et al. (2014). The DTG curve from TGA of Murchison insoluble organic matter reveals a break down occurring between 200°C and 420°C (Appendix A2.1), which is consistent with other organic studies of Murchison (Kerridge et al., 1987; Kebukawa et al., 2010). Therefore, the decomposition occurring in the Tagish Lake samples between 200°C and 400°C is attributable to the decomposition of organic matter. It is possible that some decomposition of pyrrhotite in this temperature region may occur (e.g., Garenne et al., 2014), but its contribution is expected to be minor, given the low relative abundance of pyrrhotite in these samples (Table 3.1).

Dehydroxylation of phyllosilicates (saponite and serpentine) in Tagish Lake has been designated to the temperature range of 400°C to 700°C. The majority of weight lost during TGA occurs in this temperature range (Table 3.2; Fig. 3.4). Other carbonaceous chondrite TGA studies have specified phyllosilicate dehydroxylation to occur over the temperature ranges of 400°C to 770°C (Garenne et al., 2014) and 300°C to 800°C (King et al., 2015). The TGA of saponite and serpentine mineral references completed in this study (Appendix A2.1), along with the findings of previous phyllosilicate dehydroxylation studies (Mielenz et al., 1953; Nozaki et al., 2006; Földvári, 2011; Lafay et al., 2012; Garenne et al., 2014; King et al., 2015),

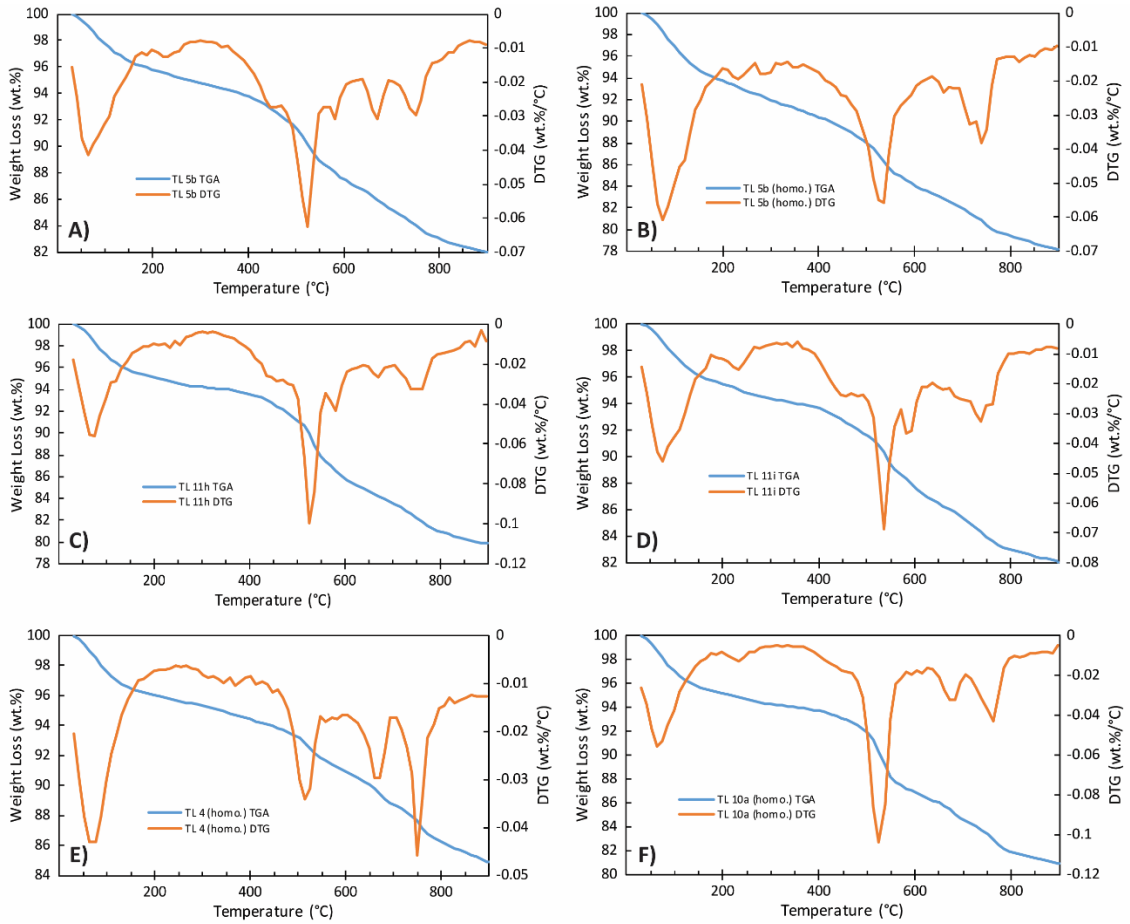

Fig. 3.2. TGA (blue) and DTG (orange) results for Tagish Lake between 30°C and 900°C from the first anayltical session. (A) TL5b; (B) Homogenized (homo.) TL5b; (C) TL11h; (D) TL11i; (E) TL4 (homo.); (F) TL10a (homo.).

reveal that both saponite and serpentine break down anywhere between 400°C and 850°C depending on their compositions. The 400°C to 700°C range for the dehydroxylation of the phyllosilicates in this study was constrained based on the findings of Nozaki et al. (2006), in which observations of bulk mineralogical changes in Tagish Lake via XRD between 400°C and 900°C revealed that saponite and serpentine were not present in Tagish Lake beyond 700°C. While the samples analyzed by Nozaki et al. (2006) are not the same as the ones analyzed in this study, the cut-off at 700°C is justified based on analysis of the same meteorite. Sulphides also break down between 400°C and 700°C (Garenne et al., 2014) which may possibly contribute to the weight loss in this temperature range. Comparing the DTG curves between 400°C and 700°C reveals similarities and differences between the results of the five Tagish Lake specimens (Figs. 3.2, 3.3). Results from both the TGA sessions show a DTG peak at ~525°C

present in all samples. The next DTG peak in the phyllosilicate temperature range occurs at ~580°C and is present in all the second TGA session samples (Fig. 3.3) as well as the first TGA session heterogeneous samples (TL5b, TL11h, and TL11i), but is absent in the homogenized samples (TL5b, TL4, and TL10a) (Fig. 3.2). The final peak occurring at ~675°C is found in all the specimens for both analytical sessions, except 11i. The ~675°C peak is absent in the first TGA session TL11i DTG curve (Fig. 3.2), and this corresponding peak temperature occurs at ~690°C in the second TGA session TL11i DTG curve (Fig. 3.3). The DTG temperature peaks between 400°C and 700°C for the two TGA sessions vary in intensity.

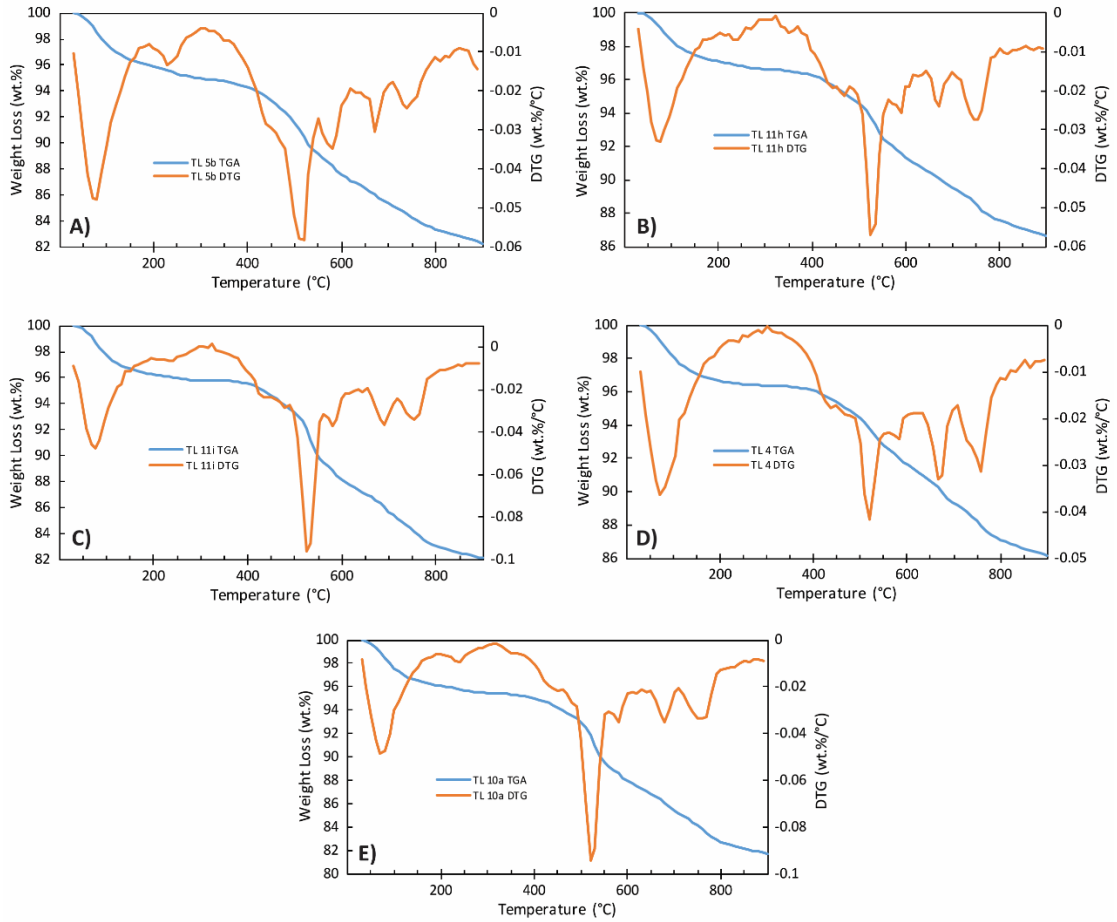

Fig. 3.3. TGA (blue) and DTG (orange) results for Tagish Lake between 30°C and 900°C from the second anayltical session. (A) TL5b; (B) TL11h; (C) TL11i; (D) TL4; (E) TL10a.

Table 3.2. TGA weight loss (wt.%) as a function of temperature for Tagish Lake.

	30 – 200°C (adsorbed water)		200 – 400°C (organics)		400 – 700°C (phyllosilicates)		700-900°C (carbonates)		Total Weight Loss		Weight Loss 200-900°C	
Specimen	1st Run	2nd Run	1st Run	2nd Run	1st Run	2nd Run	1st Run	2nd Run	1st Run	2nd Run	1st Run	2nd Run
5b	4.2 6.3*	4.1	2.0 3.3*	1.6	8.6 8.4*	9.0	3.2 3.8*	3.0	18.0 21.8*	17.7	13.8 15.5*	13.6
11h	4.9	2.9	1.5	0.8	10.1	6.7	3.7	2.9	20.2	13.3	15.3	10.4
11i	4.5	3.7	1.8	0.7	8.3	9.8	3.3	3.6	17.9	17.8	13.4	14.1
4	4.0*	3.3	1.6*	0.6	5.7*	6.8	3.8*	3.1	15.1*	13.8	11.1*	10.5
10a	4.8*	3.9	1.5*	1.1	9.1*	9.6	3.6*	3.7	19.0*	18.3	14.2*	14.4

* Indicates results acquired from samples that were crushed and homogenized by grinding in a mortar and pestle prior to analysis.

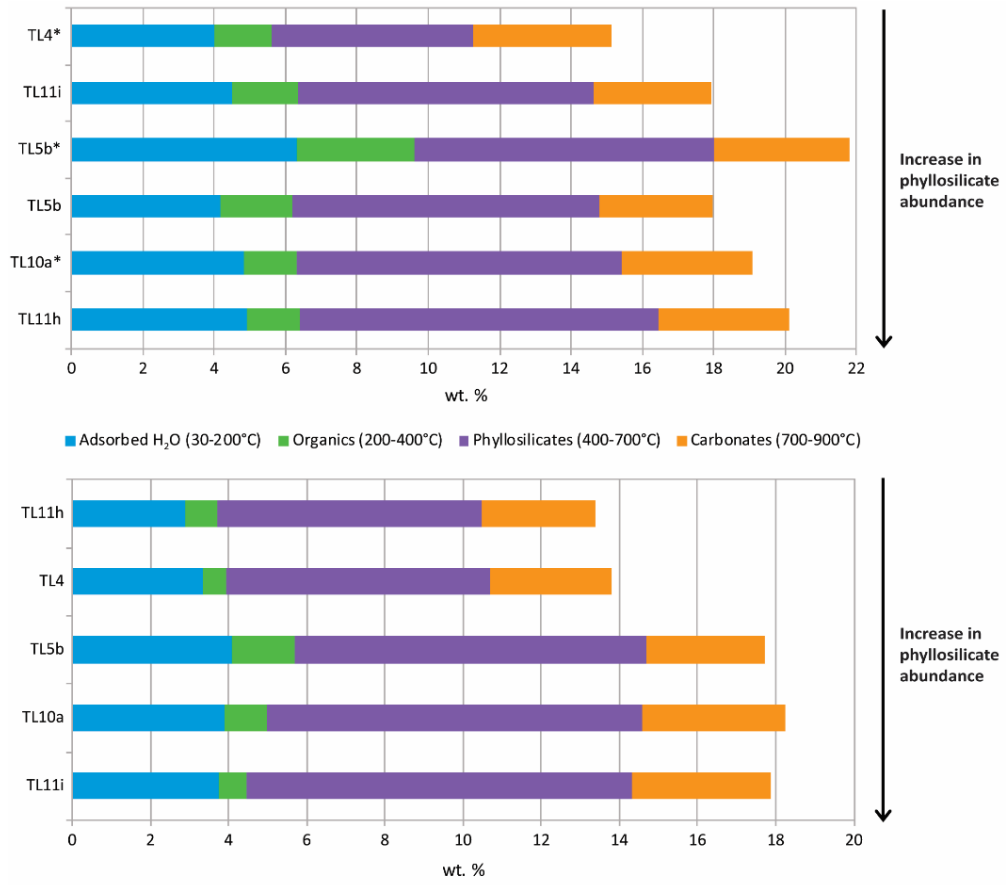

Fig. 3.4. TGA results divided into different temperature ranges corresponding to the weight loss of different mineral phases. The results are stacked based on the weight loss from the phyllosilicates (purple) between 400 – 700°C from least to greatest. **(Top)** First TGA session. Specimens marked with an asterisk (*) have been homogenized. **(Bottom)** Second TGA session.

The release of CO_2 from the decomposition of carbonates is also recorded by TGA and contributes to the total weight loss (Table 3.2; Fig. 3.4). Based on their composition, carbonates can decompose anywhere between 400°C and 1000°C (Appendix A2.1; Nozaki et al., 2006; Rodriguez-Navarro et al., 2009; Földvári, 2011; Garenne et al., 2014; King et al., 2015). Carbonate peak temperatures can be affected by the composition, crystallinity, and amount of a given carbonate mineral (Földvári, 2011). The weight loss corresponding to the release of CO_2 in Tagish Lake has been designated to temperatures between 700°C and 900°C following the temperatures specified by Garenne et al. (2014) (770°C to 900°C). One peak occurs in this temperature range at ~750°C for all Tagish Lake specimens (Figs. 3.2, 3.3). It is important to note, however, that Mg-Fe carbonate has been identified in the carbonate-rich lithology of Tagish Lake (Noguchi et al., 2002; Nakamura et al., 2003; Nozaki et al., 2006), including TL5b

(Blinova et al., 2014), which has been found to decompose at 600°C (Nozaki et al., 2006). Siderite, which is found to be relatively abundant among the Tagish Lake specimens (Table 3.1), also has low decarbonation temperatures (~450°C to 550°C; Appendix A2.1; Földvári, 2011). Therefore, it is possible that the weight loss recorded between 400°C and 700°C (Table 3.2) includes some weight loss due to decarbonation.

Under the assumption that the weight loss between 400°C and 700°C is solely from the dehydroxylation of phyllosilicates, hydrogen abundances were calculated from the OH weight loss in this temperature range (Table 3.3). Included in Table 3.3 are water/OH hydrogen abundances from Alexander et al. (2012) for comparison. The calculated values are generally in agreement with the accepted values. The H abundances calculated for TL11i are similar to the range reported by Alexander et al. (2012). Specimen TL11h shows the greatest variability in the calculated abundances, where only the result from the first TGA session is comparable to the accepted values. Similar calculated H abundances are observed between TL5b and TL10a; however, the calculated TL5b H abundances are significantly lower than the TL5b results from Alexander et al. (2012). Despite the inconsistency between the TL5b H abundances in this study and Alexander et al. (2012), the calculated H for TL5b is within the range of the reported H abundances for Tagish Lake (0.50-0.69 wt.%; Table 3.3). Specimen TL4 has the lowest calculated H abundances relative to the other specimens. The overall agreement between the H abundances from this study and Alexander et al. (2012) suggests that weight loss from mineral phases other than the phyllosilicates (i.e., carbonates, sulphides) between 400°C and 700°C is minimal.

Table 3.3. Calculated hydrogen abundances from phyllosilicate OH.

	Weight Loss 400 – 700°C		**H Abundance (wt.%)**		
	1st TGA Run	2nd TGA Run	1st TGA Run	2nd TGA Run	Alexander et al. (2012)
TL5b	8.6 8.4*	9.0	0.51 0.50*	0.53	0.68-0.69
TL11h	10.1	6.7	0.60	0.40	0.62-0.67
TL11i	8.3	9.8	0.49	0.58	0.50-0.57
TL4	5.7*	6.8	0.34*	0.40	-
TL10a	9.1*	9.6	0.54*	0.57	-

* Indicates results acquired from samples that were crushed and homogenized by grinding in a mortar and pestle prior to analysis.

3.4.3. IR Transmission Spectroscopy

The transmission spectra of Tagish Lake are shown in Fig. 3.5 between 5 and 25 μm. Included in Fig. 3.5 are spectra of reference minerals (olivine, saponite, serpentines, and carbonates) as well as the Orgueil (CI1), Murchison (CM2), and MET 01070 (CM1) carbonaceous chondrites. Phyllosilicate and olivine absorption features are of interest as the relative intensities of these features are indicative of the phyllosilicate/mafic silicate ratio, and consequently the extent of aqueous alteration (e.g., Beck et al., 2014; Garenne et al., 2014); the greater the phyllosilicate/mafic silicate ratio, the greater the degree of alteration.

Olivine (forsterite) in carbonaceous chondrites generally has characteristic absorption bands occurring at 11.2, 16.5, and 19.5 μm (Beck et al., 2014). In Fig. 3.5, the Tagish Lake specimens are stacked such that the olivine bands increase in intensity from bottom to top. Conversely, from top to bottom there is an increase in a phyllosilicate band occurring at 22 μm. The Tagish Lake spectra also reveal a phyllosilicate Si-O stretching mode at ~10 μm (Fig. 3.5). This 10 μm feature bears similarities to the saponite spectrum which has a doublet feature at higher wavelengths between 21 and 23 μm (Fig. 3.5). The 22 μm absorption band best seen in the TL11h and TL11i spectra has a subtle flat top (Fig. 3.5) which suggests that the spectra may be representative of saponite with a weak doublet feature at this wavelength. Further inspection of the Tagish Lake spectra confirmed the presence of a weak doublet feature in the 22 μm region; however, the wavelengths of the Tagish Lake doublet peaks are closer together (21.9 and 22.2 μm) than doublet peaks in both the saponite and Orgueil spectra (21.6 and 22.5 μm; Fig. 3.5, Beck et al., 2014).

Carbonates were detected in the Tagish Lake spectra from the presence of a feature at 7 μm (Fig. 3.5). Carbonates have four C-O vibrations that occur at 7 μm, 9.4 μm, 11.4 μm, and 14.7 μm (White, 1974; Izawa et al., 2010; Bonal et al., 2013). Based on the position of the 7 μm feature relative to the carbonate mineral references, the carbonate feature is indicative of dolomite, except for TL11i where the position of the 7 μm feature is indicative of calcite (Fig. 3.5). This is an interesting result given that dolomite and calcite are not abundant carbonates in Tagish Lake (Table 3.1). TL11i also stands out from the other specimens given that its spectrum has a feature occurring at 11.4 μm consistent with a carbonate rather than the 11.2 μm olivine feature (Fig. 3.5).

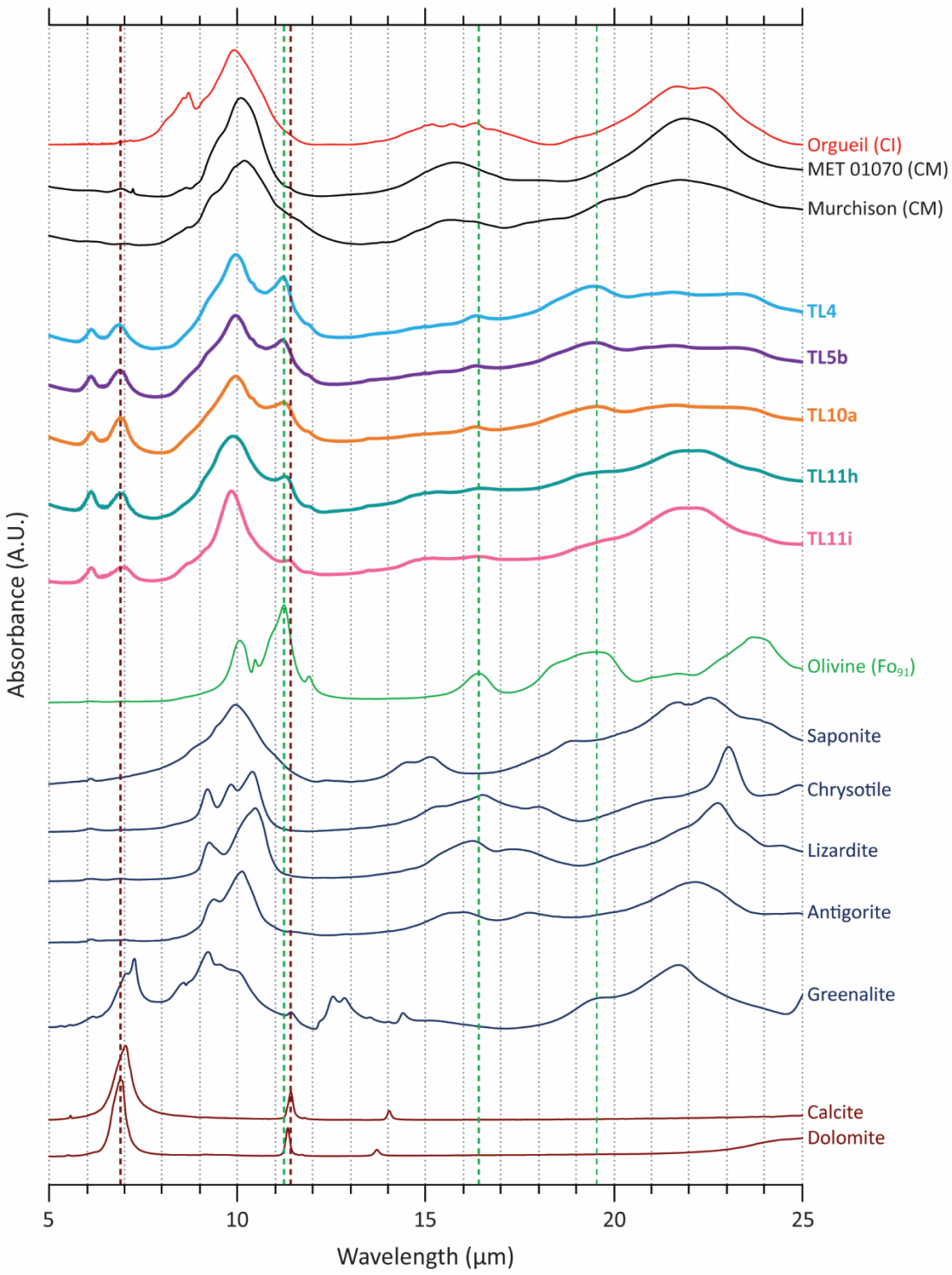

Fig. 3.5. IR spectra of the five pristine Tagish Lake specimens, Orgueil, MET 01070, Murchison, and mineral references (olivine, phyllosilicates, and carbonates). All spectra are courtesy of P. Beck from the Institut de Planétologie et d'Astrophysique de Grenoble. The Tagish Lake specimens are stacked in order corresponding to the increase in olivine features (11.2 µm, 16.5 µm, and 19.5 µm) from bottom to top.

It is clear from the IR spectra that there is diversity among the Tagish Lake specimens, which is consistent with the XRD (Table 3.1) and TGA (Table 3.2; Fig. 3.4) results. Based on qualitative analysis of the IR spectra, the phyllosilicate/olivine ratio for Tagish Lake increases in the order TL4 < TL5b = TL10a < TL11h < TL11i (Fig. 3.5).

3.4.4. Reflectance Spectroscopy

Reflectance spectra for TL5b, TL11h, TL4, and TL10a between 0.35 and 2.5 µm are shown in Fig. 3.6. The spectral slopes among the four specimens are variable, which is an interesting observation in itself given that spectral slopes are one of the characteristics used to distinguish between different asteroid types (DeMeo et al., 2009). Overall, the spectra of Tagish Lake are featureless despite the presence of an absorption band centered at 1.5 µm. This 1.5 µm feature is known as a spectral artifact which is a response of the detector due to a dip in sensitivity caused by an inadequate ratio of digital numbers between the standard and sample. The spectra acquired have a low signal-to-noise ratio which is attributable to the fact that Tagish Lake is not a very reflective material; it has a very low albedo, between 2 and 4% (Hiroi et al., 2001). Relatively featureless spectra with a low signal-to-noise ratio are characteristic of dark asteroids (Hiroi et al., 2001) such as D-, P-, T-, and C-type asteroids.

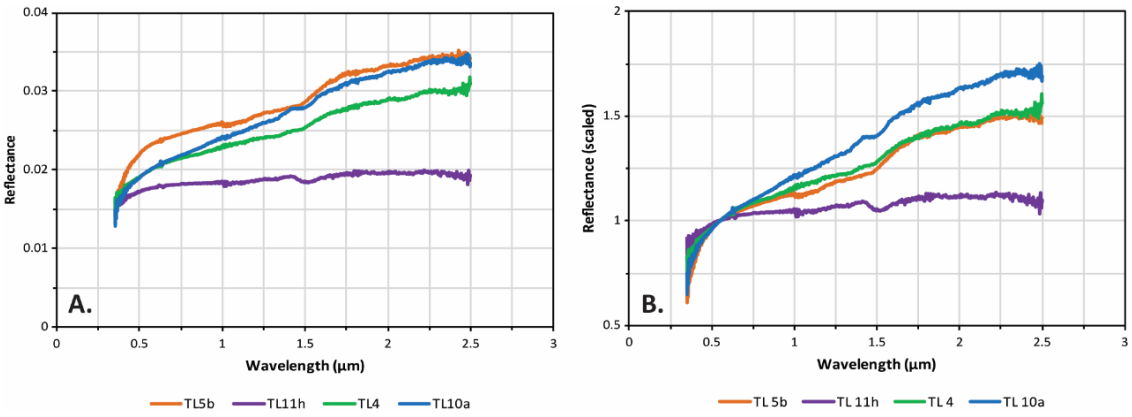

Fig. 3.6. (A) Tagish Lake reflectance spectra (0.35 to 2.5 µm). **(B)** Spectra scaled to 1 at 0.55 µm.

To match the Tagish Lake spectra to an asteroid type, the Bus-DeMeo classification system was used (DeMeo et al., 2009). The Bus-DeMeo classification system is an extension of the Bus (1999) classification system and classifies asteroid spectra measured between 0.45 µm

and 2.45 µm using Principle Component Analysis (PCA). PCA is a technique used to minimize the variance in a data set by transforming the co-ordinate system into two principle axes, known as principle components (i.e., PC1, PC2, PC3, etc.), to eliminate correlation of the data. In the DeMeo et al. (2009) study, 40 wavelength channels were transformed by PCA into 40 principle components where most of the variable data is contained in the first principle component (PC1) and the remaining variability is contained in PC2, PC3, PC4, and PC5. The reflectance data of the Tagish Lake specimens was input into the online Bus-DeMeo taxonomy classification tool created by MIT where classification is achieved by matching spectral slope and principle component values to reference data. By inputting the Tagish Lake reflectance data into the online classification tool, the slope and principle component values for each spectrum was obtained. Considering that spectral slope and principal component values overlap for some asteroid types, multiple asteroid types are output from the classification tool as possible matches. To illustrate the overlap, the slope and principle component values (PC1 and PC2) of the four Tagish Lake specimens are plotted with the 371 asteroids classified by DeMeo et al. (2009) in Fig. 3.7. In order to distinguish which asteroid type is the best match to the reflectance data, a visual inspection of the spectrum is required. DeMeo et al. (2009) developed specific criteria to follow during the visual inspection based on the presence (or absence) of characteristic absorption features.

The results of the Bus-DeMeo classification for the Tagish Lake spectra are found in Table 3.4. The variability in these results is not a surprise given the diversity in spectral slopes (Fig. 3.6), which is likely a consequence of the variance in composition, as indicated by the XRD results (Table 3.1). Distinguishing between a Xc-type and C-type from the Bus-DeMeo classification system for TL11h was difficult given how noisy its spectrum is (Fig. 3.6). In general, it is difficult to distinguish between the X- and C-type complexes (Appendix A2.2) because they overlap in their principle component values (Fig. 3.7; Bus, 1999). C-type asteroids are distinguished from Xc-type asteroids by a broad and shallow absorption feature that is centered between 1.0 and 1.3 µm (Fig. 3.8). The TL11h spectrum in Fig. 3.6 appears to dip around 1.0 µm, which could be an indication of the absorption feature characteristic of C-type asteroids. The spectrum of TL5b appears to have the broad 1.0 to 1.3 µm feature, and thus was classified as being a match to a C-type asteroid. TL4 does not appear to have the characteristic absorption feature of a C-type asteroid, or any other characteristic spectral features, and thus was classified as a X-type asteroid (Table 3.4; Fig. 3.7; Appendix A2.2)

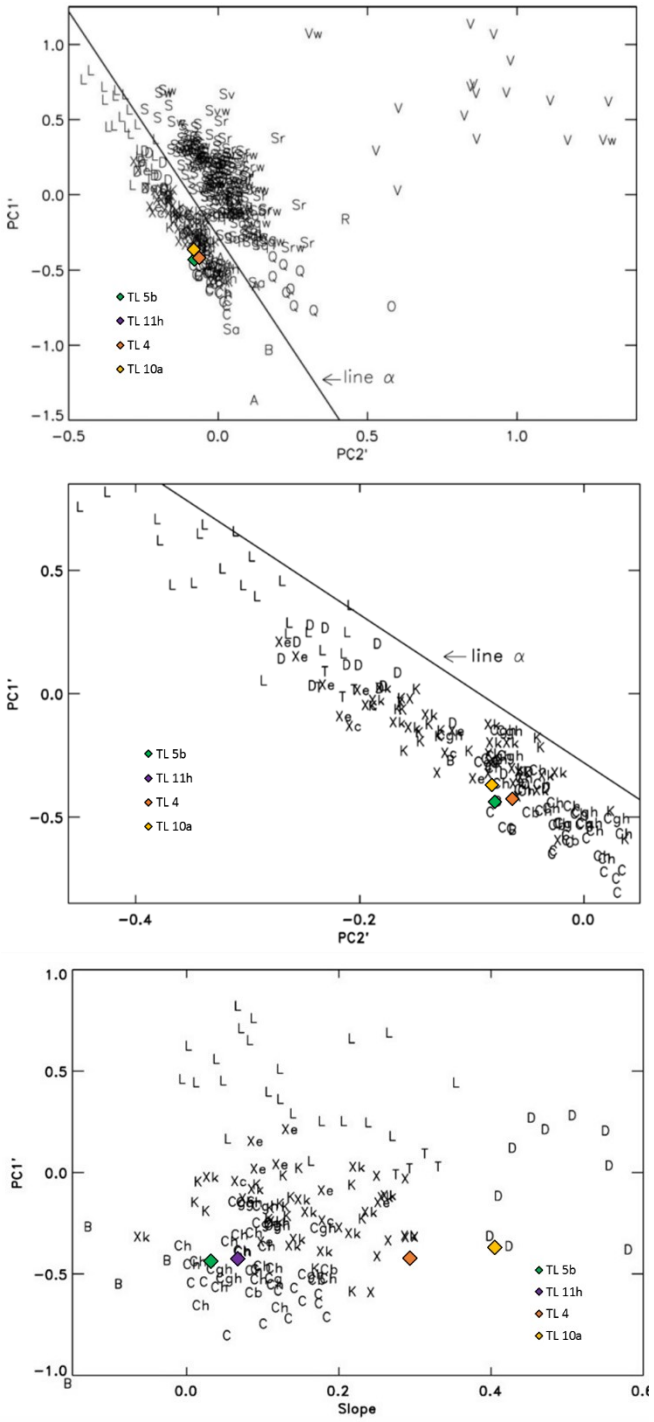

Fig. 3.7. (Top) Plot of the first two principle components with slope removed (PC1' and PC2') from the reflectance data of 371 asteroids by DeMeo et al. (2009). Line α represent the "grand divide" which splits the objects between those with and without the 2 μm absorption feature. Objects to the left of the line do not contain the 2 μm feature. The four Tagish Lake specimens have been included on this diagram and plot to the left of line α in the X- and C-complex cluster; TL4 and TL11h plot in the same location. The Tagish Lake principle component values were obtained from inputting the reflectance data into the online Bus-DeMeo taxonomy classification tool (MIT). **(Middle)** The same plot as the top diagram but to a different scale to better see the distribution of asteroids to the left of line α. **(Bottom)** A plot of PC1' vs. slope of the objects that plot left of line α. TL5b and TL11h plot in the C-complex cluster; TL4 plots near the X-type; and TL10a plots in the D-type field. Tagish Lake slope values were obtained from the online Bus-DeMeo Taxonomy classification tool (MIT). [figures from DeMeo et al., 2009]

based on its spectral slope. A D-type asteroid was matched with the reflectance data of TL10a based on its steep spectrum which is characteristic of D-type asteroids (Figs. 3.7, 3.8). For more information regarding the asteroid spectral matches (i.e., composition) refer to Appendix A2.2.

It should be noted that the Bus-DeMeo classification is designed specifically for asteroid spectral data, so caution is taken when assessing the validity of the asteroid spectral matches assigned to the Tagish Lake specimens. Furthermore, it is difficult to gather decent reflectance measurements in the lab for dark material, which can lead to difficulties in finding an asteroid match to the meteorite spectra. The results presented in this study were gathered in attempt to see how well the spectra compare to previous meteorite-asteroid connection studies which will be discussed in section 3.5.2.

Table 3.4. Bus-DeMeo classification of Tagish Lake reflectance data.

Specimen	Bus-DeMeo Classification
5b	C-type
11h	Xc-type or C-type
4	X-type
10a	D-Type

Bus-DeMeo classification determined from MIT online tool:
http://smass.mit.edu/busdemeoclass.html

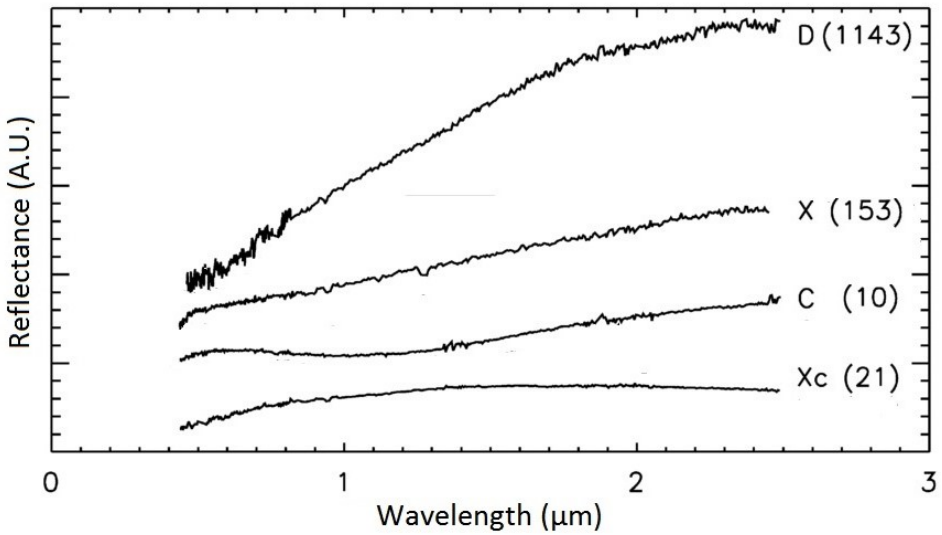

Fig. 3.8. Proto-type asteroid spectra of the spectral matches in Table 3.4. D-type – 1143 Odysseus; X-type – 153 Hilda; C-type – 10 Hygiea; Xc-type – 21 Lutetia. Image adapted from DeMeo et al. (2009).

3.5 Discussion

3.5.1. Aqueous Alteration via TGA and IR Spectroscopy

Qualitative analysis of the Tagish Lake IR spectra (Fig. 3.5) is in agreement with the reported aqueous alteration sequence of TL5b < TL11h < TL11i (Herd et al., 2011; Blinova et al., 2014). The decrease in the intensity of the olivine features and increase of the 22 μm phyllosilicate feature from top to bottom in the IR spectra (Fig. 3.5) correlates with an increase in aqueous alteration due to the replacement of olivine with phyllosilicates. It is evident from the spectra that the olivine present in Tagish Lake is forsterite-rich, consistent with XRD results (Table 3.1), based on absorption features at 11.2, 16.5, and 19.5 μm. The presence of an 11.4 μm carbonate feature in the TL11i spectra instead of the 11.2 μm olivine feature is consistent with there being less olivine in TL11i than the other Tagish Lake specimens (Table 3.1). The phyllosilicate bands (10 μm and 22 μm) in Tagish Lake appear to be saponite-like indicating that saponite is the prominent hydrous phase in Tagish Lake. The matrix of Tagish Lake is dominated by a fine-grained mixture of saponite and serpentine (Zolensky et al., 2002; Blinova et al., 2014). Classification of the phyllosilicate(s) causing the Si-O vibrations at 10 μm and 22 μm in other carbonaceous chondrites, notably CI and CM, has proven to be a difficult endeavor given that saponite and serpentine reference spectra are distinctly different from each other as well as from carbonaceous chondrite spectra at these wavelengths (Beck et al., 2010; Beck et al., 2014). The serpentine spectra have a complex band with sub-features occurring in the 10 μm region and a simple band at wavelengths between 20 and 25 μm, whereas saponite has a simple band at ~10 μm and a doublet feature around 22 μm (Fig. 3.5). Such a discrepancy between CM and CI phyllosilicate bands and phyllosilicate reference spectra has been attributed to the presence of a disordered, poorly crystalline phyllosilicate in the carbonaceous material; such phyllosilicates are known to have an unstructured absorption band around 10 μm (Beck et al., 2010; Beck et al., 2014). Alternatively, cation substitutions in serpentine (i.e., Al-Si and Mg-Al) can cause a broadening of the Si-O feature (Farmer, 1974) causing a saponite-like appearence. Regardless of the type of phyllosilicate(s) causing the 10 μm and 22 μm absorption bands in carbonaceous chondrite spectra, the presence of these two features (notably the 22 μm feature), along with the olivine bands, is very useful in determining the extent of aqueous alteration based on their intensity. From qualitative analysis of the Tagish Lake spectra, the relative intensity of the olivine and phyllosilicate bands are the same for TL5b

and TL10a (Fig. 3.5). This is not an unusual result considering these two specimens are macroscopically similar. TL4 has the most intense olivine features which implies that it is likely the least altered among the specimens. Based on these results, the intensity of the olivine and phyllosilicate features in the TL4 and TL10a spectra is strongly indicative of their relative alteration degrees.

The TGA results reveal that TL11h and TL11i have the greatest variability in the abundance of phyllosilicate water between the two TGA sessions (Table 3.2; Fig. 3.4). The significance of these variabilities is great given that the order of TL11h and TL11i relative to the other Tagish Lake specimens is different for each TGA session (Fig. 3.4); the order of TL4, TL5b, and TL10a remain constant between the two TGA sessions. Variability in phyllosilicate water abundances is also observed for TL4, but to a lesser extent. Mass differences of a given sample can result in weight loss discrepancies (Földvári, 2011); however, similar amounts of TL11h (12.1 mg and 12.9 mg) and TL11i (13.6 mg and 14.2 mg) were used in each TGA session. It is clear in this case that differences in sample amounts cannot explain the variable TGA results, especially considering that TL4 had a greater difference in sample amounts between the two runs (12.1 mg and 18.4 mg), yet has less variable phyllosilicate water abundances (Table 3.2). TL4 is an unusual specimen given its low phyllosilicate water (Table 3.2; Fig. 3.4) and hydrogen (Table 3.3) abundances relative to the other Tagish Lake specimens. These observed results for TL4 are likely in relation to its above-average grain density and porosity (Ralchenko et al., 2014). In this case, the greater porosity could account for less water, or there may be a greater abundance of non-hydrous minerals present in TL4. The latter scenario supports the case of TL4 being the least altered specimen, which is consistent with the IR spectroscopy results. Based on these observations, it is likely that TL4 represents a new lithology; a petrological study is needed to confirm this. The phyllosilicate water abundances between TL5b and TL10a are similar (Table 3.2; Fig. 3.4), which is also consistent with the IR spectra results. The minimal differences between the phyllosilicate water abundances for the homogenized and heterogenous samples of TL5b, TL4, and TL10a reveal that homogenization prior to TGA does not have a significant effect on the TGA results (Table 3.2; Fig. 3.4).

Comparing the modal abundances of minerals present in Tagish Lake derived from XRD, the relative proportions of forsterite to clays + amorphous material suggest that TL4 and TL10a are less altered than TL11h and TL11i (Table 3.1). TL10a has more clay + amorphous

material than TL5b, which is consistent with its slightly higher TGA phyllosilicate water abundances (Table 3.2). The similarity between TL5b and TL10a observed in the TGA and IR spectroscopy results supports the macroscopic observation that these two lithologies are similar. The relative proportions of forsterite between TL4 and TL5b are similar; however, TL4 has much more clays + amorphous material (Table 3.1). This observation is inconsistent with the TGA results and IR spectra considering that both methods indicate that TL4 is the least altered. In this case, it is likely that TL4 contains more amorphous material than clays. The presence of amorphous material has been proposed to be indicative of more primitive components, such as nebular condensates (e.g., Brearley, 1993; Chizmadia and Brearley, 2008); indeed, Blinova et al. (2014) argue – on the basis of Rietveld refinement results and detailed transmission electron microscope (TEM) studies of Tagish Lake matrix – that the presence of more amorphous material in TL5b is likely because it contains a relatively higher proportion of primitive, relatively unaltered material.

The discrepancy in TGA results for TL11h and TL11i suggest that these two specimens are lithologically heterogenous at the scale of sampling (e.g., Garenne et al., 2014); at least 1 gram of sample may be required to properly represent the overall lithology of TL11h and TL11i. Despite the variable TL11h and TL11i TGA results, there is no concern regarding the validity of the TGA results given that the order of TL4, TL5b, and TL10a is consistent among the TGA and IR spectroscopy results, and the calculated H abundances from the phyllosilicate water abundances are in general agreement with the literature (Table 3.3). On this basis, the results from TGA and IR spectroscopy provide sufficient evidence to incorporate TL4 and TL10a into the previously reported alteration sequence. The proposed alteration sequence from least to most altered is TL4 < TL5b ≤ TL10a < TL 11h < TL11i.

3.5.2. Parent Body Connection

Connecting Tagish Lake to an asteroid parent body is an important endeavor as such a connection can provide additional insight into Tagish Lake's extraterrestrial history including formation, organic chemistry, and parent body alteration processes. Although the Tagish Lake specimens are known to be genetically linked, matching Tagish Lake to a parent body is not an easy task given its dark nature and heterogenous composition evident by the diversity in

reflectance spectra (Fig. 3.6; Table 3.4). The heterogeneous composition of Tagish Lake is likely a result of the brecciation process(es) that occurred on the parent body.

Previous attempts to match Tagish Lake to a parent body was completed by Hiroi et al. (2001) and Hiroi and Hasegawa (2003). Initially, Hiroi et al. (2001) proposed that Tagish Lake's parent body asteroid was a D-type (Appendix A2.2) based on a spectral match and similar albedo between Tagish Lake and the D-type asteroid 368 Haidea. Later, Hiroi and Hasegawa (2003) re-visited the Tagish Lake parent body investigation to address the possibility of a T-type asteroid (Appendix A2.2) as a parent body. Hiroi and Hasegawa (2003) found that Tagish Lake also spectrally matched well with the T/D type asteroid 308 Polyxo (Fig. 3.9). Both Hiroi et al. (2001) and Hiroi and Hasegawa (2003) utilized the 3 μm hydration feature in their parent body investigations; however, acquisition of reflectance measurements for Tagish Lake beyond 2.5 μm were not possible in this study due to the darkness of the sample and small sample amounts available for analysis. It should be noted that all Tagish Lake reflectance spectra in Hiroi et al. (2001) and Hiroi and Hasegawa (2003) were acquired from powdered samples, including this study, whereas the reflectance spectra for the asteroids were obtained by telescopic measurements.

The findings from Hiroi et al. (2001) and Hiroi and Hasegawa (2003) have emphasized that different geometric viewing angles used for acquiring reflectance data can produce different results. Hiroi et al. (2001) found that Tagish Lake best matched the albedo of 368 Haidea when measured at viewing angles of i = 6° and e = -6°. These viewing angles differ in comparison from the angles used in this study which were i = 30° and e = 0°. Additionally, Hiroi and Hasegawa (2003) found that the reflectance of Tagish Lake increased in brightness with smaller incident angles. Heterogeneity of Tagish Lake was also a factor for reflectance measurements collected by Hiroi and Hasegawa (2003) as they found significant differences in the spectra of the same Tagish Lake sample measured twice ("old" and "new") with the same viewing geometry of i = 30° and e = 0° (Fig. 3.9). However, Hiroi and Hasegawa (2003) also found that the "new" sample measured with a viewing geometry of i = 14° and e = 0° compared reasonably well with the "old" (30, 0) sample (Fig. 3.9), which led them to conclude that variations in spectra due to changes in incident angles is minimal compared to the effects of sample heterogeneity. The spectra of the TL5b, TL11h, TL4, and TL10a overlain on the Hiroi and Hasegawa results (Fig. 3.9) supports the claim that heterogeneity has a strong influence on the

reflectance measurements. TL10a is the only spectrum that matches the spectra measured by Hiroi et al. (2001) and Hiroi and Hasegawa (2003); it is comparable to the (14,0) spectrum shortward of 1.4 µm, but is more similar to the old (30,0) spectra between 1.6 and 2.2 µm (Fig. 3.9). If such spectral heterogeneity as seen in Fig. 3.6 can occur under the same viewing geometries, it is most likely that Tagish Lake is too heterogeneous on the scale of sampling required for reflectance spectroscopy, which clearly makes the meteorite-parent body connection difficult.

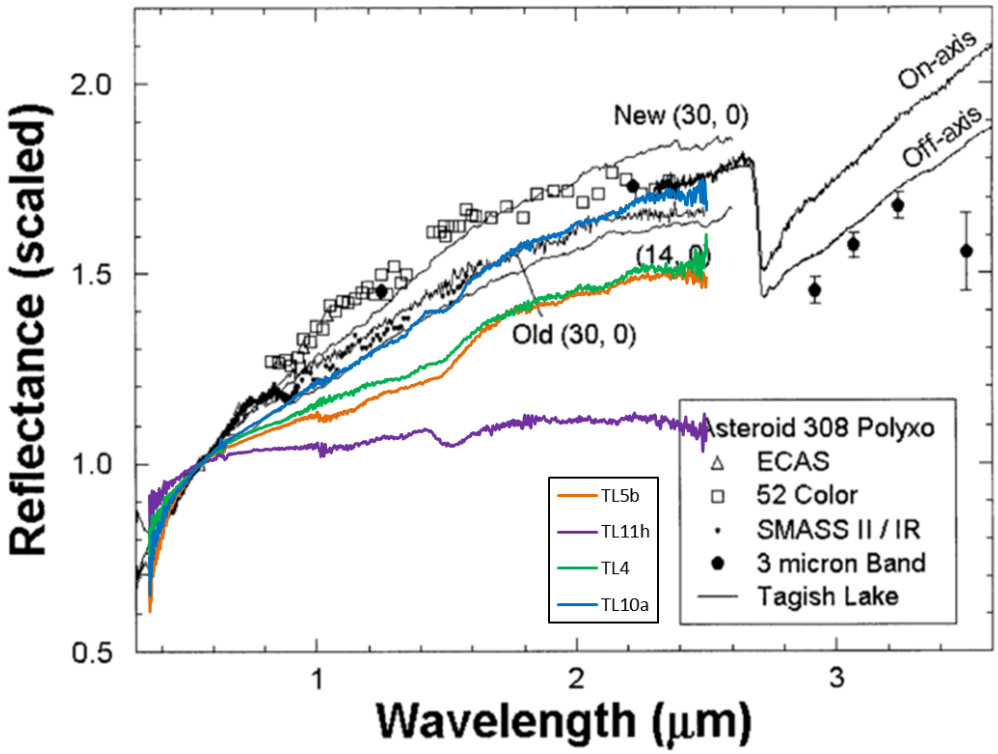

Fig. 3.9. Reflectance spectra of Tagish Lake compared to T/D asteroid 308 Polyxo from Hiroi and Hasegawa (2003). The Tagish Lake spectrum labelled as "Old" is from the Hiroi et al. (2001) study which was collected at viewing angles of i = 30° and e = 0°. The Tagish Lake "New" spectra are from Hiroi and Hasegawa (2003) obtained at incidence angles of 14° and 30° and an emergence angle of 0°. The Tagish Lake results from this study for TL5b, TL11h, TL4, and TL10a are overlain for comparison. The TL10a spectrum (D-type; Table 3.4) is the only spectrum from this study that matches with the Hiroi et al. (2001) and Hiroi and Hasegawa (2003) results. All Tagish Lake spectra were acquired from powdered samples whereas the spectra for 308 Polyxo was acquired by telescopic measurements. [from Hiroi and Hasegawa, 2003]

3.6 Future Work

The next endeavor in this Tagish Lake alteration study is to compare the extent of alteration among the five pristine Tagish Lake specimens to that of CM chondrites; the CM chondrites show a wide range in aqueous alteration (Beck et al., 2014; Garenne et al., 2014). To do this, quantitative analysis of the IR spectra is required. Such analysis is planned to be completed at the Institut de Planétologie et d'Astrophysique de Grenoble with the assistance of Pierre Beck. The goal of quantitative analysis is to obtain the relative abundance of phyllosilicate -OH (~3 μm) and olivine (11.2 μm) from the IR spectra by acquiring the band depths for these features; the greater the band depth, the greater the abundance. Comparison of the 3 μm and 11.2 μm band depths should be inversely correlated in relation to the extent of aqueous alteration (e.g., Beck et al., 2014). Similarly, the ratio of phyllosilicates (22 μm) to olivine (19.5 μm) can also be determined from quantitative analysis, which can be compared to the phyllosilicate water abundances obtained from TGA (Garenne et al., 2014). It is expected that the greater the TGA phyllosilicate water abundance of a given Tagish Lake sample, the greater the quantitative phyllosilicate/olivine ratio will be. By comparing the quantitative results to that of CM chondrites, the relative range of aqueous alteration between the different Tagish Lake specimens can be determined. It is anticipated that this range will be quite small given that the Tagish Lake specimens are genetically linked, whereas CM chondrites studied by others (e.g., Beck et al., 2014; Garenne et al., 2014) may not be, and thus span a wide range of TGA phyllosilicate water abundances and phyllosilicate/olivine ratios corresponding to different aqueous alteration degrees.

Further investigation into Tagish Lake's parent body is also likely to occur in an attempt to overcome the challenges associated with reflectance spectroscopy (low albedo; composition heterogeneity). One such endeavor may include the mixing of several Tagish Lake specimens together, or acquiring reflectance spectra at differing viewing geometries to see if a match can be made to a common asteroid parent body.

3.7 Conclusions

The analysis of Tagish Lake using TGA and IR spectroscopy has provided promising results in determining the extent of aqueous alteration among the five pristine specimens. The

diversity of the Tagish Lake specimens is reflected in both TGA and IR spectroscopy, which supports the usefulness of these analytical techniques for aqueous alteration studies. However, these methods are limited when it comes to identifying the mineral hosts of water in carbonaceous chondrites given that: 1) it is difficult to match DTG peaks to reference minerals as compositional variations of a given mineral can shift the DTG peak position (Földvári, 2011), and 2) discrepancies occur between the IR spectra of CM and CI chondrites and terrestrial phyllosilicates which are believed to be due to either the presence of disordered phyllosilicates or serpentine cation substitutions in carbonaceous chondrites (Farmer, 1974; Beck et al., 2010; Beck et al., 2014). Tagish Lake is an exception to the IR spectra phyllosilicate discrepancy because its spectra resemble saponite at ~10 μm and 22 μm, suggesting that saponite is likely the main hydrous phase in Tagish Lake.

Comparison of the TGA results and IR spectra reveals similarities in the relative order of the Tagish Lake specimens (i.e., TL5b, TL4, and TL10a), but also emphasizes variability at the scale of sampling relative to the scale of lithological variation (e.g., TL11h and TL11i). Consistencies between the XRD, TGA, and IR spectroscopy has provided enough reliable information to incorporate TL4 and TL10a into the original proposed alteration sequence of TL5b, TL11h, and TL11i (Herd et al., 2011; Blinova et al., 2014). The revised alteration sequence for the pristine Tagish Lake specimens is TL4 < TL5b ≤ TL10a < TL 11h < TL11i.

The diversity of the Tagish Lake specimens is also apparent in their reflectance spectra which have different spectral slopes (Fig. 3.6). Comparing the reflectance data to the Bus-DeMeo asteroid taxonomic system has provided several different possible asteroid matches to the different Tagish Lake specimens (D, C, X, or Xc types). Previous work by Hiroi et al. (2001) and Hiroi and Hasegawa (2003) has suggested that Tagish Lake's parent body is possibly a D- or T-type asteroid, but also emphasized the effects that compositional heterogeneities have on the spectra. Therefore, because Tagish Lake is compositionally heterogeneous with a very low albedo, difficulties arise when trying to constrain its parent body.

Chapter 4. Implications for Asteroid Mining and Conclusions

In the last five years, the asteroid mining industry has taken both the media and scientific community by storm. With the possibility of a sci-fi fantasy becoming a reality and the great innovations this industry can offer to the space industry, asteroid mining has gained the support of many investors and scientists all over the world. The groundwork necessary to bring asteroid mining to fruition is already underway by private space exploration companies (e.g., Planetary Resources and Deep Space Industries), and NASA and its partners have become invested in research projects pertaining to In-Situ Resource Utilization (ISRU). Similar to terrestrial mining, mineral exploration is a key step in the asteroid mining process. However, asteroid miners do not have the luxury of visiting "outcrops" to assess their economic potential, and therefore must rely on compositional studies of meteorites and spectral data to select valuable asteroid targets. As such, the diverse studies completed in this master's project have direct implications to the asteroid mining industry. By studying meteorites, asteroid miners can understand what type of resources are available in asteroid parent bodies and identify valuable asteroid targets with the help of the meteorite-asteroid spectral connection.

Asteroids are rich sources of volatiles, metals, and semiconductors. The relative abundances of these materials are variable and dependent on an asteroid's composition; therefore, some asteroids are more valuable than others. For example, M-type asteroids, thought to be remnants of differentiated iron cores, are a valuable source of metal, while C-type asteroids with compositions similar to carbonaceous chondrites are of interest for volatiles and water. In regards to the most desirable resources in asteroids, water is top of the list. Water can provide both rocket propellant and radiation shielding necessary for transportation purposes, and is also an essential commodity for sustaining life (Nichols, 1993; Ross, 2001; Elvis, 2014; Lewis, 2015). The volatiles which can be extracted from primitive, carbonaceous asteroids include elements essential for life (C, H, N, O, P, and S) and other components such as hydrocarbons, NH_3, and CO_2 (Nichols, 1993; Ross, 2001; Lewis, 2015). The extraction of Fe and Ni from asteroids is of interest mainly for construction material to be used in space (Ross, 2001; Lewis, 2015); extraction of these metals also supplies Co as well as byproduct PGEs (Lewis, 2015). Due to their relative scarcity on Earth, the PGEs are likely the only material to be extracted from asteroids that will be worthwhile to transport back to

Earth (Kargel, 1994; Ross, 2001; Sanchez and McInnes, 2012; Lewis, 2015). Semiconductors (i.e., Si, Al, Ga, Cu, etc.) are also valuable materials to be mined for the production of solar power cells (Sastri and Duke, 1992; Ignatiev et al., 2001).

Among the asteroids in the solar system, the near-Earth asteroids (NEAs; asteroids with orbits that cross <1.3 AU from the Sun) are the desired targets for initial asteroid mining ventures. It has been estimated that the resources available from the total NEA population alone could sustain 400 billion people until the death of the Sun (Lewis, 2015). NEAs are asteroids derived from the Main Belt (between the orbits of Mars and Jupiter) that obtain near-Earth orbits by entering into a Kirkwood gap (regions in the asteroid belt with very few asteroids) where the resonance effects of Jupiter cause their orbits to change (e.g. Shoemaker et al., 1979). Consequently, the NEAs are populated with many different spectral types (i.e., C, X, D, S, etc.); however, the S (stony), V (vestoid), C (carbonaceous), and X (some metallic) complexes are the most abundant among the NEAs (Binzel et al., 2004; DeMeo et al., 2009; Carry et al., 2016). Besides the vast resources available, the NEAs are considered desirable targets largely in part due to the minimal energy required to reach them. When considering how to get a spacecraft to a solar system object, energy is expressed as 'delta V', which is the change in velocity required to get from one object to another. The delta V necessary to reach many NEAs – e.g., from low-Earth orbit (LEO) to the object – is variable among the NEA population (Davis et al., 1993; Elvis et al., 2011). There are approximately 16,000 known NEAs (CNEOS Discovery Statistics, 2017) in which approximately 3200 have a delta V less than the Moon (6.0 km/s) (Benner, 2017). Of these 3200 NEAs, roughly 200 have a delta V < 4.5 km/s (Benner, 2017), which is referred to as ultra-low delta V (Elvis et al., 2011). In terms of diameter, there are over 500 NEAs with diameters ≥ 100 m that are more feasible to reach than the moon (delta V < 6 km/s); 9 of these are greater than or equal to 1 km (Benner, 2017). (Note that these estimates are based on the magnitude (H) of the asteroids (100 m = ~22.5 H; 1 km = ~17.5 H) assuming average albedo.) With the discovery of new NEAs occurring regularly, these estimates are destined to increase over time. Based on ultra-low delta V constraints, it has been estimated that out of the near-Earth object (NEO; includes asteroids and comets) population there are approximately 10 metallic NEOs and 18 carbonaceous NEOS greater than 100 m that would contain profitable PGE-ore and water-ore, respectively (Elvis, 2014). Given that water is so concentrated in the carbonaceous NEOs, only an 18 m carbonaceous NEO is required for a profit (Elvis, 2014); this brings the total number of water-

ore bearing NEOs to ~9000. It should be noted that these estimates by Elvis (2014) are not concrete as a small change in the variables used in his calculations can significantly change the number of NEOs. For example, changing the delta V from 4.5 km/s to 5.5 km/s for the carbonaceous NEOs (D = 18 m) results in ~90,000 potentially water-ore bearing NEOs (Elvis, 2014).

The carbonaceous NEAs are considered to be jackpot targets for asteroid mining. The compositional studies of carbonaceous chondrites have provided great insight into the wealth of water and life-sustaining volatiles that can mined from their primitive parent bodies. It is commonly reported in the literature that carbonaceous chondrites contain up to 20 wt.% water; however, such an amount appears to be representative of both adsorbed and bound water (e.g., Wiik, 1956; Jarosewich, 1990). When trying to assess how much water could potentially be mined from a carbonaceous asteroid, adsorbed water must be factored out of the equation considering that it is inherited terrestrially. The use of TGA or other step-wise heating techniques is useful for such an assessment as the type of water (i.e., adsorbed water, structural water, hydroxyl (-OH) groups) can be readily distinguished based on the weight loss occurring at different temperatures (Chapter 3). The extent of terrestrial weathering also must be considered as the abundance of hydrated minerals can be affected by such a process (e.g., Zolensky and Gooding, 1986); analyzing water abundances in meteorite falls (e.g., Tagish Lake) is most ideal. From the Tagish Lake study in Chapter 3, the greatest weight loss corresponding to the dehydroxylation (-OH loss) of phyllosilicates was 10 wt.%. Comparatively, TGA of CM chondrites by Garenne et al. (2014) showed a phyllosilicate -OH loss as high 13 wt.%. On the basis of these findings, as well as the H abundances in water/OH from Alexander et al. (2012, 2013), it appears that at most anywhere between 8 wt.% and 23 wt.% water in the form of hydroxyl (-OH) could potentially be extracted from the phyllosilicates in the most altered carbonaceous asteroids (i.e., CM and CI). As for the amount of volatiles that could be mined, Lewis (2015) claims that 46% or more of the total carbonaceous chondrite mass is attributable to volatiles. This amount is alarmingly high and not reflected in carbonaceous chondrite TGA. Assessing the total amount of mass lost between 200°C and 900°C (including bound water and organics/volatiles but excluding adsorbed water) reveals that carbonaceous chondrites lose 10 to 20% of their original weight depending on how heavily they have been altered (Chapter 3; Garenne et al., 2014; King et al., 2015). The breakdown of minerals occurs primarily between 200°C and 900°C (Chapter 3),

and with the decomposition of organics between 200°C and 400°C it is hard to imagine an additional 20 wt.% or so of volatiles available for extraction from carbonaceous material at temperatures >900°C, even with the possibility of decarbonation at these higher temperatures (e.g., Földvári, 2011). Lewis and Hutson (1993) state that autoreduction of iron oxides via carbon accounts for 40 wt.% of the total abundance of HCNO volatiles. This autoreduction process leaves a largely silicate residue with about 30% Fe-Ni metal (~20% of the original chondrite mass) (Lewis, 1996; Lewis, 2015). A review of TGA curves for Tagish Lake (Chapter 3) and CM and CI chondrites (Garenne et al., 2014; King et al., 2015) reveals that the formation of Fe-Ni metal, if any, does not result in a mass gain (i.e., an increase in the TGA curve). Conversely, some CR chondrites do show an increase in mass with increasing temperature, but this is attributed to chondrule mineralogy (Garenne et al., 2014), not autoreduced Fe-Ni metal. Given these observations, the formation of ~20 wt.% Fe-Ni metal seems quite high, especially with C as the limiting reagent. Tagish Lake, for example, has the highest C abundance among the carbonaceous chondrites (6 wt.%; Grady et al., 2002), and under the assumption that all the C (graphite) is used to reduce the iron oxides, the most Fe-metal that could be produced is 6 wt.% given a 1:1 mol ratio of FeO and C ($FeO + C \rightarrow CO + Fe^0$).

In terms of iron and nickel, the metallic iron NEAs are most desirable, especially considering that a metallic asteroid only 100 m in diameter contains enough byproduct PGEs to be a profitable target (e.g., Elvis, 2014). However, the material processing of metallic asteroids is challenging given that the metal is extremely tough and difficult to crush; iron meteorites have a crushing strength of 3600 bars (Lewis, 1992; Kargel, 1994; Lewis, 2015). Alternatively, ordinary chondrites have crushing strengths between 60 and 2600 bars (Lewis, 1992), and therefore would likely be a more cost efficient material to mine for iron, nickel, and PGEs. The potential to extract PGEs from metal has a special hierarchy relative to the other asteroid resources given that the PGEs are rare on Earth and very expensive to extract from the crust (Kargel, 1994). The PGEs are currently used for chemical production and petroleum refining catalysts, jewelry, medical and dental applications, electronic hardware, manufacturing of glass, and laboratory equipment (U.S. Geological Survey, 2017). The production of PGEs from asteroid material could reduce the market price of the PGEs (e.g., Pt currently valued at around $1000 USD/oz at the time of writing; Platinum Prices, 2017) and enable the production of new technologies that are currently on hold due to the high cost of

PGEs (Kargel, 1994); this is provided that profit is higher than transportation costs and the influx of PGEs does not crash the market. The amount of PGEs and Re in the NEA population is estimated to be worth $70,000 trillion USD (Lewis, 2015).

The PGE study in Chapter 2 was completed with intentions to provide relative abundances of PGEs in the metal phases of ordinary chondrites to be utilized in the assessment of PGE extraction from their parent body. Given that ordinary chondrites at most contain 20 wt.% Fe-Ni metal (Dunn et al., 2010), a 100 m diameter ordinary chondrite parent body is not going to be nearly as profitable a PGE-ore as a 100 m metallic asteroid. However, this is not really a concern given that ordinary chondrites are not differentiated, and therefore contain substantially greater PGE concentrations than can be found in the Earth's crust (Lewis, 2015). It has been estimated that 99.8% of the PGEs on Earth reside in the core (Lorand et al., 2008). However, there are a few known terrestrial deposits where the PGEs are enriched in concentrations that are considered profitable. For example, the Bushveld Igneous Complex in South Africa – one of the world's leading PGE producers – has ore grades between 2 and 6 ppm of Pt, Pd, Rh, and Au combined (Bushveld Igneous Complex, 2017). Elvis (2014) suggests that the grade of Ir in a metallic body specifically needed to match the terrestrial grade would be anywhere between 0.3 and 0.9 ppm. The LA-ICP-MS Ir results for ordinary chondrite kamacite from this study are around 2 ppm and up to 10 ppm in taenite (Chapter 2), which correspond to a bulk rock grade of 0.2 to 0.6 ppm (Appendix 3). Total Pt, Pd, Rh and Au in ordinary chondrites ranges from 1.0 to 2.5 ppm, based on results from this study (Appendix 3). Therefore, it is clear that the concentration of PGEs in ordinary chondrite metal are comparable to abundances in the richest terrestrial deposits. The question now becomes which ordinary chondrite parent body would be best to target. Kargel (1994) has argued that the LL chondrite parent body would be the best target given that LL chondrites can contain up to 220 ppm PGEs and Au. However, this estimate is based on bulk metal concentrations which are largely dependent on the relative proportion of taenite to kamacite (Chapter 2). The PGE study in this thesis has revealed that the variability of PGE concentrations among the ordinary chondrites is not as extreme as originally thought. When averaged, the PGE concentrations are similar among the H, L, and LL chondrites for the respective metal phases (Chapter 2). In this case, the issue of which ordinary chondrite parent body is best for mining becomes irrelevant. I conclude, however, that because PGEs

are byproducts of mining iron and nickel, the H chondrite parent body is the better target given the relatively high abundance of Fe-Ni metal in H chondrites.

Water is, without a doubt, the most precious resource for space exploration as it is critical for sustaining life. However, sending water up to space comes with a very expensive price tag; so expensive in fact that NASA has resorted to recycling water on the International Space Station (Wiedemann, 2014). Since NASA has implemented the use of private companies for space launches, putting the shipping costs of water into perspective depends on which launch company is employed. On this basis, it costs anywhere between $9,000 and $43,000 USD per pound to ship cargo to LEO (Kramer and Mosher, 2016). In other words, that is $43,000 to send one bottle of water! The goal of extracting water from asteroids is to reduce these costs. It is estimated that water could be sold in space for $5,000 USD per kilogram (~$2300/lb) in LEO or for $10,000 USD per kilogram (~$4500/lb) in geostationary orbit (Elvis, 2014). The cost of water would become almost 4 times less than what it currently is to ship to LEO.

The aqueous alteration study completed in Chapter 3 is valuable in terms of material processing for asteroid mining. Conducting TGA on carbonaceous chondrites (Tagish Lake in this case) is useful for understanding and estimating how much water could be extracted from a given carbonaceous asteroid that has undergone parent body alteration. Asteroids that have undergone higher aqueous alteration degrees (i.e., CI and CM chondrite parent bodies) are going to provide the most water. DTG curves provide insight into what temperatures are needed for water and OH extraction from hydrous minerals. It appears that temperatures as high as 700°C are needed for the extraction of OH, and even higher temperatures are necessary to extract additional volatiles (i.e., CO_2 from calcite; Chapter 3). With this being said, petrological studies of carbonaceous chondrites are still critical for assessing the economic potential of water-bearing asteroids. Knowing the exact type of hydrous minerals in a given carbonaceous chondrite will provide additional insight into the how the water is bound in mineral crystal structures. Additionally, the chemical composition of a given mineral can affect the temperature at which it breaks down and water is released (Földvári, 2011), so having a general idea of mineral compositions is also critical for asteroid mining. Transmission infrared spectroscopy is a useful method for such an investigation (Chapter 3). Since water and metal are both sought-after commodities in asteroid mining, the

question of whether a carbonaceous parent body with both water and metal (i.e., CR or CH) would be a suitable target comes to mind. CR chondrite parent bodies look promising for such an endeavor considering that CR chondrites are altered to the same degree as CI and CM chondrites (Chapter 1); however, TGA of CR chondrites has revealed that it is difficult to determine the amount of water as the increase in temperature results in a mass gain (Garenne et al., 2014) which in turn could have serious repercussions in the extraction process. Therefore, I propose that the CM or CI carbonaceous asteroid types are targeted specifically for water and volatile extraction, while ordinary chondrite-like asteroids (and possibly iron meteorites) are mined for metal.

There is still much that is needed to done before asteroid mining can become a reality, yet the work being done by asteroid mining companies and scientists are pointing the industry in the right direction. The next step forward in terms of meteorite studies would be compiling a comprehensive database of meteorites whose parent body compositions are most ideal for mining purposes (i.e., carbonaceous chondrites, ordinary chondrites). For the PGEs, the database should consist of *in situ* measurements of kamacite and taenite in a large suite of ordinary chondrites to fully understand the concentrations and variability of PGEs and other trace elements beyond what has been started in Chapter 2, especially regarding taenite concentrations in the H and L chondrites. It would also be valuable to include relative proportions of kamacite and taenite for each ordinary chondrite as these proportions are important for determining how much PGEs can be extracted from a given ordinary chondrite parent body. As for the water and volatile database, there should be a collection of TGA measurements, volatile abundances, XRD/Rietveld refinement results, and infrared spectra of CI and CM chondrites to extend the investigation on the affects that aqueous alteration has on the abundance of valuable constituents in carbonaceous materials. These databases will provide scientists and asteroid miners with the necessary data to make informative decisions when it comes to selecting asteroid targets. In addition to these databases, it is also very important to improve on the meteorite-asteroid connection using reflectance spectroscopy. As seen in Chapter 3, a variable-composition meteorite like Tagish Lake makes it difficult to narrow down a parent body match. This is mostly due to the fact that carbonaceous asteroids are very dark objects making it difficult to get decent reflectance data. It is crucial to further investigate such poor resemblances of laboratory spectra to asteroid spectra, specifically the carbonaceous objects, in order to confidently identify potential targets. The use of small

("cubesat") satellites can aid in this investigation as they can provide close-up images and spectra of an asteroid of interest that can be used in confirming the composition. Furthermore, the OSIRIS-REx mission, which launched in September 2016, is expected to return valuable data regarding the meteorite-asteroid connection issue. The work completed in this master's thesis has laid the foundation for further research of the valuable resources within chondrite meteorites and as such is an important contribution to asteroid mining industry.

References

Afiattalab F. and Wasson J. T. (1980) Composition of the metal phases in ordinary chondrites: implications regarding classification and metamorphism. *Geochim. Cosmochim. Acta* **44**, 431–446.

Alexander C. M. O., Bowden R., Fogel M. L., Howard K. T., Herd C. D. K. and Nittler L. R. (2012) The Provenances of Asteroids, and Their Contributions to the Volatile Inventories of the Terrestrial Planets. *Science* **337**, 721–723.

Alexander C. M. O. D., Howard K. T., Bowden R. and Fogel M. L. (2013) The classification of CM and CR chondrites using bulk H, C and N abundances and isotopic compositions. *Geochim. Cosmochim. Acta* **123**, 244–260.

Beck P., Garenne A., Quirico E., Bonal L., Montes-Hernandez G., Moynier F. and Schmitt B. (2014) Transmission infrared spectra (2-25µm) of carbonaceous chondrites (CI, CM, CV-CK, CR, C2 ungrouped): Mineralogy, water, and asteroidal processes. *Icarus* **229**, 263–277.

Beck P., Garenne A., Yin Z., Bonal L., Quirico E., Schmitt B., Montagnac G., Chiriac R. and Toche F. (2013) Thermal History of Sutter's Mill CM Carbonaceous Chondrite Fall From Water-Abundance and the Structure of its Organic Matter. *Lunar Planet. Sci. XLIV.* Lunar Planet. Inst., Houston. #1521(abstr.).

Beck P., Quirico E., Montes-Hernandez G., Bonal L., Bollard J., Orthous-Daunay F. R., Howard K. T., Schmitt B., Brissaud O., Deschamps F., Wunder B. and Guillot S. (2010) Hydrous mineralogy of CM and CI chondrites from infrared spectroscopy and their relationship with low albedo asteroids. *Geochim. Cosmochim. Acta* **74**, 4881–4892.

Bell J. F., Davis D. R., Hartmann W. K. and Gaffey M. J. (1989) Asteroids: The big picture. In *Asteroids II* (eds. R. P. Binzel, T. Gehrels, and M. S. Matthews). University of Arizona Press, Tuscon. pp. 921–945.

Benner L. A. M. (2017) Near-Earth Asteroid Delta-V for Spacecraft Rendezvous. *NASA JPL.* Available at: http://echo.jpl.nasa.gov/~lance/delta_v/delta_v.rendezvous.html [Accessed March 4, 2017].

Binzel R. P., Rivkin A. S., Stuart J. S., Harris A. W., Bus S. J. and Burbine T. H. (2004) Observed spectral properties of near-Earth objects: Results for population distribution, source regions, and space weathering processes. *Icarus* **170**, 259–294.

Bland P. A., Cressey G. and Menzies O. N. (2004) Modal mineralogy of carbonaceous chondrites by X-ray diffraction and Mössbauer spectroscopy. *Meteorit. Planet. Sci.* **39**, 3–16.

Blinova A. I., Zega T. J., Herd C. D. K. and Stroud R M. (2014) Testing variations within the Tagish Lake meteorite – I: Mineralogy and petrology of pristine samples. *Meteorit. Planet. Sci.* **49**, 473–502.

Bonal L., Alexander C. M. O. D., Huss G. R., Nagashima K., Quirico E. and Beck P. (2013) Hydrogen isotopic composition of the water in CR chondrites. *Geochim. Cosmochim. Acta* **106**, 111–133.

Boss A.P. and Ciesla F.J. (2014) 2.3 - The solar nebular. In *Treatise on Geochemistry, 2nd Edition* (eds. H. Holland and K. Turekian). Elsevier, Oxford. pp. 37–53.

Brearley A. J. (1993) Matrix and fine-grained rims in the unequilibrated CO3 chondrite, ALHA77307: Origins and evidence for diverse, primitive nebular dust components. *Geochim. Cosmochim. Acta* **57**, 1521–1550.

Brearley A. J. and Jones R. H. (1998) Chondritic meteorites. In *Reviews in Mineralogy, Vol. 36: Planetary Materials* (ed. J. J. Papike). Mineralogical Society of America, Washington. pp. 3-1–3-398.

Brenan J. M. and McDonough W. F. (2009) Core formation and metal-silicate fractionation of osmium and iridium from gold. *Nat. Geosci.* **2**, 798–801.

Brindley G. W. (1980) Quantitative X-Ray Mineral Analysis of Clays. In *Crystal Structures of Clay Minerals and their X-ray Identification* (eds. G. W. Brindley and G. Brown). Mineralogical Society, London. pp. 411–438.

Britt D. T., Bell J. F., Haack H. and Scott E. R. D. (1992) The reflectance spectrum of troilite and the T-type asteroids. *Meteoritics* **27**, 207.

Brown P. G., Revelle D. O., Tagliaferri E. and Hildebrand A. (2002) An entry model for the Tagish Lake fireball using seismic, satellite and infrasound records. *Meteorit. Planet. Sci.* **37**, 661–676.

Brown P. G., Hildebrand A. R., Zolensky M. E., Grady M., Clayton R. N., Mayeda T. K., Tagliaferri E., Spalding R., MacRae N. D., Hoffman E. L., Mittlefehldt D. W., Wacker J. F., Bird J. A., Campbell M. D., Carpenter R., Gingerich H., Glatiotis M., Greiner E., Mazur M. J., McCausland P. J. A., Plotkin H. and Rubak Mazur T. (2000) The fall, recovery, orbit, and composition of the Tagish Lake meteorite: A new type of carbonaceous chondrite. *Science* **290**, 320–325.

Browning L. B., McSween H. Y. and Zolensky M. E. (1996) Correlated alteration effects in CM carbonaceous chondrites. *Geochim. Cosmochim. Acta* **60**, 2621–2633.

Buchwald V. F. (1975) *Handbook of iron meteorites: History, distribution, composition and structure*. Berkeley: University of California Press.

Bunch T. E. and Chang S. (1980) Carbonaceous chondrites – II. Carbonaceous chondrite phyllosilicates and light element geochemistry as indicators of parent body processes and surface conditions. *Geochim. Cosmochim. Acta* **44**, 1543–1577.

Bus S. J. (1999) Compositional Structure in the Asteroid Belt: Results of a Spectroscopic Survey. PhD Thesis. Massacheusetts Institute of Technology.

Bus S. J. and Binzel R. P. (2002) Phase II of the Small Main-Belt Asteroid Spectroscopic Survey A Feature-Based Taxonomy. *Icarus* **158**, 146–177.

Bushveld Igneous Complex (BIC), South Africa. (2017) *Johnson Matthey*. Available at: http://www.platinum.matthey.com/about-pgm/production/south-africa [Accessed March 4, 2017].

Campbell A. J. and Humayun M. (1999a) Platinum group element microanalysis of ordinary chondrite metal grains by laser ablation ICP-MS. *9th Ann. Goldschmidt Conf.* Harvard University, Massachusetts. #7332(abstr.).

Campbell A. J. and Humayun M. (1999b) Microanalysis of platinum group elements in iron meteorites using laser ablation ICP-MS. *Lunar Planet. Sci. XXX.* Lunar Planet. Inst., Houston. #1974(abstr.).

Campbell A. J. and Humayun M. (2003) Formation of metal in Grosvenor Mountains 95551 and comparison to ordinary chondrites. *Geochim. Cosmochim. Acta* **67**, 2481–2495.

Campbell A. J. and Humayun M. (2004) Formation of metal in the CH chondrites ALH 85085 and PCA 91467. *Geochim. Cosmochim. Acta* **68,** 3409–3422.

Campbell A. J., Humayun M., Meibom A., Krot A. N. and Keil K. (2001) Origin of zoned metal grains in the QUE94411 chondrite. *Geochim. Cosmochim. Acta* **65**, 163–180.

Carry B., Solano E., Eggl S. and DeMeo F. E. (2016) Spectral properties of near-Earth and Mars-crossing asteroids using Sloan photometry. *Icarus* **268**, 340–354.

Chen J. H., Papanastassiou D. A. and Wasserburg G. J. (1998) Re-Os systematics in chondrites and the fractionation of the platinum group elements in the early solar system. *Geochim. Cosmochim. Acta* **62**, 3379–3392.

Chizmadia L. J. and Brearley A. J. (2008) Mineralogy, aqueous alteration, and primitive textural characteristics of fine-grained rims in the Y-791198 CM2 carbonaceous chondrite: TEM observations and comparison to ALHA81002. *Geochim. Cosmochim. Acta2* **72**, 602–625.

Chou C. L. and Cohen A. J. (1973) Gallium and germanium in the metal and silicates of L- and LL-chondrites. *Geochim. Cosmochim. Acta* **37**, 315–327.

CNEOS Discovery Statistics - Cumulative Totals. (2017) *Center for Near Earth Object Studies, NASA JPL*. Available at: http://cneos.jpl.nasa.gov/stats/totals.html [Accessed March 4, 2017].

Connolly H. C., Hewins R. H., Ash R. D., Zanda B., Lofgren G. E. and Bourot-Denise M. (1994) Carbon and the formation of reduced chondrules. *Nature* **371**, 136–139.

Cromwell E. F. and Arrowsmith P. (1995) Fractionation effects in laser ablation inductively coupled plasma mass spectrometry. *Appl. Spectrosc.* **49,** 1652–1660.

Davis D. R., Friedlander A. L. and Jones T. D. (1993) Role of Near-Earth Asteroids in the Space Exploration Initiative. In *Resoures of Near-Earth Space* (eds. J. Lewis, M. S. Matthews, and M. L. Guerrieri). University of Arizona Press, Tuscon. pp. 619–655.

Day J. M. D., Pearson D. G. and Taylor L. A. (2007) Highly siderophile element constraints on accretion and differentiation of the Earth-Moon system. *Science* **315**, 217–219.

DeMeo F. E., Binzel R. P., Slivan S. M. and Bus S. J. (2009) An extension of the Bus asteroid taxonomy into the near-infrared. *Icarus* **202**, 160–180.

Dodd R. T. (1981) *Meteorites: a petrological-chemical synthesis.* Cambridge University Press, New York.

Dunn T. L., Cressey G., McSween H. Y. Jr. and McCoy T. J. (2010) Analysis of ordinary chondrites using powder X-ray diffraction: 1. Modal mineral abundances. *Meteorit. Planet. Sci.* **45**, 123–134.

Elvis M. (2014) How many ore-bearing asteroids? *Planet. Space Sci.* **91**, 20–26.

Elvis M., McDowell J., Hoffman J. A. and Binzel R. P. (2011) Ultra-low delta-v objects and the human exploration of asteroids. *Planet. Space Sci.* **59**, 1408–1412.

Farmer V. C. (1974) The Layer Silicates. In *The Infrared Spectra of Minerals* (ed. V. C. Farmer). Mineralogical Society, London. pp. 331–364.

Fegley B. and Palme H. (1985) Evidence for oxidizing conditions in the solar nebula from Mo and W depletions in refractory inclusions in carbonaceous chondrites. *Earth Planet. Sci. Lett.* **72**, 311–326.

Földvári M. (2011) *Handbook of thermogravimetric system of minerals and its use in geological practice*. Geological Insitute of Hungary, Budapest.

Fry C., Melanson D., Samson C., McCausland P.J.A., Herd R.K., Ernst R.E., Umoh J., and Holdsworth D.W. (2013). Physical characterization of a suite of Buzzard Coulee H4 chondrite fragments. *Meteorit. Planet. Sci.* **48,** 1060–1073.

Gaffey M. J., Burbine T. H. and Binzel R. P. (1993) Asteroid spectroscopy: Progress and perspectives. *Meteoritics* **28**, 161–187.

Garenne A., Beck P., Montes-Hernandez G., Chiriac R., Toche F., Quirico E., Bonal L. and Schmitt B. (2014) The abundance and stability of “water” in type 1 and 2 carbonaceous chondrites (CI, CM and CR). *Geochim. Cosmochim. Acta* **137**, 93–112.

Goldstein J. I. and Michael J. R. (2006) The formation of plessite in meteoritic metal. *Meteorit. Planet. Sci.* **41**, 553–570.

Goldstein J. I. and Ogilvie R. E. (1965) The growth of the Widmanstatten pattern in metallic meteorites. *Geochim. Cosmochim. Acta* **29**, 893–920.

Grady M. M., Verchovsky A. B., Franchi A., Wright I. P. and Pillinger C. T. (2002) Light element geochemistry of the Tagish Lake CI2 chondrite: Comparison with CI1 and CM2 meteorites. *Meteorit. Planet. Sci.* **37**, 713–735.

Grimm R. E. and McSween H. Y. Jr. (1993) Heliocentric zoning of the asteroid belt by aluminum-26 heating. *Science* **259**, 653-655.

Grossman J. N. and Wasson J. T. (1985) The origin and history of the metal and sulfide components of chondrules. *Geochim. Cosmochim. Acta* **49**, 925–939.

Grossman L. and Larimer J. W. (1974) Early chemical history of the solar system. *Revs. Geophys. Space Phys.* **12**, 71-101.

Grossman L. and Olsen E. (1974) Origin of the high-temperature fraction of C2 chondrites. *Geochim. Cosmochim. Acta* **38**, 173–187.

Grossman L., Olsen E. and Lattimer J. M. (1979) Silicon in Carbonaceous Chondrite Metal: Relic of High-Temperature Condensation. *Science* **206**, 449–451.

Gualtieri A. F., Ferrari S., Leoni M., Grathoff G., Hugo R., Shatnawi M., Paglia G. and Billinge S. (2008) Structural characterization of the clay mineral illite-1M. *J. Appl. Crystallogr.* **41**, 402–415.

Guo W. and Eiler J. M. (2007) Temperatures of aqueous alteration and evidence for methane generation on the parent bodies of the CM chondrites. *Geochim. Cosmochim. Acta* **71**, 5565–5575.

Hanowski N. P. and Brearley A. J. (2001) Aqueous alteration of chondrules in the CM carbonaceous chondrite, Allan Hills 81002: implications for parent body alteration. *Geochim. Cosmochim. Acta* **65**, 495–518.

Herd C. D. K., Blinova A., Simkus D. N., Huang Y., Tarozo R., Alexander C. M. O., Gyngard F., Nittler L. R., Cody G. D., Fogel M. L., Kebukawa Y., Kilcoyne a L. D., Hilts R. W., Slater G. F., Glavin D. P., Dworkin J. P., Callahan M. P., Elsila J. E., De Gregorio B. T. and Stroud R. M. (2011) Origin and evolution of prebiotic organic matter as inferred from the Tagish Lake meteorite. *Science* **332**, 1304–1307.

Hewins R. H., Yu Y., Zanda B. and Bourot-Denise M. (1997) Do nebular fractionations, evaporative losses, or both, influence chondrule compositions? *Antarct. Meteorite. Res.* **10**, 275–298.

Hiroi T. and Hasegawa S. (2003) Revisiting the search for the parent body of the Tagish Lake meteorite -- Case of a T / D asteroid 308 Polyxo --. *Antarct. Meteorite. Res.* **16**, 176–184.

Hiroi T., Zolensky M. E. and Pieters C. M. (2001) The Tagish Lake meteorite: a possible sample from a D-type asteroid. *Science* **293**, 2234–2236.

Horan M. F., Alexander C. M. O. D. and Walker R. J. (2009) Highly siderophile element evidence for early solar system processes in components from ordinary chondrites. *Geochim. Cosmochim. Acta* **73**, 6984–6997.

Howard K. T., Alexander C. M. O. D., Schrader D. L. and Dyl K. A. (2014) Classification of hydrous meteorites (CR, CM and C2 ungrouped) by phyllosilicate fraction: PSD-XRD modal mineralogy and planetesimal environments. *Geochim. Cosmochim. Acta* **149**, 206–222.

Hsu W., Huss G. R. and Wasserburg G. J. (2000) Ion probe measurements of Os, Ir, Pt, and Au in individual phases of iron meteorites. *Geochim. Cosmochim. Acta* **64**, 1133–1147.

Hsu W., Huss G. R., Wasserburg G. J., Asylum T. L. and Fe T. (1998) Ion probe analyses of PGEs in metallic phases of chondrites: Implications for the origin of chondritic metals. *Lunar Planet. Sci. XXIX.* Lunar Planet. Inst., Houston. #1939(abstr.).

Humayun M. and Campbell A. J. (2000) Re, Os, and Ir Fractionation in Ordinary Chondrite Metal. *Lunar Planet. Sci. XXXI.* Lunar Planet. Inst., Houston. #2032(abstr.).

Humayun M. and Campbell A. J. (2002) The duration of ordinary chondrite metamorphism inferred from tungsten microdistribution in metal. *Earth Planet. Sci. Lett.* **198**, 225–243.

Hutchison R. (2004) *Meteorites: a petrologic, chemical and isotopic synthesis.* Cambridge University Press, Cambridge.

Ignatiev A., Freundlich A., Duke M., Rosenberg S. and Makel D. (2001) In-situ electric power generation to support solar system exploration and colonization: manufacture of thin film silicon solar cells on the Moon. *Aerospace Conf., IEEE Proc.,* Big Sky, Montana.

Izawa M. R. M., Flemming R. L., King P. L., Peterson R. C. and McCausland P. J. A. (2010) Mineralogical and spectroscopic investigation of the Tagish Lake carbonaceous chondrite by X-ray diffraction and infrared reflectance spectroscopy. *Meteorit. Planet. Sci.* **45**, 675–698.

Jarosewich E. (1990) Chemical analyses of meteorites: A compilation of stony and iron meteorite analyses. *Meteoritics* **25**, 323–337.

Kallemeyn G. W., Rubin A. E., Wang D. and Wasson J. T. (1989) Ordinary chondrites: Bulk compositions, classification, lithophile-element fractionations and composition-petrographic type relationships. *Geochim. Cosmochim. Acta* **53**, 2747–2767.

Kargel J. S. (1994) Metalliferous asteroids as potential sources of precious metals. *J. Geophys. Res.* **99**, 21,129-21,141.

Kebukawa Y., Nakashima S. and Zolensky M. E. (2010) Kinetics of organic matter degradation in the Murchison meteorite for the evaluation of parent-body temperature history. *Meteorit. Planet. Sci.* **45**, 101–115.

Kelly W. R. and Larimer J. W. (1977) Chemical fractionations in meteorites-VIII. Iron meteorites and the cosmochemical history of the metal phase. *Geochim. Cosmochim. Acta* **41**, 93–111.

Kerridge J. F., Chang S. and Shipp R. (1987) Isotopic characterisation of kerogen-like material in the Murchison carbonaceous chondrite. *Geochim. Cosmochim. Acta* **51**, 2527–2540.

King A. J., Solomon J. R., Schofield P. F. and Russell S. S. (2015) Characterising the CI and CI-like carbonaceous chondrites using thermogravimetric analysis and infrared spectroscopy. *Earth, Planets Sp.* **67**, 1–12.

Kong P. and Ebihara M. (1996) Metal phases of L chondrites: Their formation and evolution in the nebula and in the parent body. *Geochim. Cosmochim. Acta* **60**, 2667–2680.

Kong P. and Ebihara M. (1997) The origin and nebular history of the metal phase of ordinary chondrites. *Geochim. Cosmochim. Acta* **61**, 2317–2329.

Kong P., Ebihara M., Endo K. and Nakahara H. (1995a) Elemental distributions in metallic fractions of an antarctic ordinary chondrite ALH-77231 (L6). *Proc. NIPR. Symp. Antarct. Meteorites.* **8**, 237–249.

Kong P., Ebihara M., Nakahara H. and Endo K. (1995b) Chemical characteristics of metal phases of the Richardton H5 chondrite. *Earth Planet. Sci. Lett.* **136**, 407–419.

Kong P., Ebihara M. and Xie X. (1998) Reevaluation of formation of metal nodules in ordinary chondrites. *Meteorit. Planet. Sci.* **33**, 993–998.

Kramer S. and Mosher D. (2016) Here's how much money it actually costs to launch stuff into space. *Business Insider*. Available at: http://www.businessinsider.com/spacex-rocket-cargo-price-by-weight-2016-6/#bottle-of-water-9100-to-43180-1 [Accessed March 5, 2017].

Krot A. N., Keil K., Scott E. R. D., Goodrich C. A. and Weisberg M. K. (2014) 1.1 - Classification of meteorites and their genetic relationships. In *Treatise on Geochemistry, 2nd Edition* (eds. H. Holland and K. Turekian). Elsevier, Oxford. pp. 1–63.

Lafay R., Montes-Hernandez G., Janots E., Chiriac R., Findling N. and Toche F. (2012) Mineral replacement rate of olivine by chrysotile and brucite under high alkaline conditions. *J. Cryst. Growth* **347**, 62–72.

Lange M. A., Lambert P. and Ahrens T. J. (1985) Shock effects on hydrous minerals and implications for carbonaceous meteorites. *Geochim. Cosmochim. Acta* **49**, 1715–1726.

Larimer J. W. and Anders E. (1970) Chemical fractionations in meteorites-III. Major element fractionations in chondrites. *Geochim. Cosmochim. Acta* **34**, 367–387.

Lauretta D. S., Buseck P. R. and Zega T. J. (2001) Opaque minerals in the matrix of the Bishunpur (LL3.1) chondrite: Constraints on the chondrule formation environment. *Geochim. Cosmochim. Acta* **65**, 1337–1353.

Lee T., Papanastassiou D. A. and Wasserburg G. J. (1976) Demonstration of ^{26}Mg excess in Allende and evidence for ^{26}Al. *Geophys. Res. Lett.* **3**, 109–112.

Leroux H., Doukhan J.-C. and Guyot F. (1996) An analytical electron microscopy (AEM) investigation of opaque inclusions in some type 6 ordinary chondrites. *Meteorit. Planet. Sci.* **31**, 767–776.

Leroux H., Libourel G., Lemelle L. and Guyot F. (2003) Experimental study and TEM characterization of dusty olivines in chondrites: Evidence for formation by in situ reduction. *Meteorit. Planet. Sci.* **38**, 81–94.

Lewis J. S. (1992) Asteroid Resources. In *Space Resources Materials* (eds. M. F. McKay, D. S. McKay, and M. B. Duke). NASA SP-509, vol. 3. pp. 59–78.

Lewis J. S. (1996) *Mining the Sky: Untold Riches from the Asteroids, Comets, and Planets*., Addison-Wesley Publishing Company, Inc.

Lewis J. S. (2015) *Asteroid Mining 101: Wealth for the New Space Economy*., Deep Space Industries Inc.

Lewis J. S. and Hutson M. L. (1993) Asteroidal Resource Opportunities Suggested by Meteorite Data. In *Resoures of Near-Earth Space* (eds. J. Lewis, M. S. Matthews, and M. L. Guerrieri). University of Arizona Press, Tuscon. pp. 523–542.

Lorand J. P., Luguet A. and Alard O. (2008) Platinum-group elements: A new set of key tracers for the Earth's interior. *Elements* **4**, 247–252.

Lunine J. I., Engel S., Rizk B. and Horanyi M. (1991) Sublimation and reformation of icy grains in the primitive solar nebula. *Icarus* **94**, 333–344.

Mason B. (1963) The carbonaceous chondrites. *Space Sci. Revs*. **1**, 621–646.

McSween H. Y. Jr. (1999) *Meteorites and their parent planets, 2nd edition.* Cambridge University Press, New York.

McSween H. Y. Jr. and Labotka T. C. (1993) Oxidation during metamorphism of the ordinary chondrites. *Geochim. Cosmochim. Acta* **57**, 1105–1114.

McSween H. Y. Jr., Sears D. W. G. and Dodd R. T. (1988) Thermal metamorphism. In *Meteorites and the Early Solar System* (eds. J. F. Kerridge and M. S. Matthews). University of Arizona, Tucson. pp. 102–113.

Meftah N., Mostefaoui S., Jambon A., Guedda E. H. and Pont S. (2016) Minor and trace element concentrations in adjacent kamacite and taenite in the Krymka chondrite. *Meteorit. Planet. Sci.* **51**, 696–717.

Meteoritical Bulletin Database. (2017) *Lunar and Planetary Institute*. Available at: https://www.lpi.usra.edu/meteor/ [Accessed January 24, 2017].

Mielenz R. C., Schieltz N. C. and King M. E. (1953) Thermogravimetric analysis of clay and clay-like minerals. *Clays Clay Miner.* **2**, 285–314.

Miyazawa M., Pavan M. A., de Oliveira E. L., Ionashiro M. and Silva A. K. (2000) Gravimetric determination of soil organic matter. *Brazilian Arch. Biol. Technol.* **42**, 475–478.

Mullane E., Alard O., Gounelle M. and Russell S. S. (2004) Laser ablation ICP-MS study of IIIAB irons and pallasites: Constraints on the behaviour of highly siderophile elements during and after planetesimal core formation. *Chem. Geol.* **208**, 5–28.

Nagahara H. (1979) Petrological study of Ni-Fe metal in some ordianry chondrites. *Mem. NIPR. Spec. Issue.* **15**, 111–122.

Nakamura T., Noguchi T., Zolensky M. E. and Tanaka M. (2003) Mineralogy and noble-gas signatures of the carbonate-rich lithology of the Tagish Lake carbonaceous chondrite: Evidence for an accretionary breccia. *Earth Planet. Sci. Lett.* **207**, 83–101.

Nelson M. L., Britt D. T. and Lebofsky L. A. (1993) Review of Asteroid Composition. *Resour. Near Earth Sp.*, 493–522.

Nichiporuk W. and Brown H. (1965) The distribution of platinum and palladium metals in iron meteorites and in the metal phase of ordinary chondrites. *J. Geophys. Res.* **70**, 459–470.

Nichols C. R. (1993) Volatile Products From Carbonaceous Asteroids. In *Resoures of Near-Earth Space* (eds. J. Lewis, M. S. Matthews, and M. L. Guerrieri). University of Arizona Press, Tuscon. pp. 543–568.

Noguchi T., Nakamura T. and Nozaki W. (2002) Mineralogy of phyllosilicate-rich micrometeorites and comparison with Tagish Lake and Sayama meteorites. *Earth Planet. Sci. Lett.* **202**, 229–246.

Nolze G., Wagner G., Saliwan Neumann R., Skála R., and Geist V. (2006) Orientation relationships of carlsbergite in schreibersite and kamacite in the North Chile iron meteorite. *Mineralogical Magazine* **70**, 373–382.

Nozaki W., Nakamura T. and Noguchi T. (2006) Bulk mineralogical changes of hydrous micrometeorites during heating in the upper atmosphere at temperatures below 1000°C. *Meteorit. Planet. Sci.* **1114**, 1095–1114.

Palme H. (1982) Identification of projectiles of large terrestrial impact craters and some implications for the interpretation of Ir-rich Cretaceous/Tertiary boundary layers. In *Geological Implications of Impacts of Large Asteroids and Comets on the Earth* (eds. L. T. Silver and P. H. Schultz). Geol. Soc. Amer. Spec. Paper 190. pp. 223–233.

Palme H. (2008) Platinum-group elements in cosmochemistry. *Elements* **4**, 233–238.

Palme H. and Wlotzka F. (1976) A metal particle from a Ca,Al-rich inclusion from the meteorite Allende, and the condensation of refractory siderophile elements. *Earth Planet. Sci. Lett.* **33**, 45–60.

Petaev M. I. and Jacobsen S. B. (2004) Differentiation of metal-rich meteoritic parent bodies: I. Measurements of PGEs, Re, Mo, W, and Au in meteoritic Fe-Ni metal. *Meteorit. Planet. Sci.* **39**, 1685–1697.

Platinum Prices. (2017) *APMEX*. Available at: http://www.apmex.com/spotprices/platinum-price [Accessed March 3, 2017].

Ralchenko M., Britt D. T., Samson C., Herd C. D. K., Herd R. K. and McCausland P. J. A. (2014) Bulk physical properties of the Tagish Lake Meteorite frozen pristine fragments. *Lunar Planet. Sci. XLV.* Lunar Planet. Inst., Houston. #1021(abstr.).

Rambaldi E. R. (1976) Trace Element Content of Metals from L-Group Chondrites. *Earth Planet. Sci. Lett.* **31**, 224–238.

Rambaldi E. R. (1977a) The content of Sb, Ge and refractory siderophile elements in metals of L-group chondrites. *Earth Planet. Sci. Lett.* **33**, 407–419.

Rambaldi E. R. (1977b) Trace element content of metals from H- and LL-group chondrites. *Earth Planet. Sci. Lett.* **36**, 347–358.

Rambaldi E. R. and Cendales M. (1977) Tungsten in ordinary chondrites. *Earth Planet. Sci. Lett.* **36**, 372–380.

Rambaldi E. R., Cendales M. and Thacker R. (1978) Trace element distribution between magnetic and non-magnetic portions of ordinary chondrites. *Earth Planet. Sci. Lett.* **40**, 175–186.

Rambaldi E. R., Sears D. W. and Wasson J. T. (1980) Si-rich Fe-Ni grains in highly unequilibrated chondrites. *Nature* **287**, 817–820.

Rasmussen K. L., Malvin D. J. and Wasson J. T. (1988) Trace element partitioning between taenite and kamacite; relationship to the cooling rates of iron meteorites. *Meteoritics* **23**, 107–112.

Reddy V., Sanchez J. A., Bottke W. F., Thirouin A., Rivera-Valentin E. G., Kelley M. S., Ryan W., Cloutis E. A., Tegler S. C., Ryan E. V., Taylor P. A., Richardson J. E., Moskovitz N. and Le Corre L. (2016) Physical characterization of ~2m diameter near-Earth asteroid 2015 TC23: A possible boulder from E-type asteroid (44) Nysa. *Astron. J.* **152**, 1–7.

Reisener R. J. and Goldsteing J. I. (1999) The evolution of metal in chondrites during prograde metamorphism: the role of vapor phase transport. *62nd Ann. Met. Soc.* Meteorit. Planet. Sci., Johannesburg. #5149(abstr.).

Reisener R. J. and Goldstein J. I. (2003) Ordinary chondrite metallography: Part 2. Formation of zoned and unzoned metal particles in relatively unshocked H, L, and LL chondrites. *Meteorit. Planet. Sci.* **38**, 1679–1696.

Reisener R. J., Goldstein J. I. and Petaev M. I. (2006) Olivine zoning and retrograde olivine-orthopyroxene-metal equilibration in H5 and H6 chondrites. *Meteorit. Planet. Sci.* **41**, 1839–1852.

Rietveld H. M. (1967) Line profiles of neutron powder-diffraction peaks for structure refinement. *Acta Crystallogr.* **22**, 151–152.

Righter K., Humayun M. and Danielson L. (2008) Partitioning of palladium at high pressures and temperatures during core formation. *Nat. Geosci.* **1**, 321–323.

Rodriguez-Navarro C., Ruiz-Agudo E., Luque A., Rodriguez-Navarro A. B. and Ortega-Huertas M. (2009) Thermal decomposition of calcite: Mechanisms of formation and textural evolution of CaO nanocrystals. *Am. Mineral.* **94**, 578–593.

Ross S. D. (2001) *Near-Earth Asteroid Mining*. Space Industry Report, Caltech.

Rubin A. E. (1990) Kamacite and olivine in ordinary chondrites: Intergroup and intragroup relationships. *Geochim. Cosmochim. Acta* **54**, 1217–1232.

Rubin A. E. (1995) Petrological evidence for collisional heating of chondritic asteroids. *Icarus* **113**, 156–167.

Rubin A. E. and Wasson J. T. (1995) Variations of chondrite properties with heliocentric distance. *Meteoritics* **30**, 596.

Rubin A. E., Fegley B. and Brett R. (1988) Oxidation state in chondrites. In *Meteorites and the Early Solar System* (eds. J. F. Kerridge and M. S. Matthews). University of Arizona, Tucson. pp. 488–511.

Rubin A. E., Trigo-Rodríguez J. M., Huber H. and Wasson J. T. (2007) Progressive aqueous alteration of CM carbonaceous chondrites. *Geochim. Cosmochim. Acta* **71**, 2361–2382.

Ryan E. L. and Woodward C. E. (2010) Rectified asteroid albedos and diameters from IRAS and MSX photometry catalogs. *Astron. J.* **140**, 933–943.

Sanchez J. P. and McInnes C. R. (2012) Assessment on the feasibility of fture shepherding of asteroid resources. *Acta Astronaut.* **73**, 49–66.

Sastri S. and Duke M. D. (1992) Application of Manufactured Products. In *Space Resources Materials* (eds. M. F. McKay, D. S. McKay, and M. B. Duke). NASA SP-509, vol 3. pp. 298–306.

Schmidt G., Palme H. and Karl-Ludwig K. (1997) Highly Siderophile Elements (Re, Os, Ir, Ru, Rh, Pd, Au) in Impact Melts from three Impact Craters (Saaksjarvi, Mien and Dellen): Clues to the nature of the impacting bodies. *Geochim. Cosmochim. Acta* **61**, 2877–2987.

Scott E. R. D. and Taylor J. (1983) Chondrules and other components in C, O, and E chondrites: Similarities in Their Properties and Origins. *J. Geophys. Res.* **88**, B275–B286.

Sears D. W. and Dodd R. T. (1988) Overview and classification of meteorites. In *Meteorites and the Early Solar System* (eds. J. F. Kerridge and M. S. Matthews). University of Arizona, Tucson. pp. 3–31.

Sears D. W. and Axon H. J. (1975) The metal content of common chondrites. *Meteoritics* **10**, 486–487.

Shimaoka T. and Nakamura N. (1989) Vaporization of sodium from a partially molten chondritic material. *Proc. NIPR. Symp. Antarct. Meteorites.* **2**, 252–267.

Shoemaker E. M., Williams J. G., Helin E. F. and Wolfe R. F. (1979) Earth-Crossing Asteroids: Orbital Classes, Collision Rates with Earth, and Origin. In *Asteroids* (ed. T. Gehrels). University of Arizona Press, Tuscon. pp. 253–285.

Smith D. G. W. and Launspach S. (1991) The composition of metal phases in Bruderheim (L6) and implications for the thermal histories of ordinary chondrites - Erratum. *Earth Planet. Sci. Lett.* **102**, 79–93.

Smith D. G. W., Miúra Y. and Launspach S. (1993) Fe, Ni and Co variations in the metals of some antarctic chondrites. *Earth Planet. Sci. Lett.* **120**, 487–498.

Snelling A. A. (2014) Radioisotope dating of meteorites II: The ordinary and enstatite chondrites. *Answers Research Journal* **7**, 239–296.

Sonett C. P. (1971) The relationship of meteoritic parent body thermal histories and electromagnetic heating by a pre-main sequence T Tauri sun. In *Physical Studies of the Minor Planets* (ed. T. Gehrels). NASA SP-267. pp. 239–245.

Środoń J., Drits V. A., McCarty D. K., Hsieh J. C. C. and Eberl D. (2001) Quantitative X-Ray Diffraction Analysis. *Clays Clay Miner.* **49**, 514–528.

Sylvester P. J., Ward B. J., Grossman L. and Hutcheon I. D. (1990) Chemical compositions of siderophile element-rich opaque assemblages in an Allende inclusion. *Geochim. Cosmochim. Acta* **54**, 3491–3508.

Tagle R. and Berlin J. (2008) A database of chondrite analyses including platinum group elements, Ni, Co, Au, and Cr: Implications for the identification of chondritic projectiles. *Meteorit. Planet. Sci.* **43**, 541–559.

Tandon S. N. and Wasson J. T. (1968) Gallium, germanium, indium and iridium variations in a suite of L-group chondrites. *Geochim. Cosmochim. Acta* **32**, 1087–1109.

Tholen D. J. (1984) Asteroid taxonomy from cluster analysis of photometry. PhD Thesis. University of Arizona.

U.S. Geological Survey (2017) Mineral commodity summaries 2017. *U.S. Geological Survey,* https://doi.org/10.3133/70180197.

Van Schmus W. R. and Wood J. A. (1967) A chemical-petrological classification for the chondritic meteorites. *Geochim. Cosmochim. Acta* **31**, 747–765.

Walker R. J. (2009) Highly siderophile elements in the Earth, Moon and Mars: Update and implications for planetary accretion and differentiation. *Chemie der Erde* **69**, 101–125.

Walker R. J., Horan M. F., Morgan J. W., Becker H., Grossman J. N. and Rubin A. E. (2002) Comparative 187Re-187Os systematics of chondrites: Implications regarding early solar system processes. *Geochim. Cosmochim. Acta* **66**, 4187–4201.

Wasson J.T., Ouyang X., Wang J., and Jerde E. (1989) Chemical classification of iron meteorites: XI. Multi-element studies of 38 new irons and the high abundance of ungrouped irons from Antarctica. *Geochim. Cosmochim. Acta* **53**, 735–744.

Wasson J.T., Choi B., Jerde E.A., and Ulff-Møller, F. (1998) Chemical classification of iron meteorites: XII. New members of the magmatic group. *Geochim. Cosmochim. Acta* **62,** 715–724.

White W. B. (1974) The Carbonate Minerals. In *The Infrared Spectra of Minerals* (ed. V. C. Farmer). Mineralogical Society, London. pp. 227–284.

Wiedemann D. ed. (2014) Water Recycling. *NASA*. Available at: https://www.nasa.gov/content/water-recycling/ [Accessed March 5, 2017].

Wiik H. B. (1956) The chemical composition of some stony meteorites. *Geochim. Cosmochim. Acta* **9**, 279–289.

Willis J. and Goldstein J. I. (1983) A three-dimensional study of metal grains in equilibrated, ordinary chondrites. *J. Geophys. Res. Solid Earth* **88**, B287–B292.

Wood J. A. (1964) The cooling rates and parent planets of several iron meteorites. *Icarus* **3,** 429–459.

Wood J. A. (1967) Chondrites: Their metallic minerals, thermal histories, and parent planets. *Icarus* **49**, 1–49.

Yoldi-Martinez Z., Beck P., Montes-Hernandez G., Chiriac R., Quirico E., Bonal L., Schmitt B. and Moynier F. (2011) Hydrous Mineralogy of Carbonaceous Chondrites from Thermogravimetry-Analysis. *74th Ann. Met. Soc.* Meteorit. Planet. Sci., London. #5329(abstr.).

Yongheng C., Daode W. and Pernicka E. (1992) The compositions of six Chinese ordinary chondrites and element distributions in their different phases. *Chinese J. Geochemistry* **11**, 214–223.

Young R. A., Mackie P. E. and Von Dreele R. B. (1977) Application of the Pattern-Fitting Structure-Refinement Method to X-ray Powder Diffractometer Patterns. *J. Appl. Cryst.* **10**, 262–269.

Zanda B., Bourot-Denise M., Perron C. and Hewins R. H. (1994) Origin and metamorphic redistribution of silicon, chromium, and phosphorus in the metal of chondrites. *Science* **265**, 1846–1849.

Zanda B., Yu Y., Bourot-Denise M. and Hewins R. (1997) The history of metal and sulfides in chondrites. *Work. Parent-Body Nebul. Modif. Chondritic Mater.* Maui, Hawai'i. #4042(abstr.).

Zolensky M. E. and Gooding J. L. (1986) Aqueous Alteration on Carbonaceous-Chondrite Parent Bodies as Inferred from Weathering in Meteorites in Antarctica. *Meteoritics* **21**, 548–549.

Zolensky M. E. and McSween H. Y. Jr. (1988) Aqueous Alteration. In *Meteorites and the Early Solar System* (eds. J. F. Kerridge and M. S. Matthews). University of Arizona, Tucson. pp. 114–143.

Zolensky M. E., Nakamura K., Gounelle M., Mikouchi T., Kasama T., Tachikawa O. and Tonui E. (2002) Mineralogy of Tagish Lake: An ungrouped type 2 carbonaceous chondrite. *Meteorit. Planet. Sci.* **37**, 737–761.

Zurfluh F. J., Hofmann B. A., Gnos E., Eggenberger U. and Jull A. J. T. (2016) Weathering of ordinary chondrites from Oman: Correlation of weathering parameters with ^{14}C terrestrial ages and a refined weathering scale. *Meteorit. Planet. Sci.* **51**, 1685-1700.

Appendix 1

A1.1. Establishment of the North Chile Metal Standard

This master's project is a continuation of my undergrad thesis titled *Economic Significance of Asteroids: Insights from Chondrite Meteorites.* As part of the undergrad thesis, the North Chile (Filomena) meteorite was established as a suitable metal standard for laser ablation inductively coupled plasma mass spectrometry (LA-ICP-MS) analysis. The following is adapted from the undergrad thesis outlining the methods and results used to establish North Chile as a metal standard:

Introduction

The use of LA-ICP-MS for analyzing major- and trace-element concentrations in meteorite metal has been well-established by Campbell and Humayun (e.g., 1999b, 2003, 2004). Compositional analysis of meteorite metal via LA-ICP-MS was not previously attempted at the University of Alberta prior to this study. Therefore, it was important to develop the LA-ICP-MS method with the instruments available before analysis of unknowns could take place. One important factor in developing the LA-ICP-MS method was establishing a suitable metal standard. The iron-nickel North Chile (Filomena) meteorite was selected as a metal standard based on its well-known composition (Wasson et al., 1989, 1998; Campbell and Humayun, 1999b) and hexahedrite classification; as such it is only composed of kamacite. This study found North Chile to be a suitable metal standard for LA-ICP-MS analysis.

Methods

The LA-ICP-MS analysis of North Chile conducted in this study varies slightly from the method described in Chapter 2. For LA-ICP-MS analysis of North Chile, a New Wave UP213 laser ablation system connected to a Perkin Elmer Elan 6000 mass spectrometer was utilized. As the Perkin Elmer mass spectrometer is less sensitive than the iCAP Q mass spectrometer used in the master's study, a larger spot size (100 μm) and greater frequency (10 Hz) was necessary for analysis. The internal element standard selected was ^{60}Ni and helium gas was used for control. The ^{60}Ni standard was normalized to the mean Ni concentration from North Chile obtained

from Wasson et al. (1989). North Chile was analyzed via LA-ICP-MS on two separate occasions: 1) ~60 seconds analysis time with a background time of ~20-30 seconds (shutter closed), and 2) ~90 seconds of analysis time with a background time of ~30 seconds (shutter closed). The following isotopes were analyzed in North Chile by laser ablation ICP-MS: ^{52}Cr, ^{59}Co, ^{63}Cu, ^{69}Ga, ^{75}As, ^{102}Ru, ^{103}Rh, ^{106}Pd, ^{184}W, ^{187}Re, ^{192}Os, ^{193}Ir, ^{195}Pt, and ^{197}Au. The first LA-ICP-MS session did not include analysis of ^{102}Ru, ^{103}Rh, ^{106}Pd, and ^{192}Os due to the early stages of developing the LA-ICP-MS method for metal analysis.

Solution ICP-MS results were also gathered from a 450 mg piece of North Chile using a Perkin Elmer Elan 6000 mass spectrometer; the following method description is the same as that described for the bulk metal analysis of Bruderheim (L6) (Chapter 2). Prior to solution ICP-MS analysis, the North Chile sample was placed in a beaker with 5 mL HF and 5 mL HNO_3 and heated to 130°C until completely dry. This same process was completed once more, except with 5 mL HCl and 5 mL HNO_3. Once the beaker was dry, 10 mL of 8M HNO_3 was added to the beaker and heated for a few hours, and subsequently diluted to volume. Following this, 1 mL of the diluted solution was collected and 0.1 mL HNO_3, 0.1 mL of internal standards (In, Bi, and Sc), and 8.8 mL deionized water were added and shaken well.

The North Chile solution was analyzed for elements corresponding to the LA-ICP-MS analyzed isotopes listed above. The solution ICP-MS dwell and integration times were 20 ms and 700 ms, respectively, for all the elements except for Cu which had a dwell time of 10 ms and an integration time of 350 ms. The analysis was run with a flow rate of approximately 1 mL/minute, and measurements were made using 35 sweeps/reading, one reading/replicate and three replicates; the final results obtained are an average of the three replicates.

During optical navigation in the first LA-ICP-MS analysis session, lozenge-shaped inclusions were observed in North Chile. To further investigate these inclusions, a Zeiss EVO MA 15 scanning electron microscope (SEM) with a LaB_6 crystal source was used to obtain backscattered electron (BSE) images. The SEM was also equipped with a Bruker Silicon Drift Detector for energy dispersive X-ray (EDX) analysis, which was used to determine the composition of the inclusions. During this SEM session, BSE and secondary electron (SE) images of the North Chile laser ablation pits were also obtained. The BSE and SE images were used to assess the homogeneity of the metal from a 3-dimensional perspective and determine the

extent of melting from the laser, if any, which may cause fractionation of the elements (Cromwell and Arrowsmith, 1995).

Results/Discussion

North Chile LA-ICP-MS results for the two analytical sessions are provided in Table A1.1. The inclusions spotted in North Chile were avoided during most analyses in the first session (NC 1-6) except for the last (NC 7) in which they were specifically targeted. The results from NC 1-6 and NC 7 are similar within error; although, there are noticeable differences in Cr and Cu. Regardless, the overall similarity between NC 1-6 and NC 7 indicate that the inclusions do not affect the composition of North Chile for the elements of interest. The results from the second LA-ICP-MS session are also consistent with the results of the first analytical session (Table A1.1). The reproducibility of the North Chile results between the two LA-ICP-MS sessions provides a strong basis for establishing North Chile as a suitable metal standard. Also included in Table A1.1 are the North Chile results from the master's study (Chapter 2), which utilized the more sensitive iCAP Q mass spectrometer, and LA-ICP-MS results from Campbell and Humayun (1999b). The results from the initial study of North Chile (first and second sessions) are agreeable with both the iCAP Q and Campbell and Humayun (1999b) results. Campbell and Humayun (1999b) obtained their results using a CETAC LSX-200 (266 nm) laser ablation system coupled to an Element (Finnigan MAT) ICP-MS. Considering that the three studies utilized different laser ablation systems and mass spectrometers, the congruent results among the studies confirms that North Chile is a suitable metal standard for LA-ICP-MS analysis.

The North Chile bulk metal results via solution ICP-MS are provided in Table A1.2. For comparison, mean concentrations from the well-established compositional database of North Chile (Filomena) from Wasson et al. (1989, 1998) are given; the Wasson et al. (1989, 1998) results were obtained via instrumental neutron activation analysis (INAA). The solution ICP-MS results are higher relative to Wasson et al. (1989, 1998), except for Cr which is depleted. Cross-referencing the results in Tables A1.1 and A1.2 reveals that LA-ICP-MS results from this study compare well with the Wasson et al. (1989, 1999) INAA results. The solution ICP-MS method has since been further developed with a better agreement between analyzed results and literature values.

Table A1.1. Average trace element concentrations (ppm) of the North Chile standard from LA-ICP-MS.

	First session LA-ICP-MS		Second session LA-ICP-MS	Master's Study	Campbell and Humayun (1999b)
Element	NC 1-6	NC 7[∞]	NC 1-11		
Cr	51(11)	30[19]	54(13)	50(7)	-
Co	4579(137)	4195[432]	4600(166)	4575(299)	-
Cu	135(3)	121[11]	136(5)	134(8)	-
Ga	59(2)	60[7]	57(5)	59(5)	-
As	4.9(0.4)	3.3[1.6]	5.2(1.3)	4.7(0.6)	-
Ru	-	-	16(1)	15.3(1.0)	15.2(0.8)
Rh	-	-	3.06(0.44)	2.87(0.18)	2.86(0.13)
Pd	-	-	1.96(0.79)	1.72(0.20)	1.72(0.15)
W	2.6(0.1)	2.5[0.3]	2.9(0.6)	2.6(0.2)	-
Re	0.24(0.02)	0.21[0.07]	0.26(0.06)	0.24(0.04)	0.20(0.04)
Os	-	-	1.17(0.19)	1.10(0.11)	1.09(0.08)
Ir	3.41(0.15)	3.19[0.44]	3.67(0.59)	3.39(0.26)	3.22(0.21)
Pt	20.9(0.9)	20.9[2.66]	22.3(3.0)	20.7(1.7)	21.3(1.2)
Au	0.62(0.09)	0.63[0.34]	0.53(0.41)	0.62(0.07)	0.60(0.03)

Numbers in parentheses represent standard deviation, except for data from Campbell and Humayun (1999b) which is represented by standard error. The numbers in square brackets for NC 7 are 1 sigma error.
[∞] North Chile results with inclusions targeted.

Table A1.2. Average trace element concentrations (ppm, except for Ni) of the North Chile standard from solution ICP-MS.

Element	Solution ICP-MS	Wasson et al. (1989, 1998)
Ni (wt.%)	6.68	5.65(0.05)
Co	5541	4541(31)
Cr	64	71(8)
Cu	163	137(5)
Ga	75	59(1)
As	8.8	4.7(0.1)
Ru	21	-
Rh	-	-
Pd	2.2	-
W	5.0	2.5(0.1)
Re	0.30	0.23(0.01)
Os	<0.08	-
Ir	4.77	3.38(0.05)
Pt	29	21(1)
Au	-	0.612(0.005)

Wasson et al. (1989, 1998) results are an average from both studies.

The lozenge-shaped inclusions that were discovered during LA-ICP-MS were found throughout the entire North Chile sample during SEM analysis and have random orientation (Fig. A1.1). EDX analysis revealed them to be comprised of Fe, Ni, and P. Based on this compositional analysis, it was determined that the inclusions are rhabdite (schreibersite), a common inclusion found in the North Chile with the chemical formula $(Fe,Ni)_3P$ (Buchwald, 1975; Nolze et al., 2006). Since the SEM images show that the rhabdite crystals are found 3-dimensionally within the sample, it can be concluded that the efforts made to avoid the inclusions during the first session had no merit as the inclusions are clearly unavoidable. This explains why the analyses of NC-7 are consistent with the other results and literature values (Table A1.1).

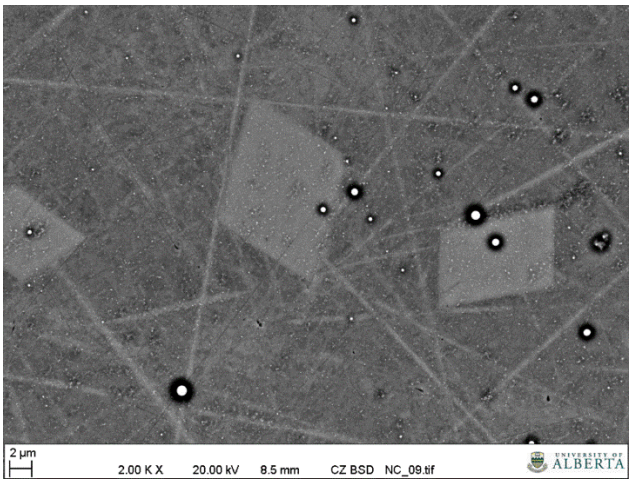

Fig. A1.1. Lozenge-shaped inclusions with different orientations found in the North Chile standard. The different orientations indicate that these inclusions are 3-dimensional within the sample.

In spite of the rhabdite crystals found locally, it was important to determine whether the kamacite metal was homogeneous throughout the sample to assess the merit of using North Chile as a metal standard. The BSE and SE images of North Chile in Fig. A1.2 confirm this homogeneity; there is no compositional variation within the metal, both adjacent to, and within, the laser pits. The SE images in Fig. A1.2 reveal that some melting did occur during laser ablation analysis given that the bottom of the laser pits are irregular. However, because the LA-ICP-MS results are consistent with the literature values, melting during LA-ICP-MS analysis is not a significant detrimental factor for this method.

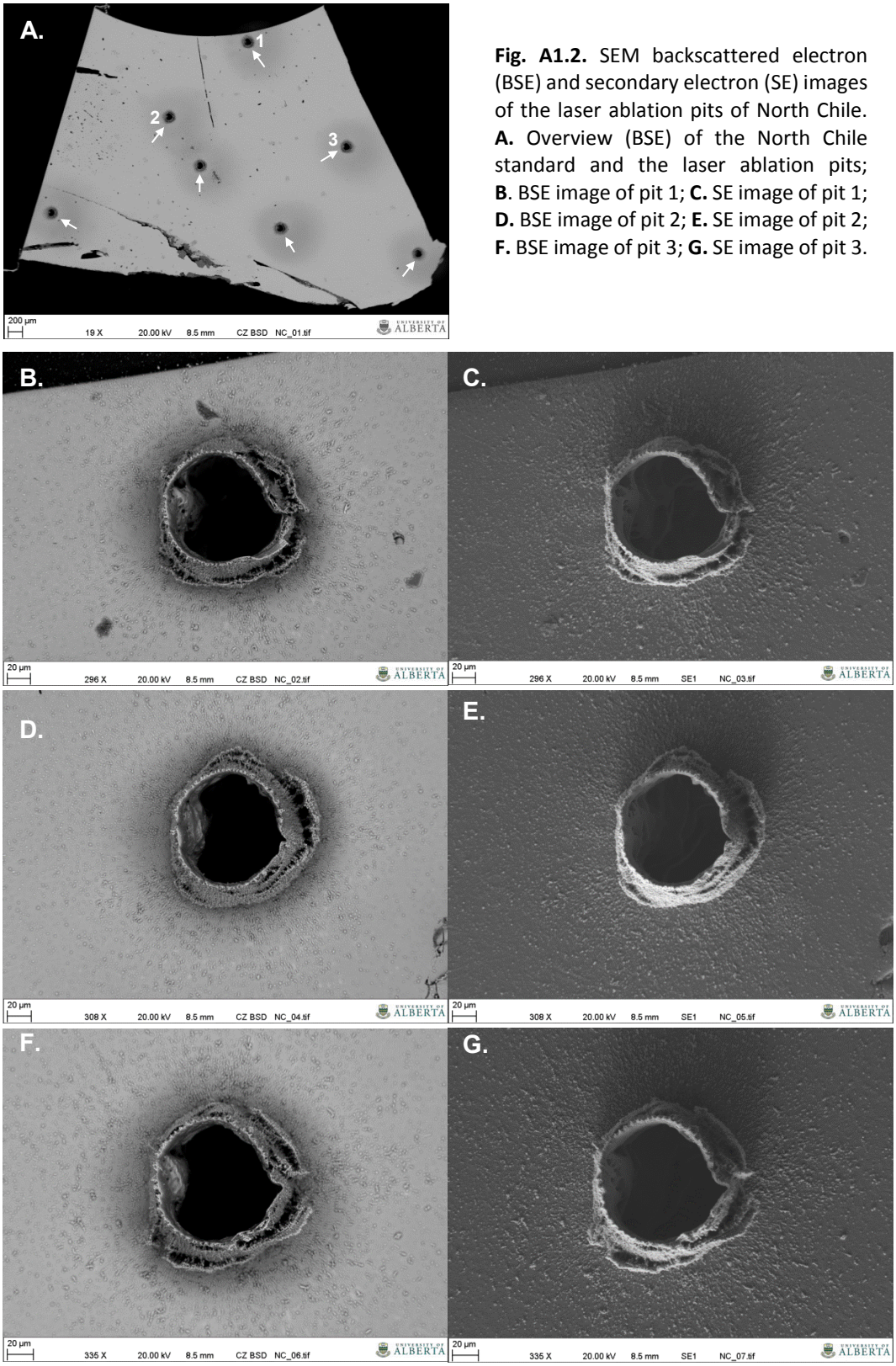

Fig. A1.2. SEM backscattered electron (BSE) and secondary electron (SE) images of the laser ablation pits of North Chile. **A.** Overview (BSE) of the North Chile standard and the laser ablation pits; **B**. BSE image of pit 1; **C.** SE image of pit 1; **D.** BSE image of pit 2; **E.** SE image of pit 2; **F.** BSE image of pit 3; **G.** SE image of pit 3.

A note on Chromium

Chromium concentrations are seen to vary in North Chile as evident by the discrepancy in values between NC 1-6 and NC 7 (Table A1.1), as well as the percent of the standard deviation relative to the mean from the different analytical sessions. Given the consistency of the other elements between NC 1-6 and NC 7, this Cr variation is not expected. It is possible that the LA-ICP-MS method is not suitable for the analysis of Cr in meteorite metal. This possibility has been confirmed from LA-ICP-MS analyses of ordinary chondrite kamacite and taenite; Cr concentrations range from below detection limits to the hundreds of ppm in any given ordinary chondrite. Therefore, Cr values are not reported for ordinary chondrite metal compositions in Chapter 2.

Conclusions

This study was successful in establishing North Chile as a metal standard for LA-ICP-MS analysis. The observed homogeneity of North Chile coupled with the LA-ICP-MS results (Table A1.1) and the similarity between LA-ICP-MS and literature values confirms that North Chile is a useful and reliable standard. The discrepancy in the solution ICP-MS results (Table A1.2) suggests that this particular method may not be reliable for bulk analysis. Despite the uncertainty of the solution ICP-MS results, the confidence of using North Chile as a metal standard for LA-ICP-MS remains high. Any unknowns analyzed by LA-ICP-MS using North Chile as a standard can be considered reliable in trace element analysis of meteorite metal.

A1.2. Ordinary Chondrite Metal Variability

The following figures show the PGE concentrations for each individual spot analyses in EOC kamacite (Figs. A1.3 to A1.10) and taenite (Figs. A1.11, A1.12) metal grains. The scale of the Y-axis has been set to specific maximum values for the kamacite (14 ppm; except for St. Séverin) and taenite (35 ppm) results to illustrate the extent of PGE variability in each metal phase for a given EOC. The sixth period PGEs (Os, Ir, and Pt) are much more variable in both kamacite and taenite than the fifth period PGEs (Ru, Rh, and Pd). Overall, Pt appears to be the most variable element, while Pd and Rh are the least variable.

H chondrite kamacite appears to be overall least variable in PGE concentrations than the other EOC groups (Figs. A1.3 to A1.10). The variability of PGEs in EOCs decreases with increasing petrologic grade for both kamacite and taenite results in response to increasing metamorphic temperatures. Buzzard Coulee (H4) is an exception to this trend given its unexpected consistency of kamacite PGE concentrations. Petrological investigation of the Buzzard Coulee meteorite has revealed that it is a monomict breccia (C. Herd, pers.comm.). Reduction of grain size and subsequent brecciation that occurred in the Buzzard Coulee parent body may have significantly homogenized the metal compositions well beyond the extent of homogenization seen in type 6 ordinary chondrites. Homogenization due to brecciation may also explain the low variation coefficients for measured physical properties (bulk density, grain density, and magnetic susceptibility) among different Buzzard Coulee fragments (Fry et al., 2013).

Note: The results for the breccia NWA 6204 (L4-6) in figures A1.3 to A1.8 are from metal that was analyzed in the L4 matrix only.

Fig. A1.3. Ruthenium (Ru) concentrations in ordinary chondrite kamacite metal.

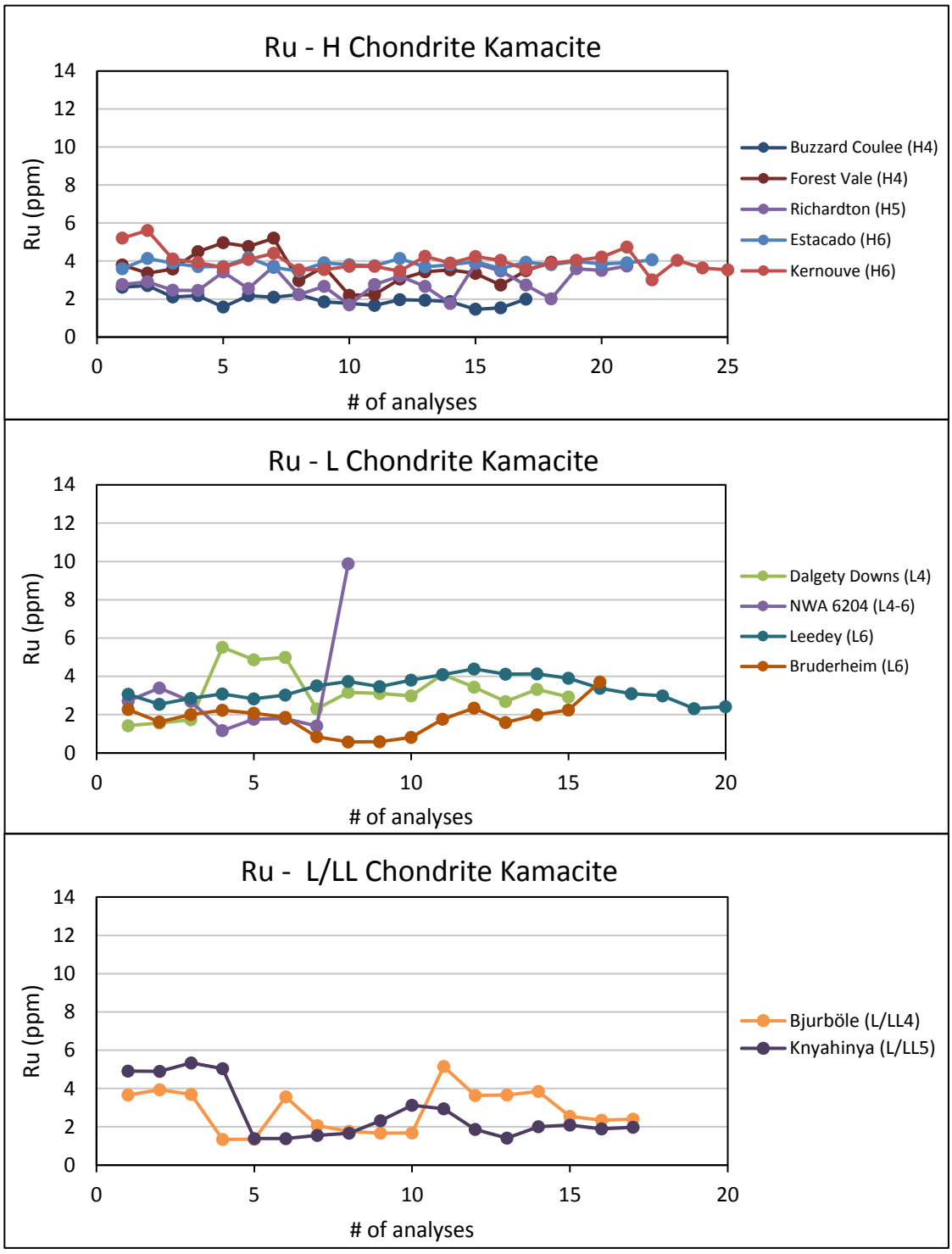

Fig. A1.4. Rhodium (Rh) concentrations in ordinary chondrite kamacite metal.

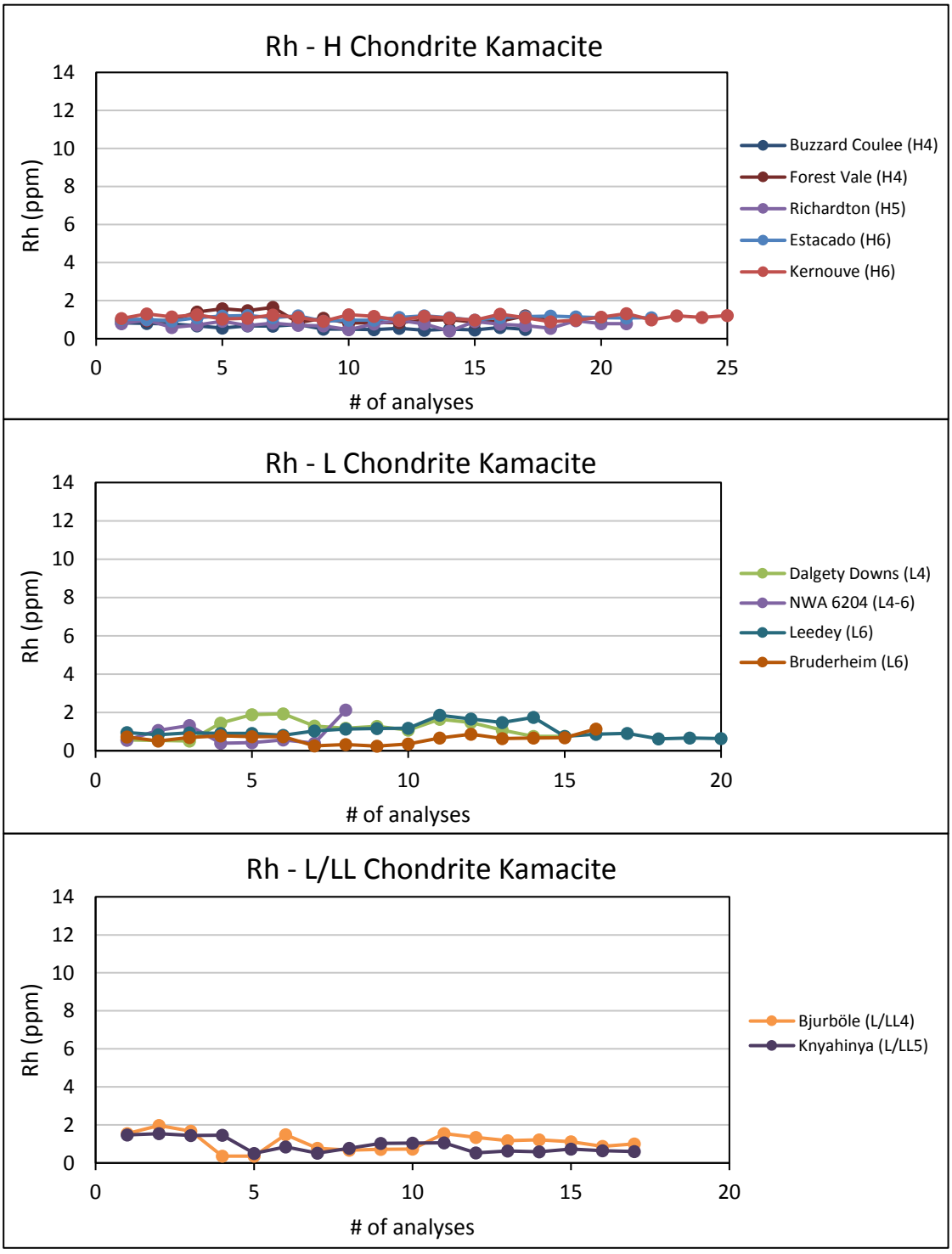

Fig. A1.5. Palladium (Pd) concentrations in ordinary chondrite kamacite metal.

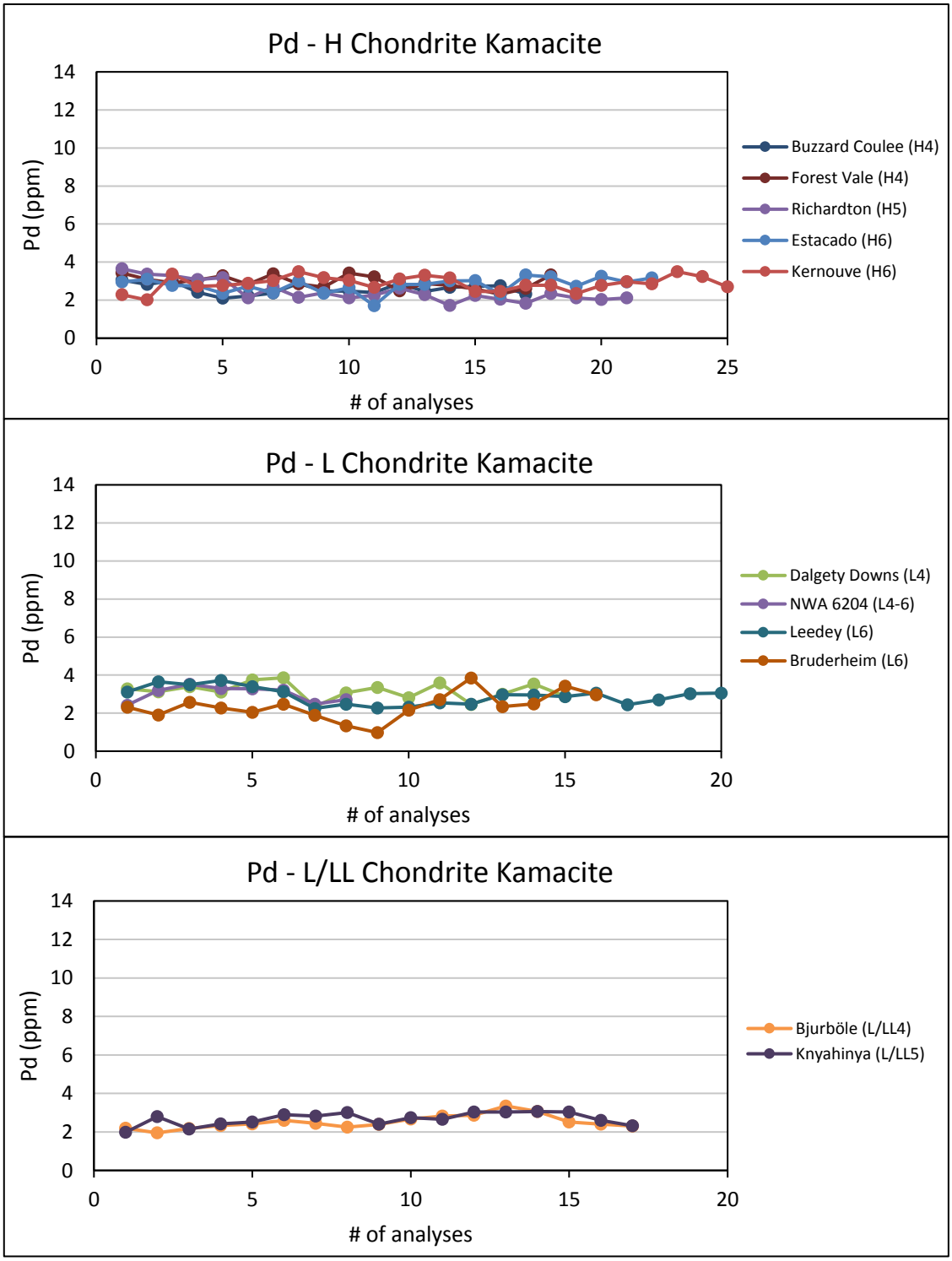

Fig. A1.6. Osmium (Os) concentrations in ordinary chondrite kamacite metal.

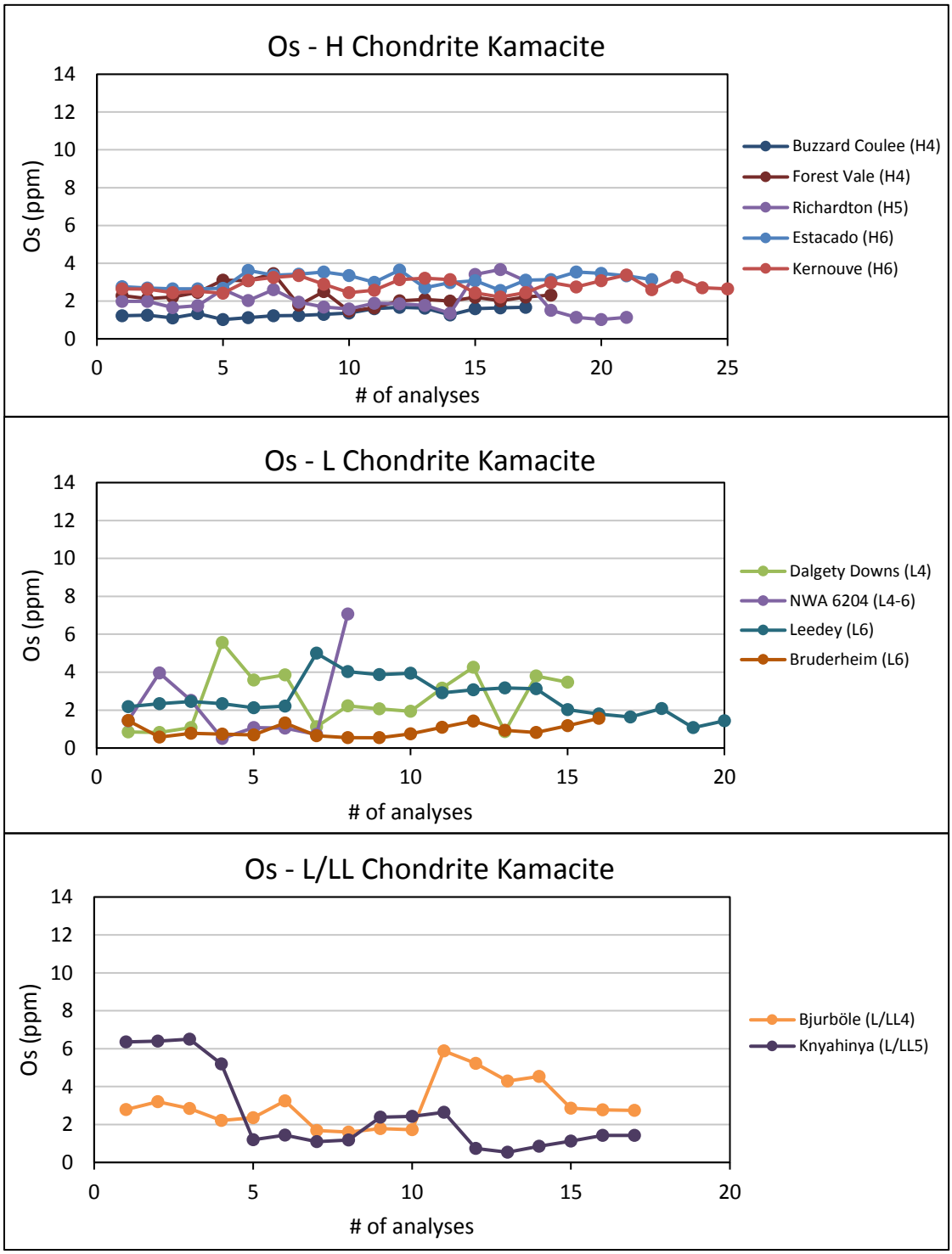

Fig. A1.7. Iridium (Ir) concentrations in ordinary chondrite kamacite metal.

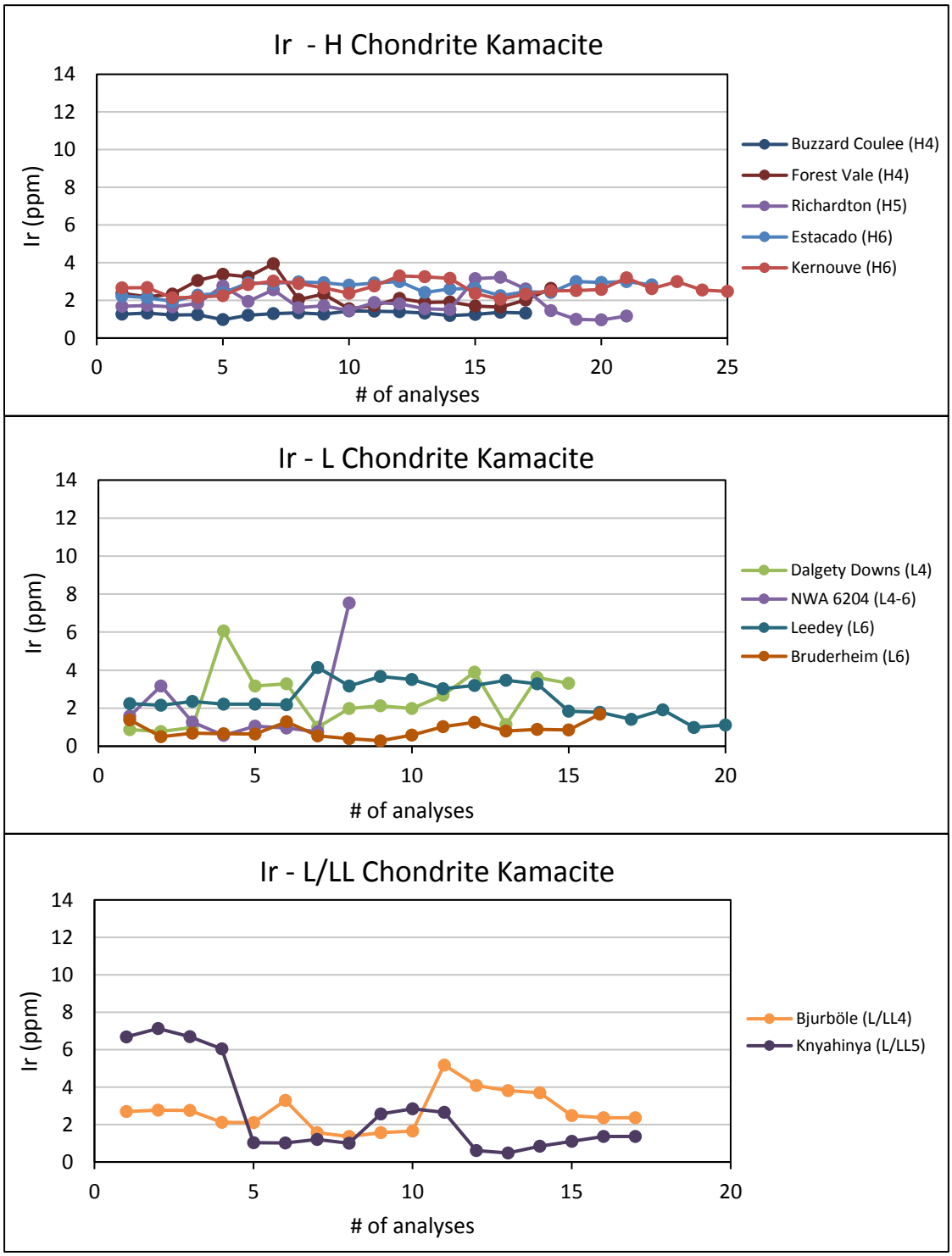

Fig. A1.8. Platinum (Pt) concentrations in ordinary chondrite kamacite metal.

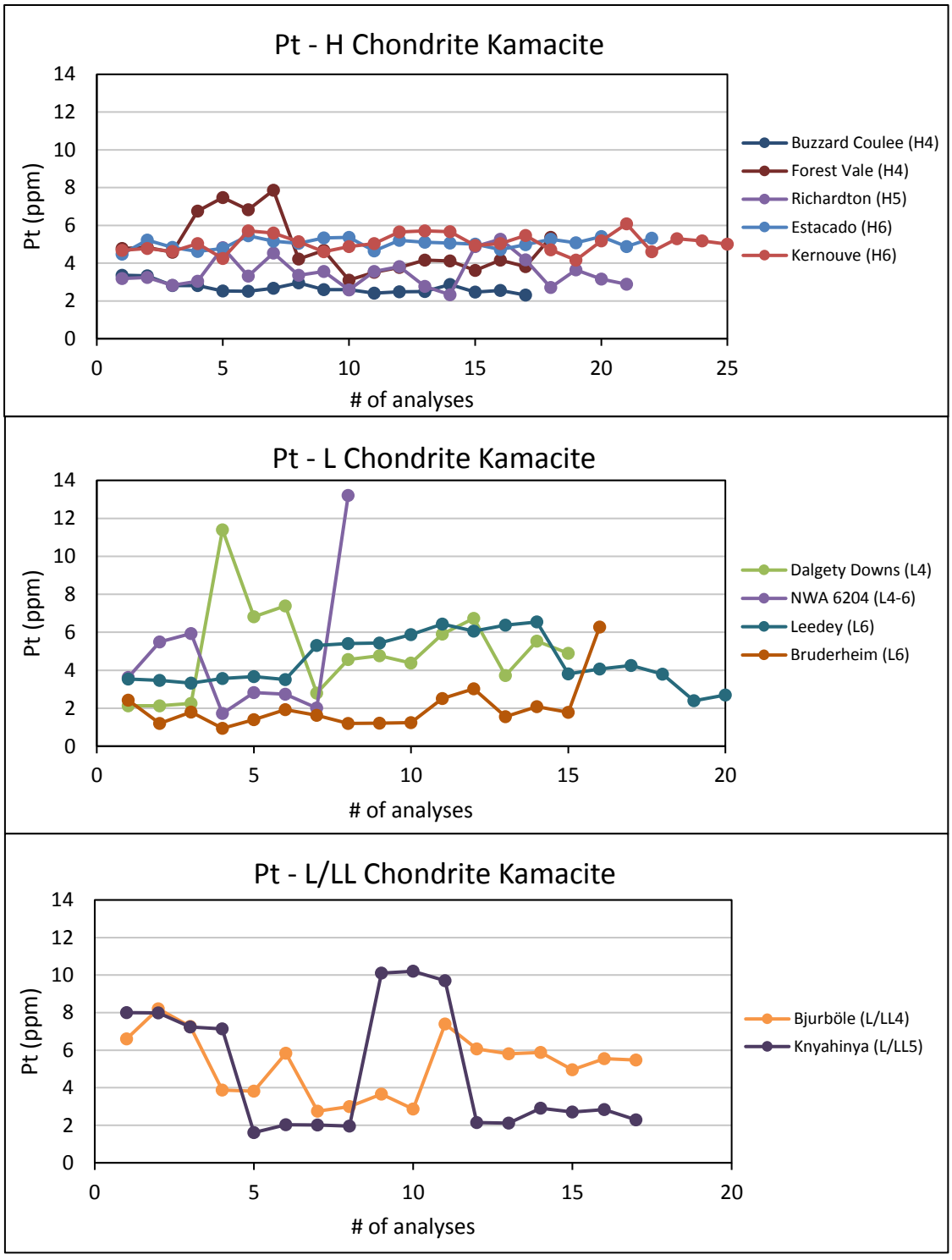

Fig. A1.9. PGE concentrations in Benares(a) (LL4) kamacite.

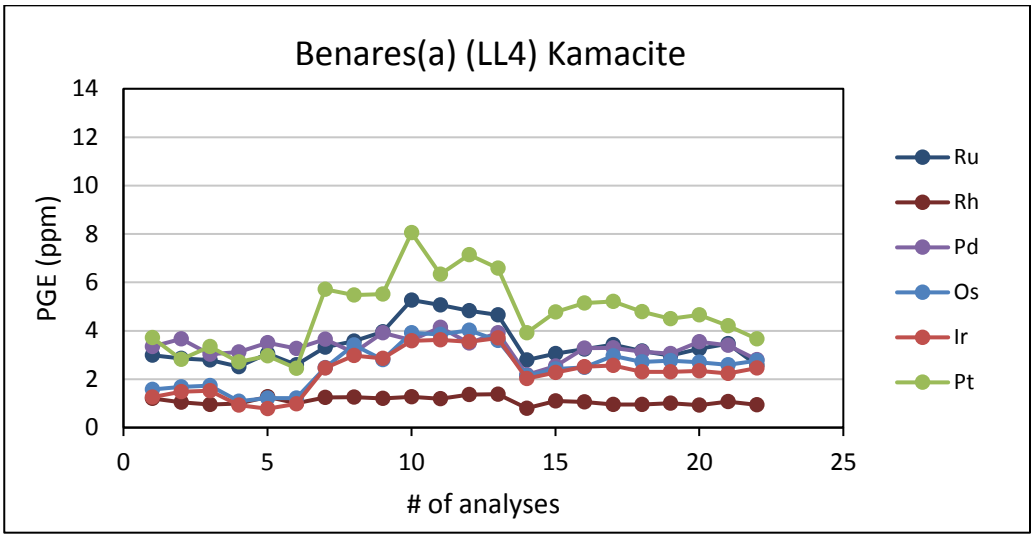

Fig. A1.10. PGE concentrations in St. Séverin (LL6) kamacite.

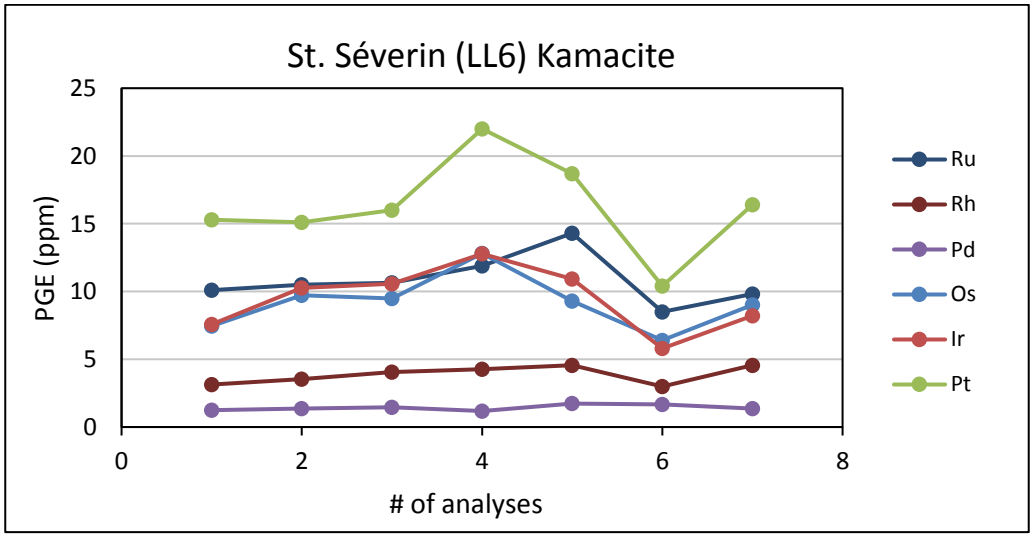

Fig. A1.11. Ruthenium (Ru), Rhodium (Rh), and Palladium (Pd) concentrations in ordinary chondrite taenite.

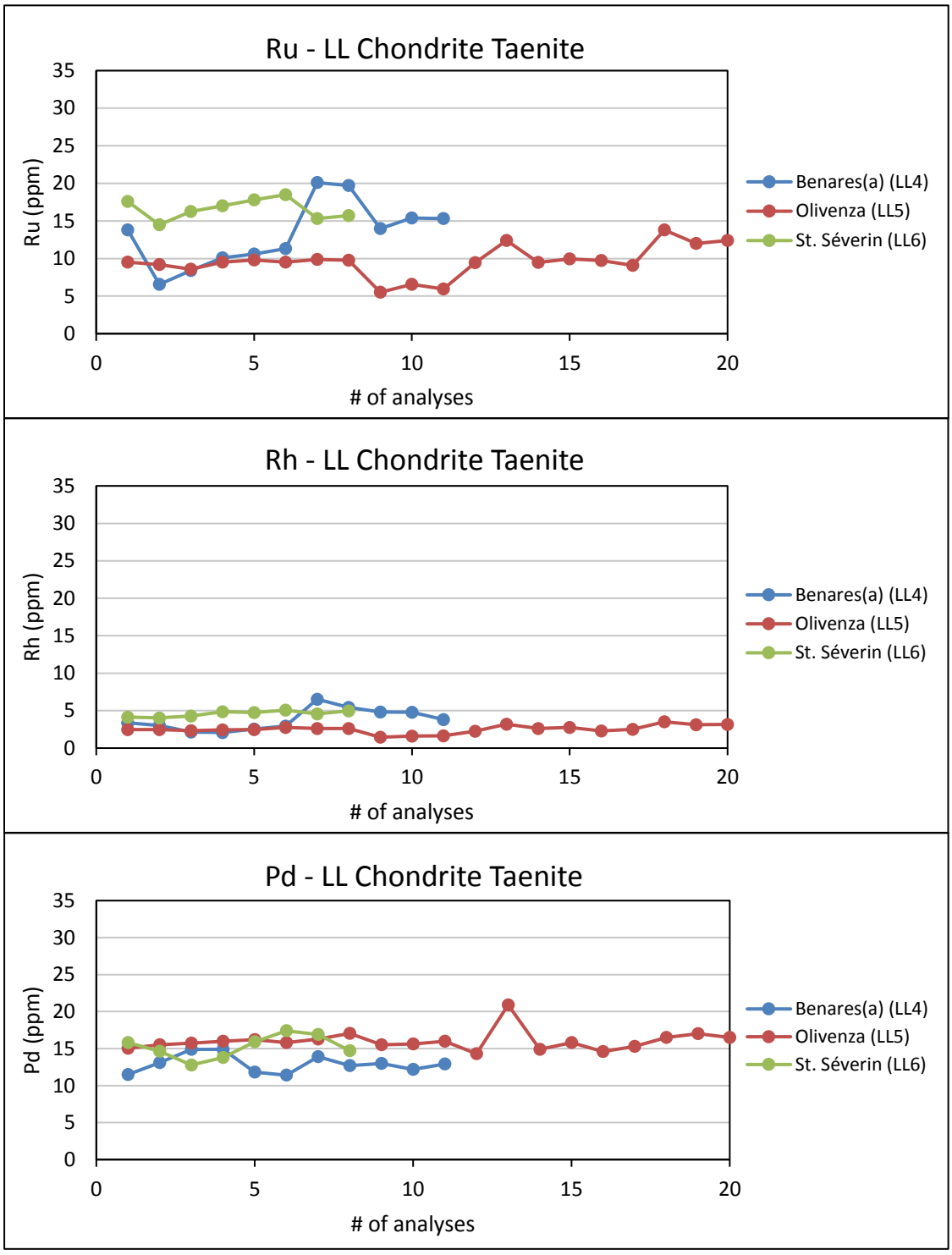

Fig. A1.12. Osmium (Os), Iridium (Ir), and Platinum (Pt) concentrations in ordinary chondrite taenite.

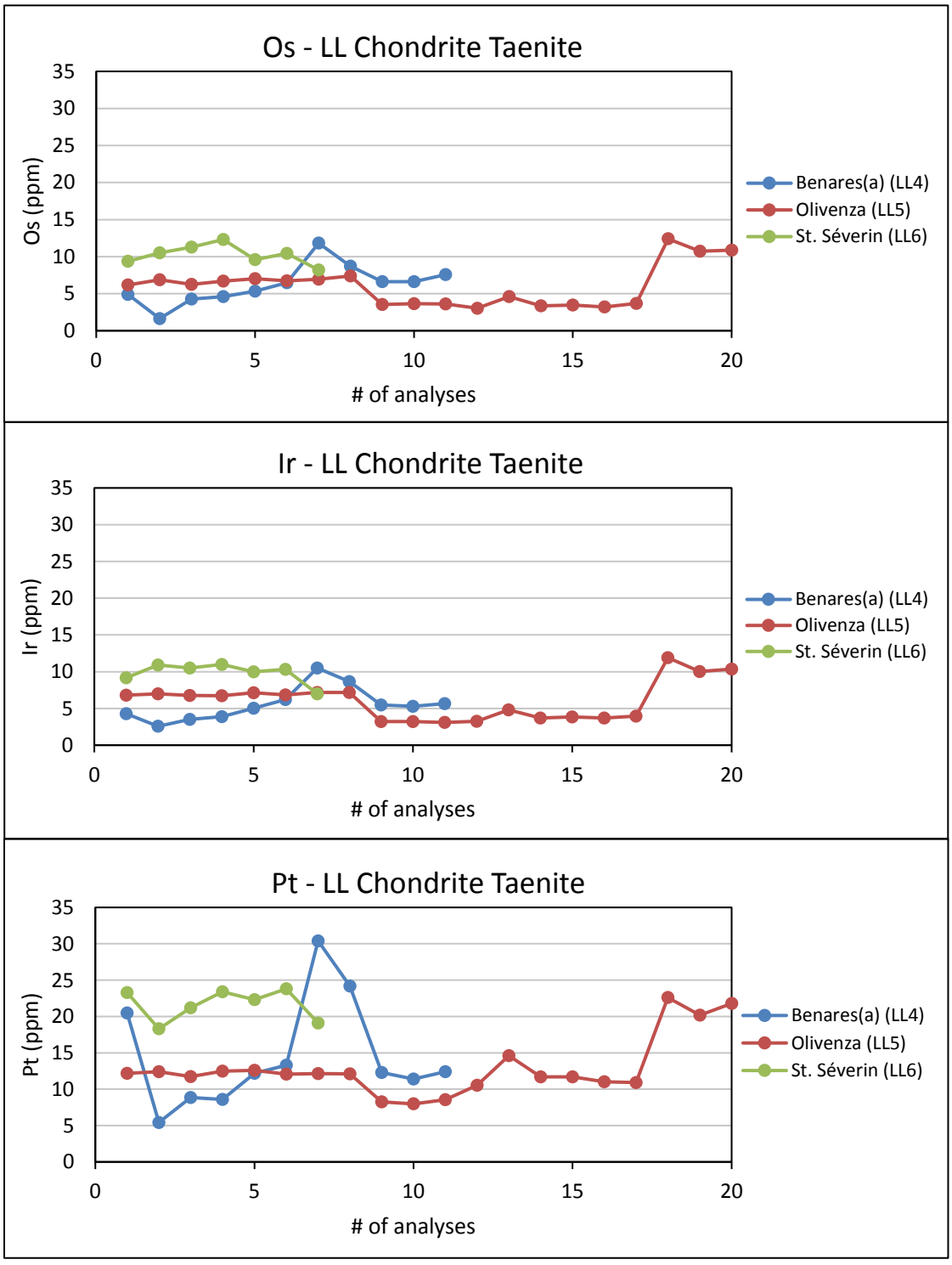

Appendix 2

A2.1. DTG curves of mineral references and Murchison insoluble organic matter (IOM) over the temperature range of 30°C to 900°C.

Fig. A2.1. DTG curve of Murchison IOM.

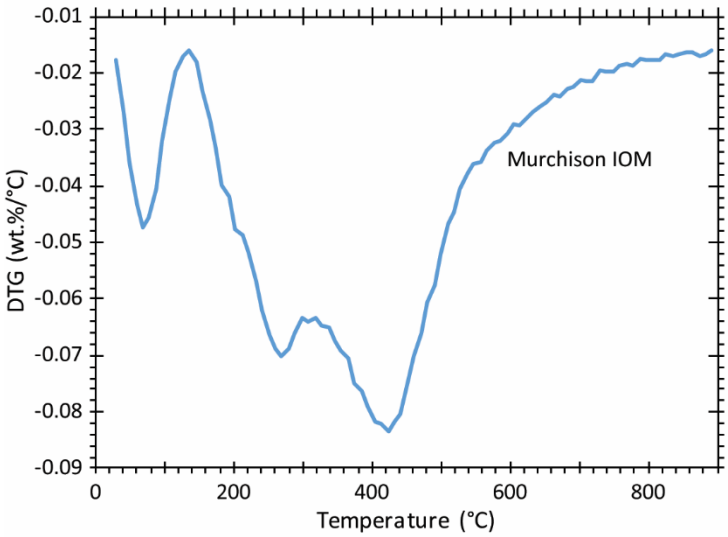

Fig. A2.2. DTG curves of carbonate standards.

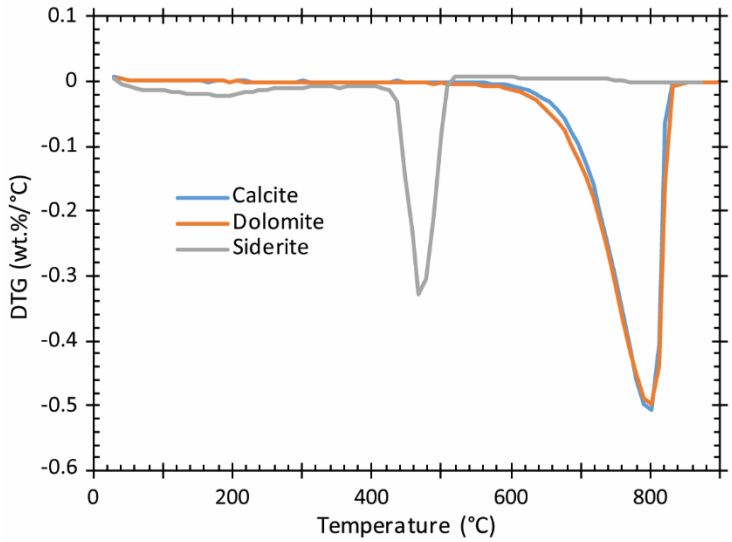

Fig. A2.3. DTG curves of serpentine minerals (greenalite and clinochlore).

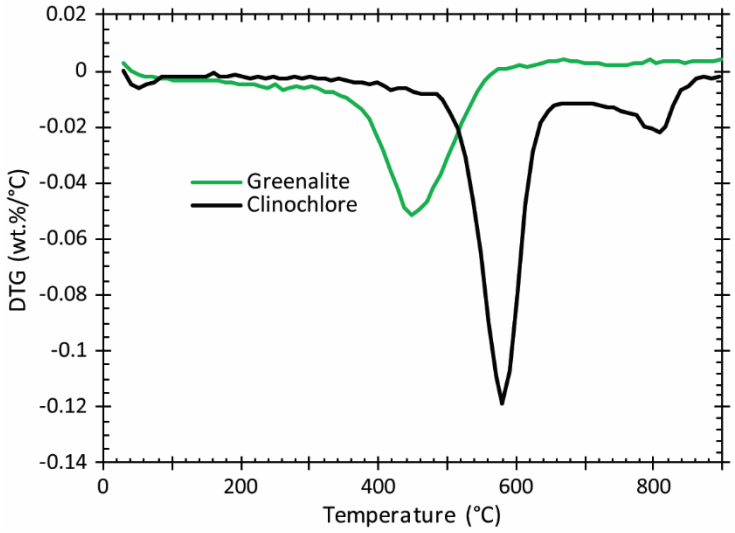

Fig. A2.4. DTG curve of saponite (clay).

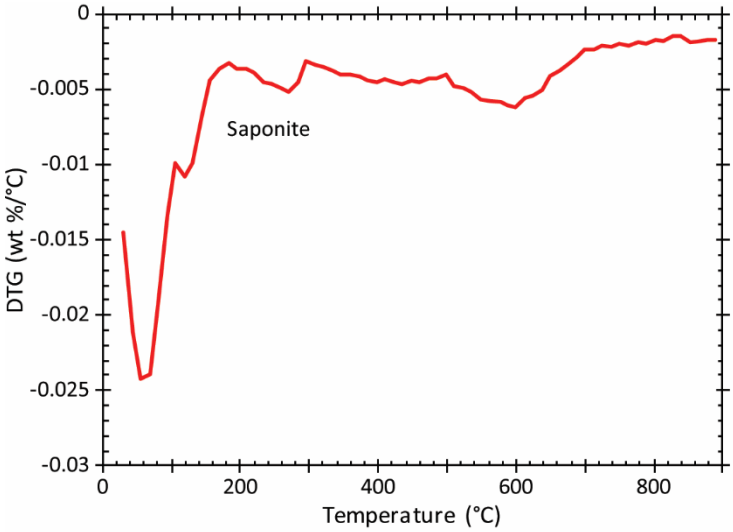

A2.2. Asteroid Taxonomy

The Bus-DeMeo classification system (DeMeo et al., 2009) has classified 24 asteroid classes based on reflectance measurements of 371 asteroids (Fig. A2.5). The asteroid types that are of interest for the discussion of Tagish Lake are D- and T-types, as well as the C- and X-complexes. Necessary background information regarding these specific asteroids is presented in this section.

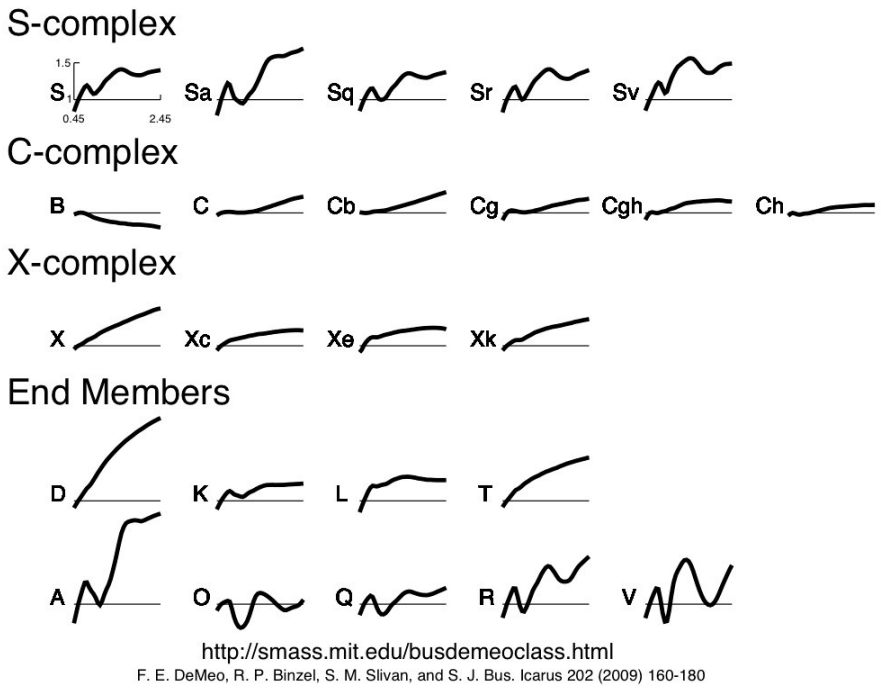

Fig. A2.5. Bus-DeMeo taxonomy key for the 24 asteroid spectral classes.

D-type

Slope value: > 0.38 (DeMeo et al., 2009)

Average albedo: 7% (Ryan and Woodward, 2010)

Spectral features: Generally featureless; however, some D-type asteroids have gentle kink around 1.5 μm (DeMeo et al., 2009)

Composition: Primitive material composed of organics, carbon, and anhydrous silicates with possible water ice interiors (Bell et al., 1989; Gaffey et al., 1993; Nelson et al., 1993)

T-type

Slope value: 0.25 < slope < 0.38 (DeMeo et al., 2009)

Albedo: 4% (Ryan and Woodward, 2010)

Spectral features: Featureless with a gently concaving downward spectra (DeMeo et al., 2009)

Composition: Either metamorphosed carbonaceous chondrite-like material (Bell et al., 1989) or bodies rich in troilite (FeS) (Britt et al., 1992; Gaffey et al., 1993)

C-complex

The C-complex consists of six asteroid subtypes: B, C, Cb, Cg, Cgh, and Ch (Fig. A2.5). These six have been grouped together based on similarities in their spectra. The C-complex was first defined by Bus (1999) and is fundamentally equivalent to the B-, C-, G- and F-classes defined earlier by Tholen (1984) based on eight-colour asteroid survey data. The B-, C-, G-, and F-classes are compositionally similar; they are composed of hydrated silicates (i.e., clays), organics, carbon, and opaques (Gaffey et al., 1993; Nelson et al., 1993). The asteroids assigned to the C-complex of Bus (1999) and DeMeo et al. (2009) can be distinguished based on differences in their spectral features. The B-type spectrum is quite distinguishable from the other C-complex types as it is linear and featureless with a negative slope (Fig. A2.5). The subgroups of the C-type asteroids (C, Cb, Cg, Cgh, and Ch) are largely distinguished based on the strength of spectral features in the ultraviolet (UV) wavelength region (Bus, 1999). Asteroids that have a spectrum with a strong UV drop-off are classed as Cg, which are similar to the Tholen (1984) G-class. Asteroids that fall under the Cgh classification have a pronounced UV drop-off, as well as a shallow absorption band occurring at 0.7 µm. Asteroids that have a slight UV drop-off as well as the shallow 0.7 µm band are classified as Ch-type. The C-type subgroup often have a slight bump occurring around 0.6 µm and also have a broad and shallow feature between 1.0 and 1.3 µm. The Cb-type have spectral shapes that are intermediate of the B- and C-subgroups (Bus and Binzel, 2002); they have a linear spectrum with a subtle positive slope onward of 1.1 µm. A summary of the C-type subgroup of the C-complex is provided below as it is most pertinent to the Tagish Lake discussion (Chapter 3).

C-type

Slope value: 0.2 < slope < 0.38 (DeMeo et al., 2009)

Average albedo: 5% (Ryan and Woodward, 2010)

Spectral features: Small bump at 0.6 μm; broad and shallow feature between 1.0 and 1.3 μm (DeMeo et al., 2009)

Composition: Primitive material composed of clays, organics, carbon, and opaques (Bell et al., 1989; Gaffey et al., 1993; Nelson et al., 1993)

X-complex

The X-complex consists of four asteroid subtypes: X, Xc, Xe, and Xk (Fig. A2.5). An Xn-type was later added to the X-complex after the publication of DeMeo et al. (2009) to classify asteroids with spectra similar to the Nysa asteroid, which have a weak to moderate narrow feature at 0.9 μm and a broad and shallow feature at 1.8 μm (Reddy et al., 2016). The X-complex classifies asteroids with spectral characteristics similar to asteroids that have been previously classified as E-, M-, or P-types by Tholen (1984). Despite having similar spectra, the E-, M-, and P-types are compositionally distinct: E-type asteroid compositions are rich in enstatite; M-type are thought to be mostly metal with some silicate component, although a 3-μm hydration feature has been observed in some M-type spectra suggesting that the M-type composition may be more diverse than originally thought; and P-type asteroids are similar in composition to D-type asteroids (primitive, organic rich material with possible water ice interiors) (Gaffey et al., 1993; Nelson et al., 1993). Due to these compositional differences, these three asteroid types have very different albedos in the order of P < M < E (Gaffey et al., 1993).

Asteroids that are a part of the X-complex of Bus (1999) and DeMeo et al. (2009) are distinguished by subtle differences in their spectral features. It is important to note that it is difficult to distinguish between the asteroid classes Cg, Cgh, Ch, Xk, Xc, and Xe using principle component analysis as their spectral features are weak and not well detected by the first few principle components (DeMeo et al., 2009). Xe-type asteroids are distinguished from the other X-complex asteroids by a hook-like absorption feature at 0.49 μm. The “e” assigned to the Xe classification is representative of the Tholen (1984) E-class (Bus, 1999). Asteroids assigned to the Xc-type are featureless, but their spectra slightly curve concave downward. The Xk-type

spectra are similar to Xc spectra; however, the Xk spectra also have a faint absorption feature between 0.8 and 1 µm. The Xc- and Xk-types were formed to classify asteroids that fall between the Tholen (1984) C-types and the K- (primitive composition similar to CV/CO chondrites; Gaffey et al., 1993) and T-type asteroids on the spectral continuum (Bus, 1999). The Xc- and Xk-types are divided by a slope value of 0.26 (Bus, 1999). Lastly, the X-complex spectra are linear and featureless with a moderate to high slope value. It is difficult to constrain the compositions of the Xc, Xk, and X-type asteroids classified by Tholen (1984) as M or P asteroids can be assigned to any of these three X-complex subgroups (DeMeo et al., 2009). In this case, albedo can be a useful indicator for composition. For the discussion of Tagish Lake, the X- and Xc-type asteroids are spectral matches to TL 4 and 11h, respectively, and are summarized below.

X-type

Slope value: 0.2 < slope < 0.38 (DeMeo et al., 2009)

Average albedo: 8% (Ryan and Woodward, 2010)

Spectral features: Featureless (DeMeo et al., 2009)

Composition: Variable; likely either M- or P-type compositions (DeMeo et al., 2009)

Xc-type

Slope value: Not specified in DeMeo et al. (2009); however, the Xc-type appear to have a slope shallower than X-type (Fig. A2.5), so slope is likely < 0.2.

Average albedo: 14% (Ryan and Woodward, 2010)

Spectral features: Featureless, but is slightly curved and concave downward (DeMeo et al., 2009)

Composition: Variable; most likely a M-type composition (DeMeo et al., 2009)

Appendix 3

Table A3.1. Ordinary chondrite PGE bulk rock grades.

	H Chondrites		L Chondrites		LL Chondrites	
Total Metal (wt. %)[a]	18.2		8.45		2.94	
Kamacite (wt. %)[a]	16.0		6.76		1.03	
Taenite (wt. %)[b]	2.2		1.69		1.91	
	LA-ICP-MS[c]	**Grade[d]**	**LA-ICP-MS[c]**	**Grade[d]**	**LA-ICP-MS[c]**	**Grade[d]**
Ir (ppm)						
Average Km	2.2	0.352	2.0	0.135	2.3	0.024
Highest Tn	9.6	0.211	9.6	0.162	9.6	0.183
	Total	*0.563*	*Total*	*0.297*	*Total*	0.207
Pt (ppm)						
Average Km	4.3	0.688	4.0	0.270	4.7	0.048
Highest Tn	21.5	0.473	21.5	0.363	21.5	0.411
	Total	*1.161*	*Total*	*0.633*	*Total*	*0.459*
Pd (ppm)						
Average Km	2.7	0.432	2.8	0.189	3.3	0.034
Highest Tn	16.0	0.352	16.0	0.270	16.0	0.306
	Total	*0.784*	*Total*	*0.459*	*Total*	*0.340*
Rh (ppm)						
Average Km	0.95	*0.152*	0.93	0.063	1.1	0.011
Highest Tn	4.6	0.101	4.6	0.078	4.6	0.088
	Total	*0.253*	*Total*	*0.141*	*Total*	*0.099*
Au (ppm)						
Average Km	1.04	0.166	1.15	0.078	1.13	0.012
Highest Tn	5.0	0.110	5.0	0.085	5.0	0.096
	Total	*0.276*	*Total*	*0.163*	*Total*	*0.108*
Total Pt, Pd, Rh, Au	-	**2.47**	-	**1.40**	-	**1.01**

[a] Gattacceca J., Suavet C., Rochette P., Weiss B. P., Winklhofer M., Uehara M. and Friedrich J. M. (2014) Metal phases in ordinary chondrites: Magnetic hysteresis properties and implications for thermal history. *Meteorit. Planet. Sci.* **49**, 652–676.

[b] Taenite wt. % calculated from total metal and kamacite fractions.

[c] LA-ICP-MS results from Chapter 2. The average kamacite (Km) values are specific to each ordinary chondrite group (LL chondrite kamacite values from Benares(a) only; Table 2.3), whereas the taenite (Tn) values are the same for all groups and correspond to the highest concentrations obtained from the LL chondrites (Table 2.4).

[d] Calculated bulk rock grade based on kamacite and taenite modal abundances in ordinary chondrites and LA-ICP-MS PGE concentrations.